




5-2017

Characterization and manipulation of lipid self-assembly to construct stable, portable synthetic lipid bilayers

Guru Anand Venkatesan

University of Tennessee, Knoxville, gvenkate@vols.utk.edu

Follow this and additional works at: https://trace.tennessee.edu/utk_graddiss

 Part of the [Biological Engineering Commons](#), [Biomedical Devices and Instrumentation Commons](#), and the [Other Biomedical Engineering and Bioengineering Commons](#)

Recommended Citation

Venkatesan, Guru Anand, "Characterization and manipulation of lipid self-assembly to construct stable, portable synthetic lipid bilayers. " PhD diss., University of Tennessee, 2017.
https://trace.tennessee.edu/utk_graddiss/4432

This Dissertation is brought to you for free and open access by the Graduate School at TRACE: Tennessee Research and Creative Exchange. It has been accepted for inclusion in Doctoral Dissertations by an authorized administrator of TRACE: Tennessee Research and Creative Exchange. For more information, please contact trace@utk.edu.

To the Graduate Council:

I am submitting herewith a dissertation written by Guru Anand Venkatesan entitled "Characterization and manipulation of lipid self-assembly to construct stable, portable synthetic lipid bilayers." I have examined the final electronic copy of this dissertation for form and content and recommend that it be accepted in partial fulfillment of the requirements for the degree of Doctor of Philosophy, with a major in Biomedical Engineering.

Stephen A. Sarles, Major Professor

We have read this dissertation and recommend its acceptance:

Pat Collier, Jaan Mannick, Christopher A. Baker

Accepted for the Council:

Dixie L. Thompson

Vice Provost and Dean of the Graduate School

(Original signatures are on file with official student records.)

Characterization and manipulation of
lipid self-assembly to construct stable,
portable synthetic lipid bilayers

A Dissertation Presented for the

Doctor of Philosophy

Degree

The University of Tennessee, Knoxville

Guru Anand Venkatesan

May 2017

© by Guru Anand Venkatesan, 2017
All Rights Reserved.

*To my mom and dad,
Poongothai and Venkatesan*

my brother,

Ramesh

and my grandfather,

Srinivasan.

Acknowledgements

I would like to express my deepest gratitude to my advisor, Dr. Andy Sarles, for his guidance and support throughout my graduate school. Andy has been a great role model and a friend. He has patiently taught me to become a better writer, speaker and researcher. His dedication to things that he cared about, work ethics, mentorship and sense of humor has always inspired me. I have learned a tremendous amount from Andy and will forever be indebted to him.

Dr. Pat Collier has been instrumental in my work and deserves many thanks for his scientific insights. I would like to thank Dr. Jaan Mannik and Dr. Christopher Baker for their valuable inputs. I would also like to acknowledge the financial support offered through Air Force Office of Scientific Research (AFOSR) Basic Research Initiative (Les Lee's M4 program).

I consider myself very fortunate for joining the Bioinspired Materials and Transduction Laboratory, where I had the opportunity to learn and work alongside great labmates and friends: Graham Taylor, Nima Tamaddoni, and Mary-Anne Nguyen. I would like to extend a special thanks to Graham Taylor for being a great friend and a role model, and for pushing me to get out of my comfort-zone. Finally, I would like to acknowledge my parents, brother and friends for providing me with love and constant encouragement.

Abstract

The overarching goal of this research work is to further our understanding of lipid self-assembly and its organization at an oil-water interface to support the development of synthetic lipid bilayer systems that can be used in biologically relevant fields such as membrane biophysics, protein electrophysiology, development of synthetic biomolecules, drugs, nanoparticles and other applications. Self-assembly kinetics and interfacial properties of lipid monolayers formed at a liquid-air and liquid-liquid interface are characterized using Langmuir-Blodgett trough and pendant drop tensiometer. Insights gained from these studies not only allow us to answer questions related to droplet interface bilayer (DIB; a promising technique to assemble artificial lipid membranes) formation but also enable us to manipulate properties of monolayer in order to improve the potential of droplet interface bilayer by, a) increasing the number of phospholipids that can form DIBs, b) improving the success rate of DIB formation, and c) enhancing the electrical stability of bilayers formed. Owing to its wide range of applicability, novel efforts towards improving the durability and portability of DIB system are presented. In addition, this research work aims at using Nanoscribe direct laser writing — a state-of-the-art 3D printing device, to build 3D micro-scaffolds that can support lipid monolayers and bilayers that are suitable for high resolution optical studies.

Table of Contents

1	Introduction and Literature Review	1
1.1	Introduction	1
1.1.1	Phospholipids	2
1.1.2	Self-Assembly and Langmuir Monolayers	5
1.1.3	Langmuir Compression Isotherm and Phases of Lipid Monolayer	7
1.1.4	Lipid Bilayer	10
1.1.5	Model Membranes	16
1.2	Background and Literature Review	20
1.2.1	Droplet Interface Bilayers (DIB)	20
1.2.2	Monolayer formation: "Lipid-in" vs "Lipid-out"	21
1.2.3	Membrane Composition in DIBs	24
1.2.4	Durability and Portability	26
1.2.5	Horizontally-oriented Lipid Bilayers	27
1.3	Vision	29
1.4	Scientific Gaps, Objectives and Research Plan	30
1.4.1	Scientific Gaps	30
1.4.2	Research Objectives	31
1.5	Document Overview	32
2	General Methods	33
2.1	Materials and Preparation	33

2.1.1	Lipid-in solution preparation.	33
2.1.2	Lipid-out solution preparation	33
2.1.3	Lipid-chloroform preparation for compression isotherm	34
2.1.4	SEBS-hexadecane organogel preparation	34
2.2	Dynamic Light Scattering	35
2.3	Interfacial Characterization	35
2.3.1	Pendant Drop Tensiometer	35
2.3.2	Langmuir Compression Isotherm	37
2.4	DIB formation and characterization	37
2.4.1	Liquid-in-liquid DIB formation	37
2.5	Contact Angle Measurement	38
2.6	Electrical Characterization	38
2.6.1	Resistance and Rupture Potential	40
2.6.2	Specific Capacitance and Thickness	41
2.6.3	Alamethicin Ion-channel Gating	43
2.7	Nanoscribe 3D printing	43
2.8	PDMS Microfluidic Channel Fabrication	45
2.8.1	Plasma Bonding PDMS Chip on Glass Coverslip	46
3	Kinetics of Lipid Self-assembly at an Oil/Water Interface: Dynamic Interfacial Tension Measurements and MD Simulation	47
3.1	Introduction	47
3.2	Results	48
3.2.1	Interfacial Tension Measurements	48
3.2.2	DIB Formation vs Lipid Type and Placement	52
3.2.3	Electrical Measurements	53
3.2.4	Comparison to Simulation Results Performed at UIUC	53
3.3	Discussion	58
3.4	Validity and Limitations of the Proposed Model	70

3.4.1	Limitations of the Model	71
3.5	Conclusion	72
4	Evaporation-induced Compression of Monolayers to Enable Droplet Interface Bilayer Formation using Unsaturated Lipids	74
4.1	Introduction	74
4.2	Approach	75
4.2.1	Description of Novel Procedure: Evaporation of Water Droplets to Compress Lipid Monolayer	75
4.2.2	Pendant Drop Tensiometry with Step-wise Volume Reduction	76
4.3	Results	77
4.3.1	Improved DIB Formation Success Rate	77
4.3.2	Dynamic Interfacial Tension Measurements	78
4.3.3	Langmuir Compression Isotherm	82
4.4	Discussion	84
4.4.1	Explanation for improved DIB formation success rate	86
4.4.2	Decrease in Area/lipid: comparing compression isotherm with IFT	89
4.4.3	Required Volume Reduction and Period of Evaporation	91
4.5	Summary	92
5	Improving Bilayer Stability and Portability Using Polymer Encapsulation	93
5.1	Introduction	93
5.2	Objective and Approach	94
5.2.1	Liquid-in-gel DIB formation	94
5.2.2	DIB Durability Test	96
5.3	Results and Discussion	97
5.3.1	Rheology Measurement	97
5.3.2	Encapsulation of DIB	97

5.3.3	Capacitance vs temperature	100
5.3.4	Characterization of encapsulated DIB	101
5.3.5	Wax-encapsulated DIBs	113
5.3.6	Conclusions	113
6	3D-Printed Microscaffolds for Horizontally-oriented Suspended Bi-layer Formation	117
6.1	Introduction	117
6.2	Research Objective and Approach	119
6.2.1	Scaffold Designs	119
6.3	Method	119
6.4	Results and Discussion	121
6.4.1	Manual Solution Exchange	121
6.4.2	Microfluidics for Sequential Solution Exchange	121
6.5	Summary and Future Directions	125
7	Summary and Conclusions	127
7.1	Research Overview	127
7.1.1	Contributions	128
	Bibliography	132
	Appendices	164
	A Lipid Composition of Biological Membranes	165
	B Exponential Model for Lipid Self-assembly	167
	C DI Water Evaporation Rate at Oil-Air Interface	169
	Vita	170

List of Tables

1.1	Techniques to assemble model membranes	18
1.2	Key differences between lipid-in and lipid-out approach	24
3.1	Success Rates of DIB Formation and Measured Electrical Properties of the Bilayers	53
3.2	Measured physical properties of DIBs	69
3.3	Qualitative determination of suitable minimum lipid concentration . .	70
4.1	DIB Formation Success Rates	78
4.2	DIB measured electrical parameters	79
4.3	Compression isotherm parameters for pure monolayers.	82
5.1	Electrical and physical properties of liquid-in-liquid and liquid-in-gel DIBs	102
A.1	Lipid composition of biological membranes	165
A.2	Phospholipid fatty acid chain composition in human red blood cell . .	166

List of Figures

1.1	(a) Basic structure of Glycerophospholipids. (b) Chemical structure of DPPC molecule. (c) Schematic and chemical structure of phospholipids showing two distinct regions: hydrophilic head in blue box and hydrophobic tails in orange box. All lipids possess same 1,2-dipalmitoyl (DP) tail groups with different head groups: phosphatidylcholine (PC), phosphatidylethanolamine (PE), phosphatidylglycerol (PG), phosphatidylserine (PS), phosphatidylinositol (PI) and phosphatidic acid (PA).	3
1.2	Chemical structure of phospholipids with identical head groups made up of phosphatidylcholine (PC) and distinct tail groups; DLPC (12C fatty acid chain), DPPC (16C fatty acid chain), DPhPC (12C fatty acid chain with 4-methyl groups attached to each tails), POPC (tail groups of different lengths: 16C & 18C, monounsaturated in 18C chain), DOPC (18C chains with 1 double-bond in each tail group), and 18C polyunsaturated tail groups.	4
1.3	3D structures showing different shapes of lipids (a-c) and their corresponding self-assembled structures (d-f). In solutions, conical shaped lysophospholipids self-assemble to form micelle structures, cylindrical shaped phosphatidylcholines form a bilayer and inverse conical shaped phosphatidylethanolamines form an inverse micelle. . .	6

1.4	Surface pressure-area isotherm for a typical lipid monolayer showing various phases: gaseous, liquid-expanded (LE), liquid-condensed (LC), and solid. LC-LE marks LE and LC coexistence. Inset shows a schematic of a LB trough.	8
1.5	Cartoon of a lipid bilayer membrane reproduced from Escribá et al.[1]. Illustration shows different lipid types in different colors organized into microscopic domains with some domains carrying integral membrane proteins.	11
1.6	Lipid composition of biological membranes. Note: Charts represent the proportions of various lipids and not the spatial distribution in the membrane. Refer to Appendix (Table A1) for references and percentages; data taken from Yeagle et al.[2]	12
1.7	Fatty acid chain length and unsaturation of phospholipids found in human red blood cells. SPM: sphingomyelin, PC: phosphatidylcholine, PE: phosphatidylethanolamine. Refer to Appendix (Table A2) for references and percentages; data taken from Vance et al.[3]	13
1.8	Double-bond composition of phospholipids in membranes. Data taken from Vance et al.[3]	14
1.9	(a) Schematic illustration of model membranes: (a) liposome, (b) giant unilamellar vesicle (GUV), (c) black lipid membrane (BLM)formed across a pore, and (d) solid supported lipid bilayer (SSLB).	18
1.10	Schematic illustration of DIB formation procedure. (A) and (B) shows lipid-in (lipids placed in water) and lipid-out (lipids placed in organic solvent) methods to form monolayers on aqueous droplets (C). After incubating for appropriate time period, droplets are brought into contact to form a DIB (D).	20
1.11	A simple schematic (a), select few applications of DIB (b-e) and usage of digital microfluidics to form multiple DIBs (f). Images reproduced from previously published works. Refer text for appropriate citations.	22

1.12	(a) Schematic showing a lipid bilayer placed within the short working distance offered by high-resolution microscopes. (b) One of the few existing methods to form horizontal bilayers within this working distance. Image reproduced from Bartsch et al.[4] (c) Droplet hydrogel bilayer (DHB) - image reproduced from Gross et al.[5]	28
2.1	IFT measurement setup using a pendant drop tensiometer: (A) inverse oil drop formed at the tip of the needle placed under aqueous bulk, (B) pendant drop of water under oil bulk. (C) IFT data measured with pendant drop and inverse pendant drop approach for both DPhPC-in and DPhPC-out cases are compared.	36
2.2	A droplet interface bilayer with an equivalent electrical circuit.	38
2.3	Electrical characterization. (A) shows the input triangular voltage to measure the membrane capacitance shown in (B). (C) shows a sample plot of current versus voltage that is used to calculate membrane resistance.	40
2.4	Specific capacitance measurement procedure.	42
2.5	Schematics showing steps involved in printing and developing parts that are fabricated using Nanoscribe direct laser writing.	44
2.6	Schematics showing the steps involved in development of PDMS chip for microfluidics.	45
2.7	Schematic showing plasma oxidation and assembly steps involved to develop a microfluidic chip containing 3D printed scaffold in its liquid chamber.	46
3.1	Interfacial tension versus time measured at an oil-water interface containing 2mg/ml of either DPhPC or DOPC lipids placed in the aqueous buffer or hexadecane.	49

3.2	Interfacial tension versus time for: (a) 2, 0.2, and 0.002 mg/ml DPhPC-in concentrations; and (b) 10, 2, 0.2, 0.02 and 0.002 mg/ml DPhPC-out concentrations; (c) 4 different old DPhPC-out concentrations; (d) fresh DPhPC-out, hydrated DPhPC-out, fresh DOPC-out, and hydrated DOPC-out.	50
3.3	Interfacial tension versus time: (a) 2mg/ml DPhPC-out with and without stirring; and (b) 2mg/ml DOPC-out with and without stirring the lipid-out solution for a 1 μ l droplet. Arrows mark the beginning of 30 s periods of stirring.	51
3.4	Current-voltage curves for DPhPC and DOPC (a) lipid-in; (b) lipid-out. Slopes are plotted between -75 mV and 75 mV to calculate resistance of the bilayers (inverse of slopes).	54
3.5	DPhPC and DOPC lipid assembly free energy curves as a function of the distance from the pristine OW interface. (a) & (c) shows free energy curves for DPhPC and DOPC micelle (lipid-in), respectively; (b) & (d) shows free energy curves for DPhPC and DOPC inverse micelle (lipid-out), respectively.	55
3.6	Free energy curves for (a) DPhPC-in micelles, (b) DPhPC-out inverse micelles, (c) DOPC-out inverse micelles, and (d) DPhPC-out swollen inverse micelles w.r.t. the distance from the OW interface with different packing density monolayers.	56
3.7	DLS measurements showing size distribution in terms of scattering intensity for a a) fresh DPhPC-out sample, b) 10-day old DPhPC-out sample, and c) hydrated "swollen" DPhPC-out sample, d) fresh DPhPC-in liposome sample, and e) 10-day old DPhPC-in sample. . .	57
3.8	Estimated lipid flux rate versus time for a) DPhPC-in and DPhPC-out, b) DOPC-in and DOPC-out, c) DPhPC-in and DOPC-in, and d) DPhPC-out and DOPC-out at 2mg/ml concentration. Note: Only non-zero values are plotted.	62

3.9	Estimated lipid flux rate versus surface pressure for, a) DPhPC-in and DPhPC-out, b) DOPC-in and DOPC-out, c) DPhPC-in and DOPC-in, and d) DPhPC-out and DOPC-out at 2mg/ml concentration. Note: Only non-zero values are plotted.	63
3.10	Schematic representation of lipid self-assembly at an oil-water interface following rupture mechanism (a: lipid-in, c: lipid-out) and extraction mechanism (b: lipid-in, d: lipid-out). Schematic (d) depicts the swollen inverse micelles through uptake of water.	66
3.11	DPhPC-in surface pressure data and calculated fit using equation 5 for, a) the entire length of data with a single mk_a , and b) estimating mk_a values for 4s segments. Inset: A zoomed-in view of the same plot to show the short 4s data segments and its fit. c) Comparison of experimental surface pressure and back-calculated surface pressure from the model for DPhPC-in at 2 mg/ml.	71
4.1	Schematic illustrating the steps involved in conventional procedure (a, b) and in proposed procedure (a, c and d) to form a DIB.	76
4.2	Representative data showing change in IFT due to spontaneous assembly of DOPC monolayer (blue; fixed-volume mode) and step-wise reduction in volume (red).	77
4.3	Change in interfacial tension with time measured using fixed-volume pendant drop tensiometer.	80
4.4	Representative IFT traces showing change in tension (blue) induced by step-wise reduction in droplet volume (red) for DPhPC (a), DOPC (b) and POPC (c). Change in IFT w.r.t. droplet volume for data shown in (a-c) is plotted in (d).	81
4.5	Change in IFT induced by step-wise volume change for multiple trials of DOPC (a) and POPC (b) monolayers. Dotted lines in the figure are only for guiding the eye.	81

4.6	Compression isotherm (a) and inverse compressibility modulus (b) for DPhPC (blue solid line), DOPC (red dotted line) and POPC (yellow dashed line). Each curve is average of 3 or more measurements. Black horizontal dashed line corresponds to the bilayer-monolayer equivalence pressure of 40 mN/m.	83
4.7	Sketch showing organization of DPhPC (a), DOPC (b) and POPC (c) molecules and hexadecane molecules in a monolayer formed at a hexadecane-water interface before and after compression. The chemical structures of lipids are provided in inset with arrows pointing at the double-bonds found in the fatty acid chains.	88
4.8	Compression isotherms indicating collapse pressures (shaded circles) and estimated pressure corresponding to spontaneously assembled monolayer (unshaded circles).	89
4.9	Comparing percentage change in Volume, Surface Area and Radius of 300 nl droplet.	90
5.1	Procedure for assembling a single DIB using: A) the liquid-in-liquid method, and B) the liquid-in-gel method. Note: electrodes not shown for clarity.	95
5.2	Schematic of experimental setup for durability test.	96
5.3	Loss modulus (A), storage modulus (B), and complex viscosity (C) of 10 mg/ml SEBS/hexadecane mixture plotted with respect to angular frequencies at various temperatures (25-55°C). A dog-bone shaped specimen made from 50 mg/ml SEBS/hexadecane shows flexibility and shape retaining property of the organogel (D).	98
5.4	Micrographs of a DIB formed in molten 10mg/ml SEBS-gel (A) and cooled to room temperature (B). Scale bar represents 500 μm	100

5.5	Change in nominal bilayer capacitance and temperature with time as a DIB formed in SEBS-gel is cooled (A) and heated (C). Change in capacitance of the same bilayers plotted w.r.t. temperature as the system is cooled (B) and heated (D).	101
5.6	Electrical resistances of A) liquid-in-liquid, B) Liquid-in-gel (20°C), and C) Liquid-in-molten gel (50°C) are calculated by finding the slope of the current versus voltage plot.	104
5.7	Electrowetting behavior of DIB SEBS-gel and liquid-in-liquid DIB at RT (blue) and 50°C (red); the increase in capacitance of bilayer with applied voltage is plotted according Equation 1 (A). (B) Bright-field microscopic images of a single DIB at 0 and 150 mV applied voltage in molten and gelled SEBS.	105
5.8	Appearance of hexadecane-filled gap between the droplet phase and SEBS-gel phase due to the evaporation of droplet phase.	107
5.9	Single-channel alamethicin recording at +175 mV applied voltage at room temperature (A-C). (D) Histogram of conductance levels corresponding to trace in A. Normalized conductance ratios with respect to the first conductance level are found to be 1:2 (1st to 2nd level), 1:4 (1st to 3rd), 1:5 (1st to 4th) & 1:9 (1st to 5th).	109
5.10	Electrical activity of Alamethicin at +175 mV applied voltage at 50°C (A) & (B). C) The histogram of conductance levels corresponding to the trace shown in (A).	109
5.11	Measured values of applied acceleration that triggered bilayer failure for liquid-in-liquid and liquid-in-gel DIBs, plotted with respect to excitation frequency (A). Bar graph comparing the average accelerations at failure across all frequencies (n = 14; left), and at 50 & 60 Hz (n ≥ 4; right) (B). Error bars represent ± one standard deviation.	111

5.12	DIB formed in 40% hexadecane-paraffin wax at 50°C (A) and cooled to room temperature (B). A wax-encapsulated DIB formed at the tip of two hanging electrodes held in air (C). Shrinkage of paraffin upon solidification causes bilayer size reduction or rupture.	114
5.13	Demonstrating the portability and improved handling of SEBS-encapsulated DIBs: A) DIB formed on a flexible, open substrate, and B) DIB submerged under water testifying physical shielding from environment. C) Application of indirect force to perturb the DIB.	115
6.1	3D models of various designs tested in this Chapter (a-c). (a) and (b) shows the Design style 1 (container-style scaffolds; for bilayer with two different aqueous volumes) while (c) shows the Design type 2 (ring-type; for bilayer surrounded with single aqueous volume). (d) shows a microfluidic chip containing a 3D printed scaffold placed in its liquid chamber.	118
6.2	Procedure showing sequentially dispensing different solutions using a pipette.	120
6.3	(a) Front view of the fully assembled microfluidic chip enclosing the 3D printed scaffold. Red box shows the zoomed-in view of the printed scaffold placed in the liquid chamber. (b-d) show the experimental procedure to assemble a lipid bilayer. First, aqueous solution 1 is filled in the liquid chamber and in the micro-wells of scaffold (b). Following this, lipid/alkane solution is passed through the chamber (c). This displaces the aqueous solution 1 from the chamber leaving behind the volume filled in the micro-well. A lipid monolayer is formed at the water-oil interface on top of the micro-well. Finally, aqueous solution 2 is passed through to replace the lipid/alkane and form a bilayer at the opening of the micro-well (d).	122

6.4	Brightfield microscopic images of cube-scaffolds shown in Figure 6.1(a) (Design 1.a). (a) Image of an empty substrate and (b) shows scaffolds partially filled with aq. solution 1 and the chamber filled with aq. solution 2, separated by a layer of lipid/alkane. The dark circles seen on top of the cubes in inset are expected to be lipid bilayers.	123
6.5	Fluorescent images showing CF-filled micro-wells (a), and a possible lipid bilayer assembled on top of a micro-well (b). Inset shows a zoomed-in, contrast-adjusted image of (b). (c) shows the same scaffold without the trapped CF found in (b). 3D view of design 1.b is shown in Figure 6.1(b).	124
6.6	Brightfield (a, b) and phase contrast (c) microscopic images showing printed ring-type scaffolds. (Design 2 in Figure 6.1(c))	125
7.1	Summary of scientific gaps and contributions.	128
B.1	Values of left hand side of Equation 3 plotted versus time for DPhPC-in and DOPC-in.	168
C.1	Rate of evaporation of DI water droplet held close to Hexadecane-Air interface. Volumes are estimated from droplet diameter by assuming a spherical droplet. Droplet diameter is measured using MATLAB image processing.	169

Chapter 1

Introduction and Literature Review

1.1 Introduction

Biomimetics is the imitation of structural and/or functional concepts and models found in nature to create physical models and engineering designs that are useful for scientific and technological advancement. Humans have gained inspiration from nature for numerous different applications; invention of trains from caterpillars, flights from birds, and artificial photosynthesis from plants, to name a few. Other biomimetic approaches involve developing structures and materials that mimic what is found in nature in a microscopic and submicroscopic scale. For instance, numerous superhydrophobic surfaces have been developed by structurally imitating the nanoscale structures that are found on a lotus leaf. Such an approach to structurally and functionally mimic the complex natural systems also enables us to better understand the system and probe them in ways that is often tedious if not impossible to perform in their native state. One such structure that scientists have been interested in for nearly a century is lipid bilayer — a 5-10 nm thick membrane that surrounds a cell and many of its organelles. These membranes are made up of highly regulated lipids and numerous other biomolecules playing unique roles to support and orchestrate the nominal behavior of nearly all cells. For this reason,

the lipid membrane structure, organization and functions are being heavily studied to understand the various roles that they play using both live cells and biomimetic models.

This work seeks to further our understanding of lipid self-assembly and its behavior at a liquid-liquid interface to support and advance synthetic lipid bilayer systems, also referred to as model membrane, that can be used to study biologically relevant fields such as membrane biophysics, protein electrophysiology, and towards the development of synthetic biomolecules, drugs and nanoparticles for various applications. The findings from this work is also found to be useful in other fields which uses emulsions, such as paint, petroleum, food and drug industries. Specifically, attempts to understand the self-assembly kinetics and organization of phospholipids at an oil-water interface and to apply engineering concepts to fabricate stable synthetic lipid bilayers that are more biologically relevant, physically durable, portable and suitable for high resolution optical probing will be addressed here.

1.1.1 Phospholipids

Phospholipids are a class of lipids that form the major component of membranes found in living cells. These biomolecules are made up of a polar head group attached to non-polar tail groups through a glycerol, hence the term Glycerophospholipids (see Figure 1.1(a) & (b)). Because of this physically distinct molecular construct, with a hydrophilic (water-loving) polar end and a hydrophobic (water-fearing; or lipophilic: fat-loving) non-polar end, these molecules are also categorized as amphiphiles (loving both water and fat).[6]

Head Groups of Phospholipids

Based on the head group moiety attached to the glycerol, properties such as shape, hydrophilicity, packing, etc. varies significantly. Figure 1.1(c) shows 6 different phospholipids with identical tail groups (1,2-dipalmitoyl-) but distinct head groups

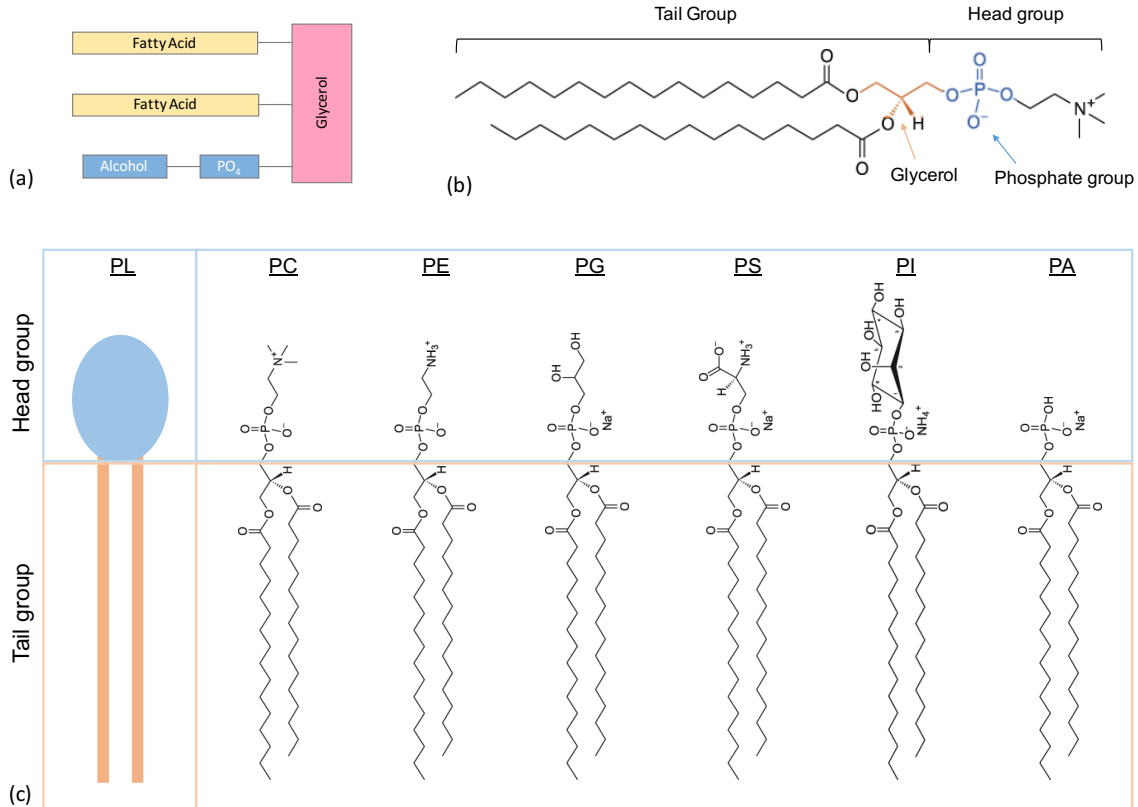


Figure 1.1: (a) Basic structure of Glycerophospholipids. (b) Chemical structure of DPPC molecule. (c) Schematic and chemical structure of phospholipids showing two distinct regions: hydrophilic head in blue box and hydrophobic tails in orange box. All lipids possess same 1,2-dipalmitoyl (DP) tail groups with different head groups: phosphatidylcholine (PC), phosphatidylethanolamine (PE), phosphatidylglycerol (PG), phosphatidylserine (PS), phosphatidylinositol (PI) and phosphatidic acid (PA).

that are commonly found in cell membranes. These head groups are named, phosphatidylcholine (PC), phosphatidylethanolamine (PE), phosphatidylglycerol (PG), phosphatidylserine (PS), phosphatidylinositol (PI) and phosphatidic acid (PA). While all head groups are negatively charged, PC and PE also possess positively charged amine, making them zwitterionic.

Tail Groups of Phospholipids

Tail groups of phospholipids can be made up of a wide range of non-polar chains that vary in length and complexity. Figure 1.2 shows few examples of different tail groups

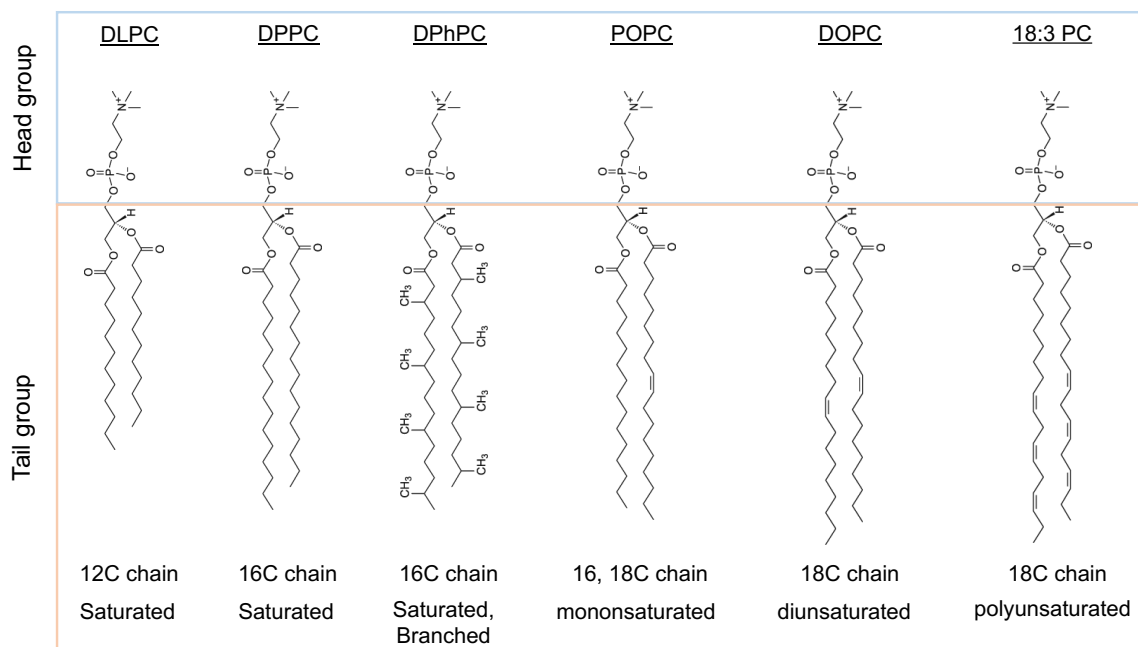


Figure 1.2: Chemical structure of phospholipids with identical head groups made up of phosphatidylcholine (PC) and distinct tail groups; DLPC (12C fatty acid chain), DPPC (16C fatty acid chain), DPhPC (12C fatty acid chain with 4-methyl groups attached to each tails), POPC (tail groups of different lengths: 16C & 18C, monounsaturated in 18C chain), DOPC (18C chains with 1 double-bond in each tail group), and 18C polyunsaturated tail groups.

(with identical head groups) found in membrane phospholipids. The length of lipid molecule varies based on the number of carbons present in the fatty acid. Fatty acid chains with 12C to 18C are commonly found in cell membranes. In general, lipids with longer fatty acid chains are found to have higher transition temperature.[7] These fatty acid groups can either be unbranched or branched with methyl groups. Fatty acid chains can also be saturated or unsaturated i.e., absence and presence of C-C double-bond in the chain groups, respectively. Based on the number of chains that possess unsaturations and the number of unsaturations in each chain, phospholipids are further classified as saturated, monounsaturated, diunsaturated and polyunsaturated phospholipids.

Shapes of Phospholipids

The innate shape of a phospholipid is determined based on the volume and shape of head group and tail group moieties attached to the glycerol backbone. For instance, inositol occupies more volume when compared to a simple phosphate and choline group, and thus, makes PI's has a larger head group than PA's and PC's. Similarly, number of tail groups, and their lengths, saturation level, and presence/absence of branches are found to affect the volume occupied by the tail groups. Presence of branches and unsaturations in the fatty acid chains increases the volume occupied by the lipid. Thus, the shape of the lipid molecule as a whole is defined by the combination of head and tail group sizes, and they broadly fall under three different shapes as shown in Figure 1.3(a-c). A lipid with a single fatty acid chain (e.g. lysophospholipid) and/or a large head group (e.g. polyphosphoinositide) are known to take an inverse conical shape. Conversely, a conical shape is realized by the lipids which have smaller head group than the tail groups (e.g. phosphatidylethanolamines and phosphatidic acid). Lastly, lipids which has comparably sized head group and tail groups occupy a cylindrical shape (e.g. phosphatidylcholines and phosphatidylserines).[8, 9]

1.1.2 Self-Assembly and Langmuir Monolayers

Because of the amphiphilic nature of phospholipid molecules, when mixed in solutions at a concentration above a threshold (critical micelle concentration, CMC), they self-assemble to form aggregates with well-defined structures. Figure 1.3(d-f) shows self-assembled structures that are spontaneously formed by lipids when placed in polar and non-polar solvents. In an aqueous solution to minimize the contact of non-polar hydrophobic tail groups with the polar water molecules, thus resulting in self-assembled structures such as micelles and vesicles (Figure 1.3(d & e)).[10-12] When placed in non-polar solvents such as alkanes, soybean oil, lipids self-assemble to form inverse micelles.[13-15] The type of self-assembled structure is determined

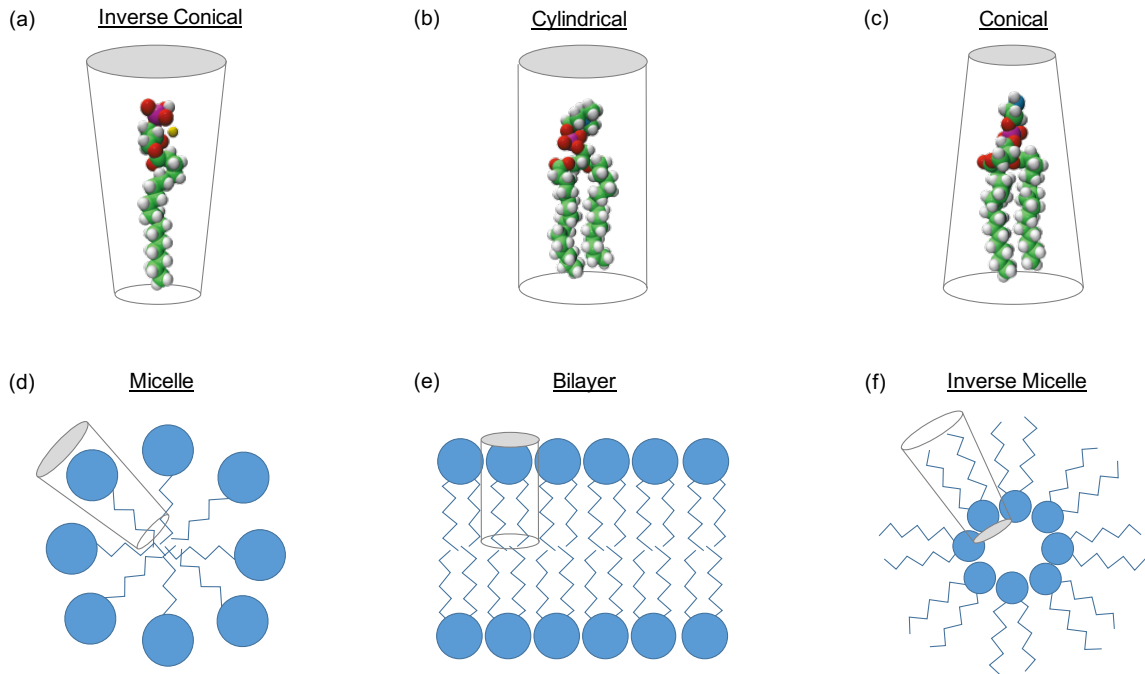


Figure 1.3: 3D structures showing different shapes of lipids (a-c) and their corresponding self-assembled structures (d-f). In solutions, conical shaped lysophospholipids self-assemble to form micelle structures, cylindrical shaped phosphatidylcholines form a bilayer and inverse conical shaped phosphatidylethanolamines form an inverse micelle.

by the factors including innate shape of lipids, temperature, hydrophile-lipophile balance (HLB), types of solvent and solutes.[10, 13] More interesting and useful self-assembly phenomena are found to take place when both polar and non-polar solvents are brought into the picture.[16–18]

Lipid molecules self-assemble at an air-water as well as oil-water interface to form a monolayer. Such monomolecular layer consisting of one or more types of surface active molecule at a liquid-air, liquid-liquid interface is known as Langmuir monolayer, named after Irving Langmuir. Like surfactants, lipids self-assembled at an air-water or oil-water interface reduces the surface tension of the interface.[19, 20] For instance, a pristine air-water interface has a surface tension of 72 mN/m at room temperature. When a phospholipid monolayer is spread at the same air-water interface, the tension can be reduced to <20 mN/m.[21, 22] A more drastic change is noticed at an oil-water

interface; the interfacial tension can be found to decrease from 44 mN/m to <2 mN/m with the addition of lipid monolayer.[23] The extent to which the surface/interfacial tension is reduced is determined largely by the packing density of the monolayer: in general, tighter packing leads to lower tension.[24]

This 2D coverage of amphiphilic biomolecules and the resulting reduction in tension are found to play vital roles in the nominal survival of individual cells to an entire organism. Lipid droplets that store fatty acids in the form of neutral lipids thereby protecting cells from lipotoxicity are covered with phospholipids monolayer that prevents it from fusing with nearby lipid droplets and other cellular organelles.[25] Lipid monolayer is found to play an essential role in the human respiratory system as well; the outer most layer of the lungs is covered with a highly regulated monolayer of lipids and pulmonary surfactant proteins to maintain low tension at the air-alveoli interface.[19]

1.1.3 Langmuir Compression Isotherm and Phases of Lipid Monolayer

Langmuir-Blodgett trough is a century old laboratory apparatus that is used to study the behavior of a monolayer that is spread on an air-water interface. The apparatus accurately measures the surface tension of the interface (using a Wilhelmy plate and an electrobalance) while laterally compressing the monolayer that is spread on the surface. With the knowledge of the number of surfactant molecules present in the monolayer (surface number density) and the surface pressure ($\Pi = \gamma_0 - \gamma$; γ_0 is the surface tension of pristine interface while γ is the surface tension with monolayer) of the interface, the area occupied by a single surfactant molecule can be estimated at varying extents of compression.[26] The results obtained from LB trough are often times plotted as surface pressure-area (Π - A) isotherm that reveals the 2D physical state of monolayer.

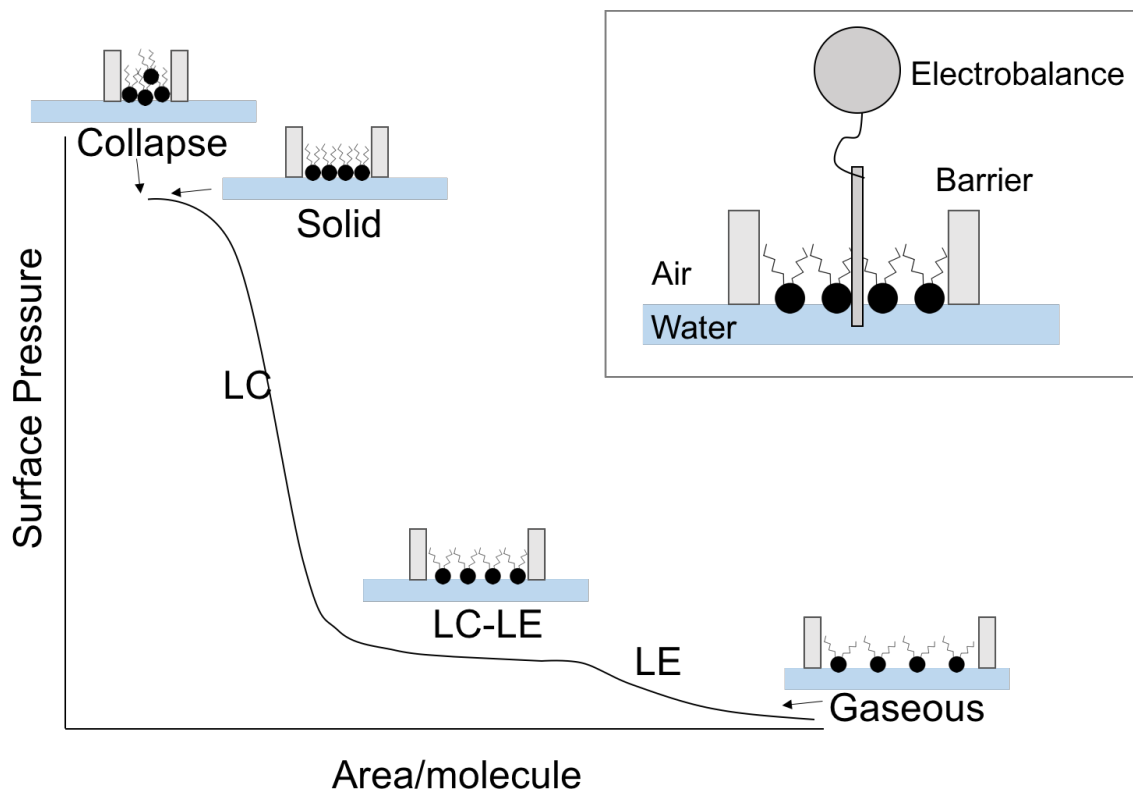


Figure 1.4: Surface pressure-area isotherm for a typical lipid monolayer showing various phases: gaseous, liquid-expanded (LE), liquid-condensed (LC), and solid. LC-LE marks LE and LC coexistence. Inset shows a schematic of a LB trough.

When a lipid monolayer that is spread on an air-water interface is dynamically compressed, the monolayer goes through various phases, namely: gaseous, liquid-expanded (LE), liquid-condensed (LC), and solid. In Figure 1.4, initially, the surface pressure is considered zero when no lipid is spread at the interface (IFT equals γ_0). As the lipid molecules are spread at a clean interface, the area occupied each lipid molecule is at its highest. As the barriers begin to move inward, the area occupied by the film decreases; reducing area available for each lipid changes the phase of lipid monolayer from gaseous (no interaction between neighboring lipid molecules) to LE/LC phase (lipids are close enough to interact with one another). As the monolayer is compressed further, the monolayer reaches a maximum packing state (a solid phase), beyond which, further compression will lead to collapse or buckling

of monolayer and exclusion of lipids in the subphase.[27] This phase is indicated by the maximum achievable surface pressure for the monolayer and is often called as the collapse or buckling pressure. Varying the composition, temperature and even the rate of compression is reported to have significant effects on this compression isotherm plots.[28–31] LB troughs are also being used in conjunction with optical techniques such as Brewster Angle Measurement (BAM), fluorescence correlation spectroscopy (FCS) and fluorescence recovery after photobleaching (FRAP) to study the diffusion behavior of lipids and other biomolecules in a monolayer at various compression states and temperatures.[32–36]

Monolayer Phase and Biology

In biology, the phase in which the monolayer exists is known to have drastic impact on its functional behavior, and therefore its composition is tightly regulated. For instance, the composition and the phase of lipid monolayer that forms the inner wall of lungs is found to play crucial roles in preventing the lungs from collapsing during our regular respiratory cycles.[28] Extensive body of literature can be found to utilize LB trough to characterize the dynamic behavior (changing packing density, lateral compression, reduction in tension, phase, etc.) of lung surfactant.[19, 28, 29, 37] Protein binding and insertion activity are found to be highly dependent on the packing density of lipids in the monolayer of lung alveoli and lipid droplets.[38–41] Such packing density dependent protein binding, insertion and activity are also seen at the plasma membrane and membranes of endoplasmic reticulum, lipid droplets. The innate shape of lipid is found to have an impact on the monolayer self-assembly too, which then alters different interfacial properties associated with it.[42, 43]

Despite the structural differences, understanding the behavior of lipid monolayer is also found to be useful in answering numerous questions regarding lipid bilayers. Because of the simplicity and usefulness of this experiment, monolayers (a half-bilayer) are often studied to understand the packing properties, lateral compressibility and behavior of a lipid bilayer. Especially, above a threshold surface pressure known as

bilayer-monolayer equivalence pressure (>40 mN/m), the monolayer spread on air-water interface is considered a close model to study lipid bilayers.[26]

1.1.4 Lipid Bilayer

As the name suggests, lipid bilayer is made up of two sheets of lipid monolayer held together by hydrophobic interactions between the tail groups.[44] Cells and several cell organelles such as mitochondria, endoplasmic reticulum, lysosomes, etc. are surrounded by a lipid bilayer membrane. In these membranes, lipids, along with other biomolecules such as cholesterol, carbohydrates and transmembrane proteins, acts as a functional unit that performs various tasks pertaining to the cell or organelle that it encompasses.[45] Figure 1.5 shows a graphical illustration of a cell membrane reproduced from a recently published article.[1] These 5-10 nm thick membranes, due to the hydrophobic region formed in between the two leaflets, act as a semipermeable barrier that is essential for nominal survival and functioning of a living cell; the highly regulated composition and structural makeup determines the chemical species that can be passively or actively transported across the membrane to support various cellular activities such as ingestion, excretion, communication, etc. In addition, various toxins and drugs are targeted to specific cell types based on the types of biomolecules that are expressed on these membranes.[46] For these reasons, lipid bilayers in live cells have been studied in detail for nearly a century.

Lipid Composition of bilayers

Cell membranes are made up of numerous different types of lipids that vary in size, shape, charge, etc.[47] Figure 1.6 shows the proportions of different lipids found in plasma membrane of *E. coli*, Sindbis virus, and membranes of rat liver endoplasmic reticulum and mitochondria. Phosphatidylethanolamines (PE) is the chief component of *E. coli* plasma membranes with nearly no phosphatidylcholines (PC) or cholesterol. On the other hand, PCs are a major component of eukaryotic membranes. Figure

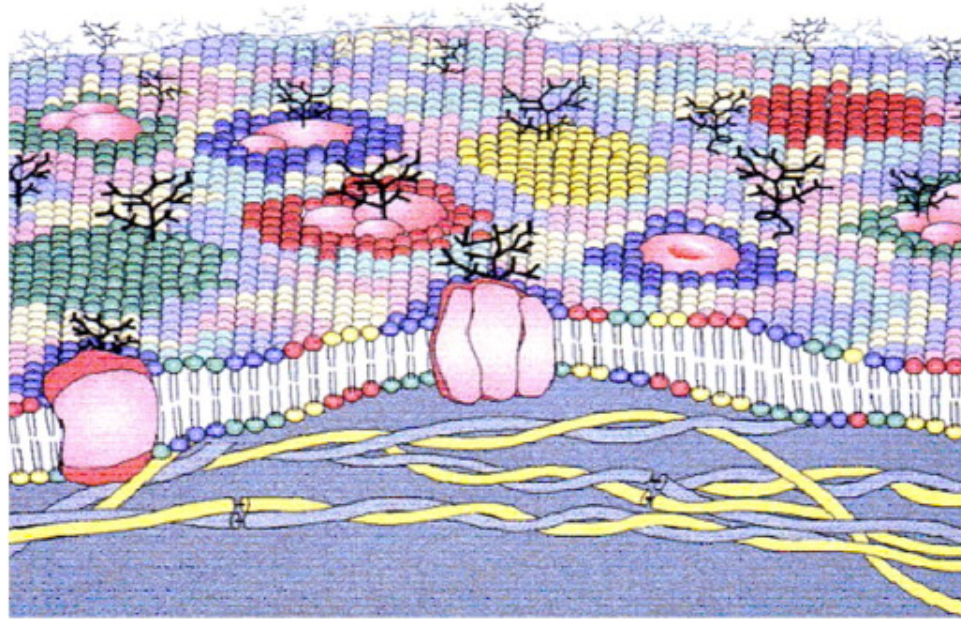


Figure 1.5: Cartoon of a lipid bilayer membrane reproduced from Escribá et al.[1]. Illustration shows different lipid types in different colors organized into microscopic domains with some domains carrying integral membrane proteins.

1.6(d) signifies the difference in membrane composition between the two leaflets of the same membrane. The outer leaflet of the mitochondrial membrane of rat liver cells is reported to have higher proportion of PCs and PIs when compared to the inner leaflet. Such differences in composition between the two leaflets of the same membrane is due to the differences in packing density caused by the curvature of the membrane.[2]

■ Cholesterol
 ■ PC
 ■ SPM
 ■ PE
 ■ PI
 ■ PS
 ■ PG
 ■ Other

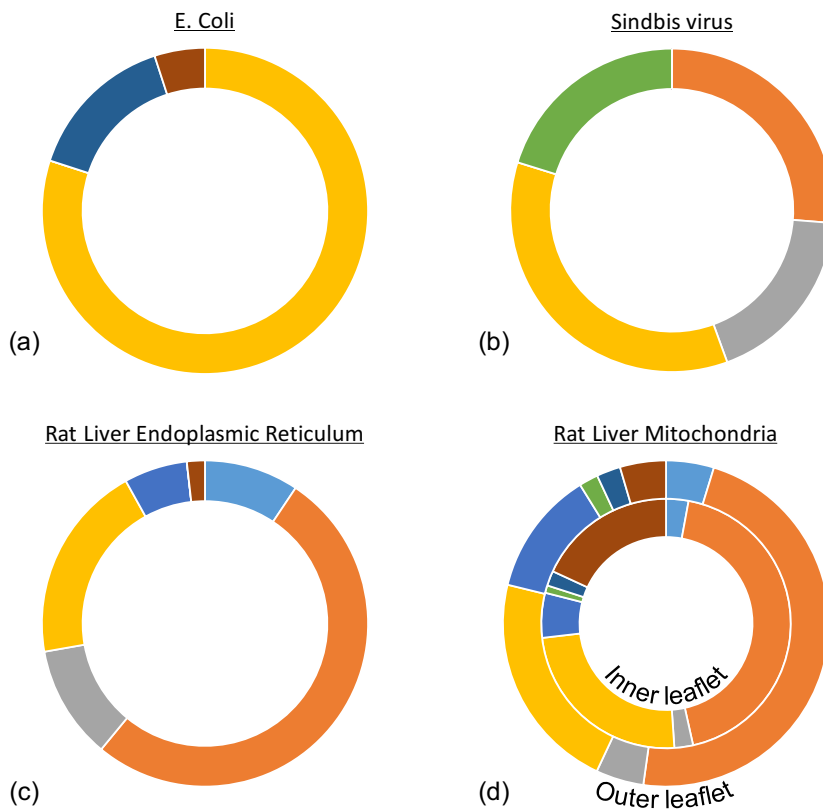


Figure 1.6: Lipid composition of biological membranes. Note: Charts represent the proportions of various lipids and not the spatial distribution in the membrane. Refer to Appendix (Table A1) for references and percentages; data taken from Yeagle et al.[2]

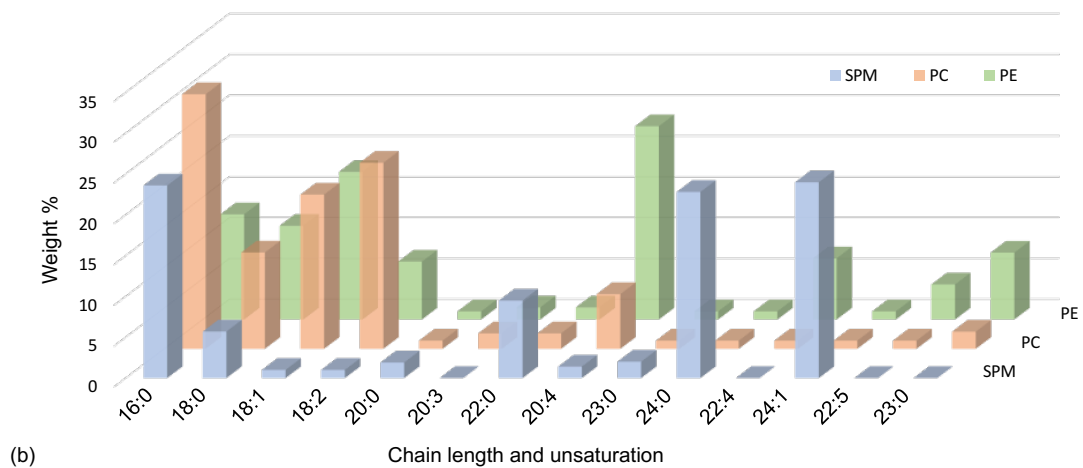
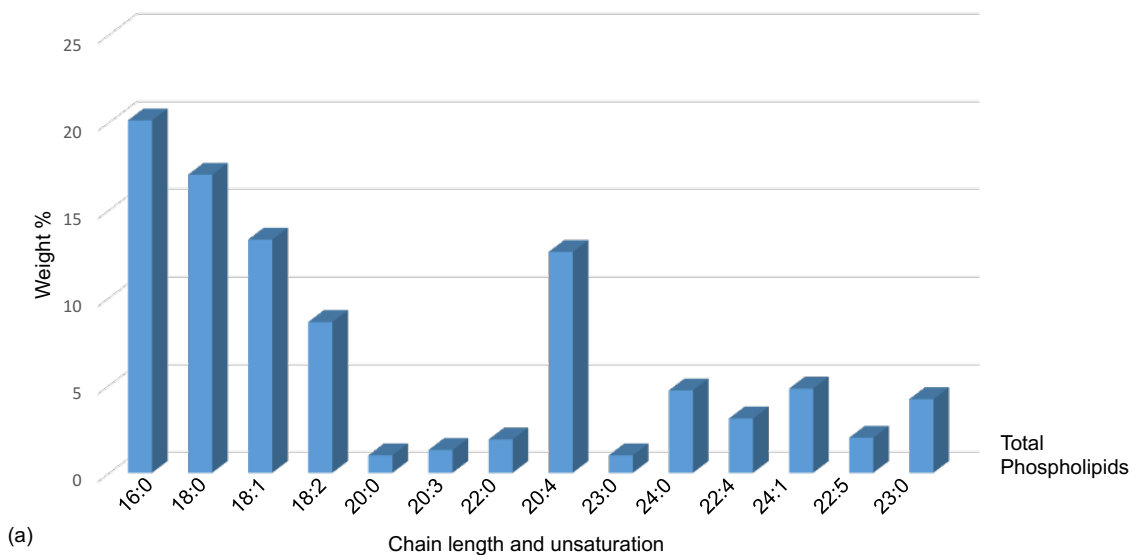


Figure 1.7: Fatty acid chain length and unsaturation of phospholipids found in human red blood cells. SPM: sphingomyelin, PC: phosphatidylcholine, PE: phosphatidylethanolamine. Refer to Appendix (Table A2) for references and percentages; data taken from Vance et al.[3]

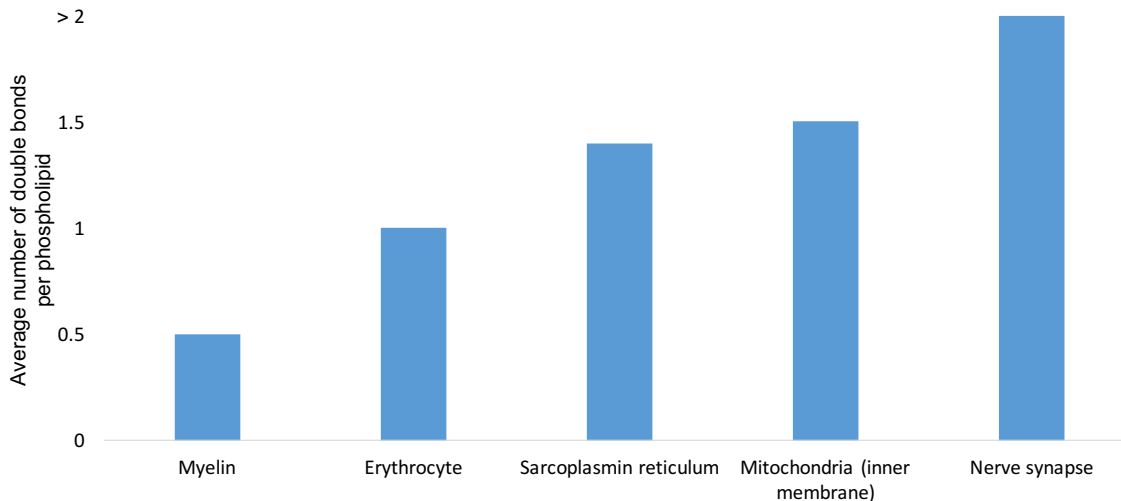


Figure 1.8: Double-bond composition of phospholipids in membranes. Data taken from Vance et al.[3]

As discussed in an earlier section, tail groups of lipids found in membranes can vary significantly. Figure 1.7 shows the proportions of different fatty acid chains present in human red blood cells. The tail groups can vary in both fatty acid chain length (16-carbon to 24-carbon) and number of double-bonds in each chain (0 to 5 double-bonds per chain). Figure 1.7(a) indicates that majority of tail groups has 16, 18 or 20 carbons with fewer number of phospholipids with larger (20-24C) chains. Figure 1.7(b) presents the chain length and unsaturation distribution for 3 major lipids types (SPM, PC and PE) found in human RBCs.[3] The presence of double-bonds brings a specific set of physical attributes to a membrane and thus, its role in nominal functioning of membrane cannot be ignored. Figure 1.8 shows the average number of double-bonds found per phospholipid in the membranes of different cells and cellular organelles.

Lipid Bilayer Properties

The composition of membranes determines its biophysically significant structural and functional properties. Each of the lipids mentioned above play unique roles

in regulating crucial properties of the membrane. Changing the lipid composition of these membranes can bring about changes in a variety of its properties. Membranes composed of lipids with saturated fatty acid chains are less fluidic due to the high van der Waals interaction between neighboring tail groups. On the other hand, presence of lipids with unsaturated fatty acid chains creates defects in the packing and decreases the tail-tail interaction between neighboring molecules and therefore, increases the membrane fluidity of the membrane. Membranes with high amount of unsaturated fatty acid chains remain fluid at lower temperatures when compared to that of saturated lipids. In animals, the membrane fluidity of a membrane is determined by the ratio between saturated and unsaturated lipids as well as by the amount of cholesterol, which increases the ordering and helps keep the membrane fluid at low temperatures while stabilizing the membrane at high temperatures.[48] This lateral packing-dependent physical property of the membrane is known to directly affect its permeability.[42, 49]

Similar to phases of lipid monolayer discussed in section 1.1.3, lipid bilayers too have distinct phases with significantly different properties. Based on temperature, a lipid bilayer can exist in one of two phases: gel phase at temperatures below and liquid phase at temperatures above the transition temperature (T_m) of the lipid.[50] In its gel phase ($T < T_m$), the lipids are highly ordered and are tightly-packed where the lipids are spatially constrained and their lateral diffusivity is found to be minimum.[51] As the temperature is increased, the bilayer transitions from a gel phase to a liquid phase, where the lipids can diffuse more freely (spatially less constrained) in the same leaflet or flip-flop between opposing leaflets of the bilayer. Various laboratory techniques such as Differential scanning calorimetry (DSC),[52, 53] Nuclear magnetic resonance (NMR),[54] X-ray [55, 56] and other techniques[57] have been used to characterize this temperature dependent behavior of lipid bilayers. Over the last few decades, these techniques have been used to precisely determine the transition temperatures of nearly all lipids. Other techniques such as TIRF, FCS and FRAP have been used to measure the diffusion coefficient of lipids in different phases. Such

techniques reveal that lateral diffusion of lipids in a gel phase is measured to be 10^{-11} cm²/s whereas 10^{-8} cm²/s for liquid phase.[51] This seemingly insignificant and microscopic, in-plane diffusion of lipid molecules play a huge role in dynamic lateral organization of lipids in cell membrane and are necessary for the formation microdomains called lipid rafts, which are often the binding sites for proteins and viruses.[58, 59]

While the presence of a lipid-based membrane was confirmed in 19th century, the structural make-up was confirmed by H. Fricke only in 1924. An abundant body of literature exists as a result of numerous researchers attempting to understand various different aspects of lipid bilayers for nearly a century.[46] However, we are yet to come to a complete understanding of the behavior of lipid bilayers and the various roles each biomolecule play in various aspects of a living cell. Scientists are still uncovering new information with the usage of advanced and more powerful scientific methods and tools that are made available by advancements in engineering. Among these scientific methods that can be used to understand the behavior of lipid bilayer is usage of an artificially assembled mimic of lipid bilayers called model membranes.

1.1.5 Model Membranes

Lipid bilayers, along with several other biomolecules, perform a variety of important functions in each and every cell. Replicating lipid bilayer structures in laboratory would allow researchers to investigate deeper into the various processes individually and collectively, with higher degrees of freedom in terms of controlling the relevant composition and conditions. Such structures that are created using laboratory techniques in order to structurally and functionally mimic the lipid bilayers found in living cells using natural or synthetic lipids are called model membranes. Table 1.1 lists some of the commonly used techniques to assemble model membranes that are either planar (e.g. black lipid membranes; BLMs) or non-planar (e.g. giant unilamellar vesicles; GUVs). Schematics of these model membranes are shown in

Figure 1.9. Each of these techniques has its own set of advantages and disadvantages. For instance, while GUVs are suitable for high resolution microscopy and calorimetric techniques, they do not offer easy control on altering lipid or aqueous volume compositions.[60, 61] Liposomes - a spherical lipid bilayer with an enclosed aqueous volume, are being used both in research as well as in clinical applications as a drug carrier.[62]

Planar bilayers such as BLMs, on the other hand, are highly convenient for performing electrophysiological experiments that are typically tedious to perform on a live cell.[63, 64] One of the earliest techniques to assemble planar membranes involved painting a lipid containing oil solution across a pore formed in a hydrophobic partition (often made of Teflon) placed between two aqueous volumes.[65] A bilayer is formed spanning this pore as the oil gets spontaneously excluded to bring the opposing monolayers closer. This half-a-century old technique first demonstrated by Mueller is commonly referred to as "painted" bilayers or black lipid membranes (BLM) because of its dark visual appearance in reflected light. A modified method to assemble a BLM involves "folding" two monolayers that were pre-assembled at an air-water interface.[66] Over the last few decades, several modified experimental setups and methods have been proposed by researchers to broaden the application of BLMs in various fields.[67]

Table 1.1: Techniques to assemble model membranes

Technique	Procedure	Type	Electro phys.	Optical Access	Asymmetry	Notable Advantages	Disadvantages
Liposome	Extrusion or sonication	Non-planar	No	No	Yes; Difficult.	Easy to prepare. High stability.	Too small for microscopy
Giant unilamellar vesicle (GUV)	Electroformation, centrifugation, or jetting through BLM	Non-planar	No	Yes	Yes. Difficult.	High biological relevance.	Fragile, tedious procedure.
Black lipid membrane (BLM)	Painting/folding	Planar	Yes	No	Yes	Asymmetric bilayers	Limited life time (<1 hour), residual solvent
Solid supported lipid bilayer (SSLB)	Langmuir-Blodgett technique/vesicle fusion	Planar	No	Yes	Yes	High stability and life time	Substrate affects diffusion properties of bilayer
Droplet interface bilayer (DIB)	Connecting lipid-coated aqueous droplets under a suitable solvent	Planar	Yes	No	Yes	Simple setup, scalability, ability to form networks	Not ideal for optical techniques, residual solvent

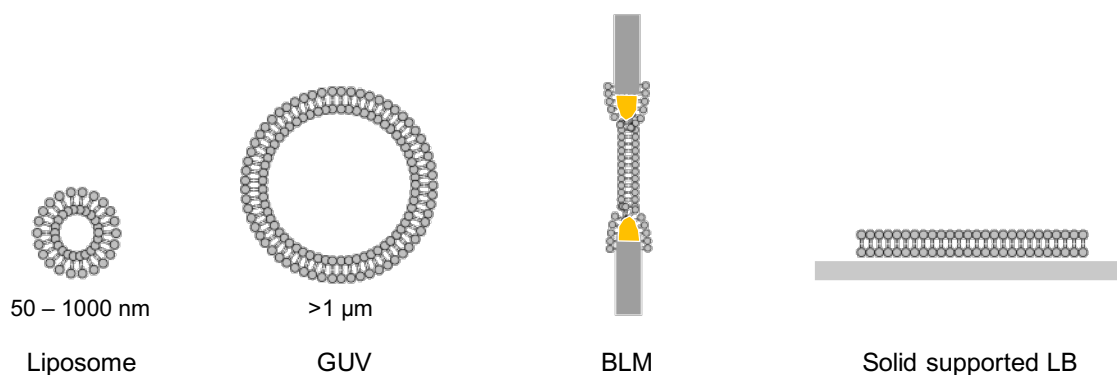


Figure 1.9: (a) Schematic illustration of model membranes: (a) liposome, (b) giant unilamellar vesicle (GUV), (c) black lipid membrane (BLM) formed across a pore, and (d) solid supported lipid bilayer (SSLB).

Solid supported lipid bilayer (SSLBs) is another type of planar bilayer that are typically formed on solid supports such as glass, mica, silicon wafer, etc.[68, 69] SSLBs are widely useful as they offer highly stable bilayers that can be patterned on solid substrates. Another compelling advantage of SSLBs, over vertical BLMs is the ability to visualize and perform high resolution optical microscopic techniques such as single-particle tracking, total internal reflection fluorescence (TIRF), Förster resonance energy transfer (FRET), fluorescence correlation spectroscopy (FCS).[69, 70] Such optical techniques performed on model membranes have revealed several useful information regarding the physical state and behavior of lipid bilayers under different conditions. However, studies have shown that behavior of lipids and other biomolecules in SSLBs can be altered by the solid support that is in direct or indirect contact with one leaflet of the bilayer.[71–75]

An alternate technique to achieve a planar bilayer free of direct solid support is called suspended lipid bilayers (SLB). Similar to BLMs, suspended bilayers are formed across a pore in a hydrophobic material. The difference between BLMs and suspended being the orientation of the bilayer: suspended bilayers are perpendicular to the direction of view from an inverse microscope while BLMs are parallel to the direction of view. Several different designs and methods to assemble suspended bilayers have been demonstrated.[76, 77] Many of these designs include electrodes embedded in the substrates, thus allowing for simultaneous electrical and optical probing of BLMs that enables the *in vitro* study of functional properties of biomolecules such as gating responses of ion channels while visualizing the bilayer.[4, 77, 78] Advances in microfabrication and microfluidic techniques have enabled automated formation of arrays of BLMs on a single substrate, thereby increasing the throughput of experiments performed.[79, 80]

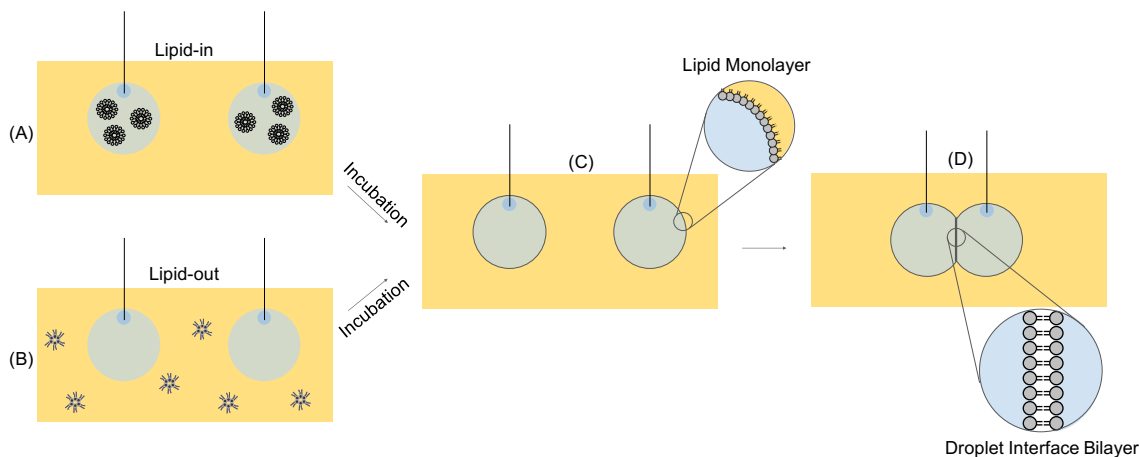


Figure 1.10: Schematic illustration of DIB formation procedure. (A) and (B) shows lipid-in (lipids placed in water) and lipid-out (lipids placed in organic solvent) methods to form monolayers on aqueous droplets (C). After incubating for appropriate time period, droplets are brought into contact to form a DIB (D).

1.2 Background and Literature Review

1.2.1 Droplet Interface Bilayers (DIB)

The droplet interface bilayer (DIB) is one of the newer techniques employed to construct planar lipid bilayers between two aqueous droplets (see Figure 1.10).[81, 82] When two or more lipid-coated water droplets are brought into contact under a suitable organic solvent, droplets spontaneously adhere to one another (instead of coalescing) to form a DIB. This adhesion process is driven by the interaction between the two opposing monolayers and the exclusion of solvent from the space between them. The energy of adhesion can be estimated by calculating the reduction in Gibbs free energy given by $\Delta F = 2\gamma_m(\cos\theta - 1)$, where θ is the contact angle between the droplets (see Figure 2.4) and γ_m is the monolayer tension. These DIBs are found to be stable for hours to days.[83, 84] The presence of aqueous solutions on either side of the DIB allows for easy electrical access and enables electrical interrogation of proteins and peptides.

Since its innovation in 2006, DIB has been the basis for several innovative biomolecular material systems. Engineered applications of single- and multi-membrane DIB networks range from the development of electrical rectifier circuits,[85] energy conversion platforms,[86] 3D-printed tissues capable of mechanical actuation,[87] bioinspired sensors,[88] and for use in the study of selective transport of ions and molecules (see Figure 1.11).[89] A light sensing DIB network was also been demonstrated by using the light sensitive channel, bacteriorhodopsin.[86] The DIB platform has also been implemented for studying the electro-physical activation and characterization of various transmembrane peptides and proteins such as alamethicin and α -hemolysin.[90, 91] Recently, mechanical[92] and chemical activation[93] of MscL channels from *E. coli* were demonstrated by two independent groups using the DIB platform. These applications highlight several advantages of DIBs, including their easy assembly and rearrangement, the ability to control both droplet and bilayer compositions, and a wide-range working temperature.[94] Another unique advantage of the DIB technique is its scalability in number and scale: while a single DIB can be assembled between two droplets, multiple DIBs can be formed by connecting additional droplets in 2 and 3 dimensions to form complex networks.[95] DIBs can also be formed across a wide range of length scales, between droplets of micron- to millimeter-size; DIBs formed between droplets size ranging femtoliters to several microliters have been demonstrated by several researchers.[83, 96] Application of digital microfluidics to create multiple DIBs are also being heavily explored to maximize the throughput of experiments conducted using these bilayers.[97–100]

1.2.2 Monolayer formation: "Lipid-in" vs "Lipid-out"

A DIB is formed by connecting two lipid monolayer-coated aqueous droplets placed under a suitable oil. This technique hinges on the ability of lipids to spontaneously self-assemble to form a "well-packed" monolayer at an oil-water interface, as absence of or failure to achieve suitable monolayers will lead to droplet coalescence.

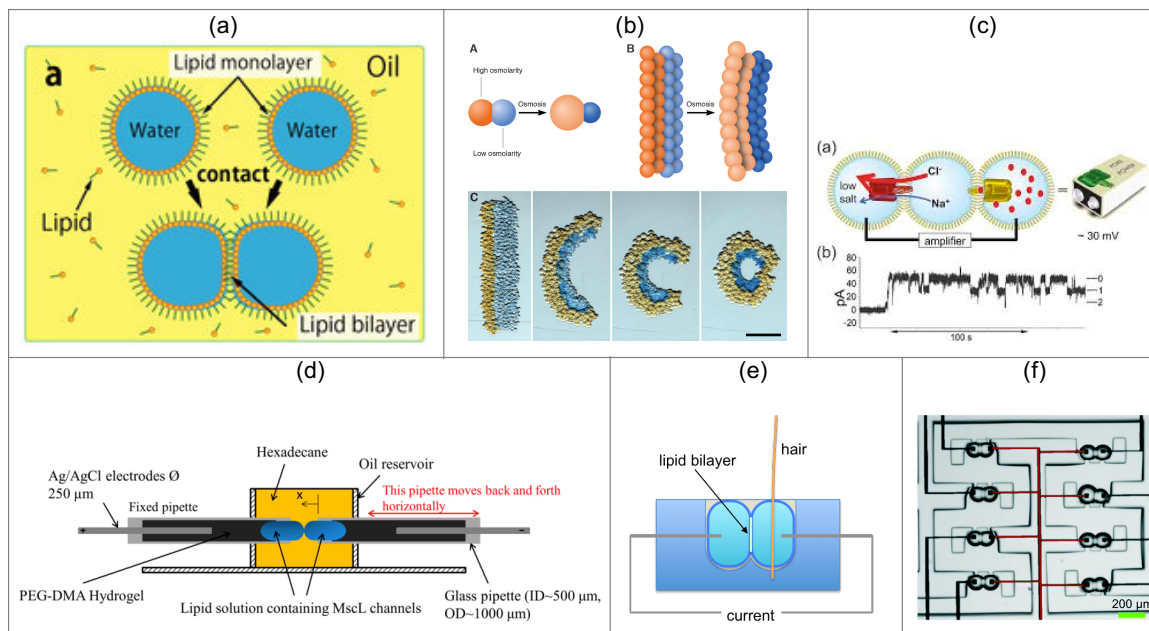


Figure 1.11: A simple schematic (a), select few applications of DIB (b-e) and usage of digital microfluidics to form multiple DIBs (f). Images reproduced from previously published works. Refer text for appropriate citations.

Monolayers can be formed using two different approaches, known as "*lipid-in*" and "*lipid-out*", that differ in the placement of phospholipids in the multiphase system (see Figure 1.10(a & b)). Phospholipids are incorporated as liposomes into the aqueous droplets in the lipid-in approach, while, in the lipid-out technique, phospholipids are dispersed in the external oil phase in the form of inverse micelles. Both approaches seek to provide suitable conditions for assembling a lipid monolayer upon the diffusion and adsorption of lipids to the oil-water interface,[101, 102] yet each has specific advantages in assembling planar lipid bilayers. For instance, asymmetric lipid bilayers with different lipid compositions in each leaflet of the bilayer can be formed with lipid-in technique, but not with lipid-out technique in which a common lipid mixture is present in the oil surrounding all droplets.[82] On the other hand, the lipid-out technique offers simpler preparation of lipid solution since dispersing lipids in oil avoids the need for freeze-thaw, extrusion, or sonication steps necessary for liposome preparation. Also, a wider range of phospholipid types are known to dissolve in

alkanes than form liposomes, making the lipid-out technique amenable to more types of membranes, including complex mixtures.[24, 94, 101] Recent reports show that incorporation of saturated lipids into the oil phase allows for sufficient monolayer formation at room temperature, whereas it is required to heat droplets containing liposomes with the same lipid to a temperature above the gel-liquid phase transition of the saturated lipid to enable sufficient assembly.[24] The lipid-out method also helps to maintain a lipid-free environment within the aqueous droplets that can be used to eliminate lipid and protein exchange between liposomes and interfacial bilayers and permit a wider range of chemical species in the droplet that may otherwise degrade liposomes.

From a bilayer formation standpoint, there are other differences. For certain lipids such as DPhPC, Lipid-in aqueous droplets (200-500 nl) can be routinely connected within 5 minutes of placing them in the oil,[84, 94] unlike the lipid-out technique, in which 30 minutes or more is often required before the droplets can be brought into contact (see Table 1.2).[84, 103, 104] This time required between placing the aqueous droplets in oil and bringing them into contact during which the lipid monolayer assembles is called the *incubation time*. Insufficient incubation time, i.e. connecting droplets *too soon*, leads to droplet coalescence instead of bilayer formation. Especially in attempts to form DIBs with lipid-out technique that requires a longer incubation time, droplets tend to fail more often than to form a bilayer. In some cases, such as DPhPC placed in hexadecane (DPhPC/Hexadecane), the success rate of forming a DIB can be as low as 5%. This undesired behavior was attributed to a lack of "*well-packed*" monolayer. While other factors such as contaminants, mainly detergents, that maybe found in surrounding oil or aqueous droplets, degraded lipids, unclean or *sticky* substrates may all lead to droplet coalescence, the lower success rate of lipid-out DIBs was often attributed to poor and/or slow monolayer formation.

The self-assembly kinetics or the differences in phospholipid packing in the monolayer achieved from the lipid-in and lipid-out approaches have never been quantitatively characterized to identify why lipid-out approach is slower and less

Table 1.2: Key differences between lipid-in and lipid-out approach

	Property	Lipid-in	Lipid-out
Solution	Number of lipids that can be used	Low	High
	Solution preparation	Tedious	Simple
	Using saturated lipids	May require heating	Heating not required
	Lipid-protein interaction	High	Low
Bilayer	Incubation time required	Low (3-5min)	High (10-20min)
	DIB formation success rate	High	Low
	Bilayer stability	High	Low
	Electrical resistance and workable voltage range (rupture potential)	High	Low
	Bilayer asymmetry	Possible	Not possible

effective in promoting lipid organization than lipid-in approach. Abundant literature is available on stabilization of oil-in-water emulsion focusing on time required for self-assembly of surfactants such as sodium bis (2-ethylhexyl) sulfosuccinate (AOT) and sodium dodecyl sulfate (SDS) to reach a level of packing density that averts droplet fusion.[20, 105, 106] Few studies focusing on the interfacial self-assembly of natural surfactants has also been published.[107, 108] Several works focusing on the spreading kinetics of liposomes to form a monolayer at air-water interface are found in the literature. [109–112] These studies focus on determining the factors affecting the rate at which monolayer forms and have theorized possible mechanisms in which lipids from bulk adsorb to form a monolayer. Lipid packing in a monolayer formed at an oil-water interface has been explored by few researchers. [113–115] However, very few studies have been performed in regards to water-in-oil emulsions focusing specifically on the kinetics of phospholipid self-assembly for DIB formation.[116]

1.2.3 Membrane Composition in DIBs

As discussed in section 1.1.4, native cell membranes are made up of several types of lipids that vary in head group, tail group, number of unsaturations, charge, etc. The structural and functional properties of membrane-associated proteins and peptides

can differ based on the nature of lipids that is surrounding them. For example, lipid head group's charge is known to significantly affect the insertion of pHLIP's (pH low insertion peptide) into a model membrane.[117] While the significance of lipid composition influencing membrane-associated biomolecules are undeniable, DIB model membranes formed thus far, to a large extent, fail to represent the compositions and heterogeneity of natural lipids. Specifically, we observe that most DIB studies have only focused on the use of 1 lipid type. As identified by Taylor and Sarles, DPhPC - a lipid native to archaeal organisms, has predominantly been the lipid of choice for DIB research.[94] This noticeably high interest towards DPhPC-based DIB arise from the fact that DPhPC lipids quickly self-assemble to form well-packed monolayers and produce highly resistive and stable bilayers with high success rates.

The prevalence of using DPhPC versus other lipids (e.g. DOPC) in DIBs studies thus far may in fact point to difficulties in being able to obtain stable membranes from these types of lipids. Lack of published works using these lipids and experiments in our own lab support this hypothesis; we find that it is very difficult to assemble DIBs from unsaturated lipids such as DOPC and POPC. Recent advances in DIB platform has attempted to utilize E-coli and brain total lipid extracts, which are composed of both saturated and unsaturated lipids of varying lengths, to form stable bilayers by employing heat to induce monolayer formation.[94] Other efforts to form DIBs with unsaturated lipids involve creating lipid blends with different proportions of DPhPC.[104, 118, 119] Few other works have demonstrated the usage of surfactants such as SPAN80 and SDS to assemble and stabilize the bilayer formed with unsaturated lipids which typically fail to form DIBs.[120, 121] Nevertheless, formation of DIBs with pure unsaturated lipids, such as DOPC and POPC, that are highly relevant to eukaryotic cell membranes has been poorly explored.

1.2.4 Durability and Portability

Due to the fragile nature of synthetic lipid bilayers, DIB platform has largely been limited to laboratory usage. Researchers have made efforts to make DIBs more durable and portable by modifying the procedure, solution or bilayer composition, and substrate design. Jeong et al. demonstrated that mixing emulsion stabilizers such as SPAN 80 increases the bilayer stability.[120] While this approach was proven to form DIBs without affecting the functionality, the mechanical durability and portability of the bilayer is not improved. One of the first attempts to improve portability of DIB includes freezing the precursors (aqueous droplets placed in non-polar solvents) until use.[122, 123] This allows the DIB precursors to be stored for extended period of time and even to be transported. However, this approach does not allow portability after the bilayer is formed. Other attempts include modifying the substrate that holds the DIB assembly. Kawano et al. used a portable patch clamp amplifier (Tecella) along with an open-style droplet chambers with porous, parylene film separations to assemble DIBs in an outdoor environment. While they successfully demonstrated portability of the substrate and its ancillary system, the system cannot be moved after the bilayer is formed.[83] Sarles et al. fabricated a PMMA/PDMS embodiment with integrated electrodes that can hold a DIB. This method successfully improved the durability and portability of the bilayer assembly and allowed the users to move, shake and invert the substrate without rupturing the bilayer.[124] However, this design does not permit easy reconfiguration of droplet assembly after enclosing the content. Another successful demonstration of improving bilayer portability includes usage of hydrogels in place of aqueous droplets.[125] This system is qualitatively reported to have an improved durability and longevity; however, usage of hydrogel is known to affect diffusion behavior of biomolecules in the bilayer.[71, 72]

1.2.5 Horizontally-oriented Lipid Bilayers

High-resolution optical techniques such as FCS, TIRF and FRAP have been used extensively to study the biophysical properties of lipids and proteins in monolayers and bilayers. These techniques have been used to quantify various biologically relevant properties such as lateral diffusion, domain formation, and lipid-protein interaction using model membranes.[32–36, 126, 127] Several groups have demonstrated the usage of model membrane platforms that allow simultaneous recording of electrical and optical measurements.[4, 77, 78] Such platforms provide great advantage of simultaneously probing model membranes to obtain better understanding of pore forming proteins and peptides. However, usage of these high resolution optical techniques that use high magnification objective lenses reduces the working distances down to 100-200 μm (see Figure 1.12(a)).[128] That is, the model membrane must be positioned within 100-200 μm from the objective.

Because of the low working distance restriction posed by high-resolution microscopy, solid supported lipid bilayers (SSLBs) - a technique in which artificial lipid bilayers are placed within few 100 nm from the surface of substrate (as shown in Figure 1.9), are found to be the most suitable technique to assemble model membranes within this range.[69, 70, 129] Numerous works have been published over the last few decades demonstrating the applicability of SSLBs to study molecular level behaviors.[70] However, as one leaflet of the bilayer is in direct or indirectly (in case of tethered lipid bilayers) contact with a solid support, the behavior of lipids and other molecules are found to deviate significantly from that of live cells. Particularly, the lateral and transverse diffusion of lipids are greatly affected by the direct physical contact posed by solid surfaces used in SSLBs.[71–75]

Droplet hydrogel bilayer (DHB), a modified DIB technique in which an aqueous droplet with a lipid monolayer is connected to a thin layer of lipid monolayer-coated planar hydrogel that is spread on a glass surface, is another technique that is suitable for high-resolution microscopy (see Figure 1.12(c)).[130] Similar to

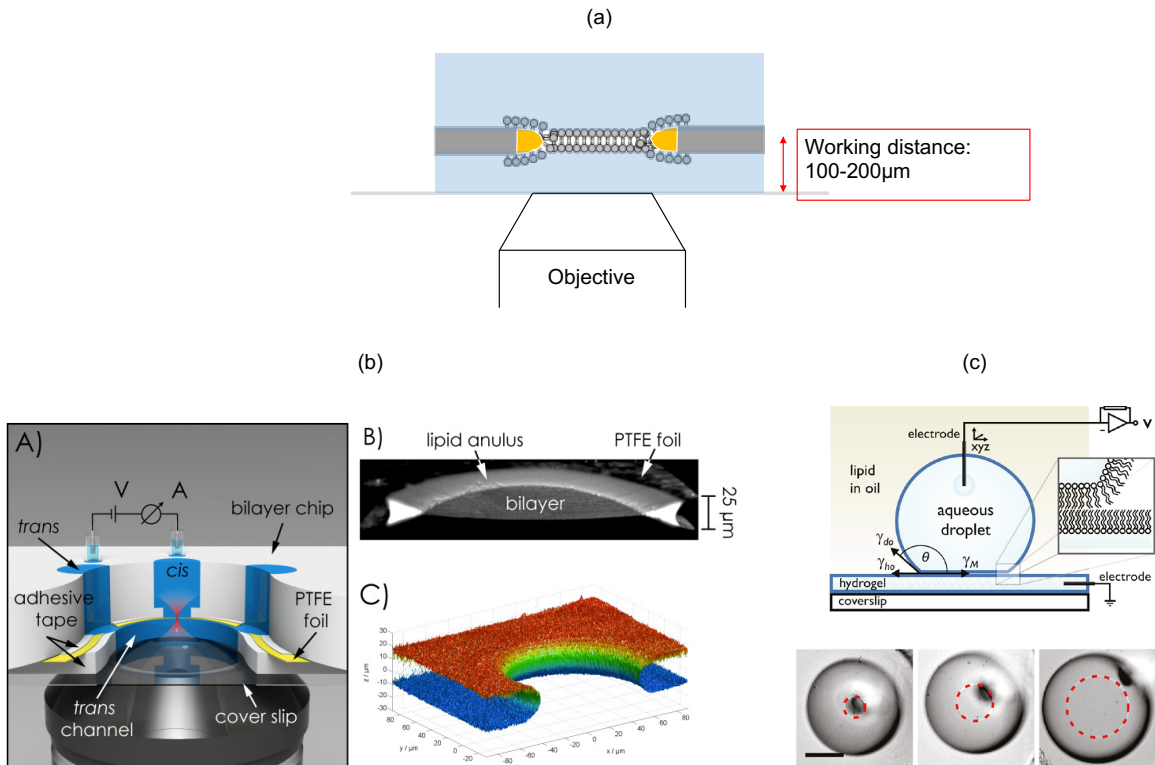


Figure 1.12: (a) Schematic showing a lipid bilayer placed within the short working distance offered by high-resolution microscopes. (b) One of the few existing methods to form horizontal bilayers within this working distance. Image reproduced from Bartsch et al.[4] (c) Droplet hydrogel bilayer (DHB) - image reproduced from Gross et al.[5]

DIB, DHB provides electrical access, simple experimental setup and procedure, easy reconfiguration (droplet composition, bilayer area, etc.) and ability to form networks. This capability has enabled researchers to accurately measure specific capacitance of bilayer[131] and application of high resolution optical techniques to simultaneously track electrical and optical behavior of single protein pore activities, and to directly measure diffusion coefficients of lipids and proteins in the bilayer has also been performed.[130, 132] However, similar to SSLBs, effect of underlying hydrogel on the properties of bilayer cannot be ignored.

Unlike SSLB and DHB, SLB technique forms a planar bilayer that spans across a microscopic pore without using a direct support that affects the diffusion properties

of the bilayer. When such a bilayer is oriented horizontally and positioned within the working distance, they form the ideal model membranes for high resolution microscopic studies. Various different designs have been proposed to assemble horizontal BLMs that are suspended using hydrophobic supports made up of Teflon, Parylene, plastics and other materials.[4, 77, 133–136] Microfabrication techniques have also been used to develop scaffolds with microscopic wells or nano-pores across which spans the model membrane.[76, 137–141] Lipid bilayers formed using these microfabricated chips have been found effective for using high-res. microscopic techniques such as FRET and other single particle tracking techniques.[142, 143] Simultaneous optical and electrical measurements have also been enabled using these microfabricated chips (see Figure 1.12(b)).[4, 137, 142] However, the major drawback with these devices is the tedious, and often, expensive fabrication procedure required to develop the chips. In addition, such complex fabrication process makes it hard to iterate on scaffold designs and dimensions. Thus, an easy-to-fabricate approach that enables the assembly of horizontally-oriented lipid bilayers within short-working distance is still needed in model membrane community.

1.3 Vision

Model membrane systems have been an eminent tool both for understanding biophysical behavior of biomolecules as well as for the development of novel membrane-based smart materials. Specifically, the attractive properties of DIBs such as scalability, high longevity and their ability to form networks and to be used for electrophysiological measurements have motivated several researchers to utilize this platform in the development of new types of multifunctional, membrane-based materials that employ the functionalities of a wide range of membrane-bound biomolecules for applications such as sensing, energy conversion, information and energy storage, monitor response and actuation. Therefore, this work aims to advance DIB platform by better understanding the fabrication process and by developing

novel methods to improve the quality of bilayers formed. Additional works performed towards fabricating new types of suspended lipid bilayers are also discussed here.

1.4 Scientific Gaps, Objectives and Research Plan

1.4.1 Scientific Gaps

The literature review provided above identifies several significant scientific gaps:

Gap 1: There is a lack of explanation for why lipid-in technique leads to higher DIB formation success rate than lipid-out. In addition, there is a lack of quantitative understanding of differences in self-assembly kinetics between lipid-in and lipid-out technique used for monolayer formation. Shedding light on kinetics of lipid monolayer formation and spatial organization of lipids in monolayer could provide answers to anecdotal observations regarding lipid placement and incubation time, and insights to improve DIB formation success rates.

Gap 2: There is a lack of quantitative explanation for why monolayers formed with unsaturated lipids are not suitable for DIB formation. Understanding the spatial organization of lipids at OW interface will help develop methods to enable DIB formation with a wider range of lipids.

Gap 3: Conventional DIBs are formed with two immiscible liquid phases placed in an open substrate, consequently making it prone to spillage, contamination and requires delicate handling with very limited portability. Thus, a convenient and robust DIB platform with an significantly improved durability and portability without compromising the basic functionalities of a lipid bilayer is still needed.

Gap 4: Currently existing methods to form horizontally-oriented suspended lipid bilayer suitable for high resolution microscopy is either tedious to fabricate or do not accurately represent membranes of living cells. Therefore, there is a need for a new

platform that will enable formation of horizontally-oriented lipid bilayers within the short 100-200 μm working distance of high-resolution microscope objectives.

1.4.2 Research Objectives

The following objectives attempts to address the scientific gaps mentioned above:

Objective 1 (*addressing Gap 1 & 2*). Use dynamic interfacial tension measurements to understand the differences in self-assembly kinetics and organization of phospholipids (DPhPC, DOPC and POPC) at an OW interface when placed in water versus hexadecane. Measuring the interfacial tension will help us answer a) why monolayer formation takes longer for lipid-out, b) why DIB formation success rate is lower for lipid-out when compared to lipid-in, and c) why unsaturated lipids have low or zero DIB formation success rates.

Objective 2 (*addressing Gap 1 & 2*). Develop methods to reduce incubation time and improve bilayer formation success rate for lipid-out technique. Develop an active-packing technique to achieve monolayers suitable for DIB formation using unsaturated lipids (DOPC and POPC).

Objective 3 (*addressing Gap 3*). Develop new methods to transform DIB, a lab-based technique, into a more portable and durable material system that is easier to handle without compromising membrane integrity, functionality or losing advantages of a conventional DIB system. This goal will be addressed by examining the usage of a polymer-based organogel to immobilize aqueous droplets in a DIB system in order to achieve the above-mentioned goals.

Objective 4 (*addressing Gap 4*). Construct and characterize 3D microscaffolds for supporting horizontally-oriented SLBs that are positioned within the short working distance offered by high resolution optical techniques. The proposed approach is

to use a Nanoscribe direct writing instrument to 3D print micro-scaffolds that can support lipid monolayers and bilayers within 100-200 μm from the objective.

1.5 Document Overview

This introductory chapter provided the inspiration and background information on lipid self-assembly, monolayer, bilayer and cellular membranes. Various techniques to assemble synthetic lipid bilayers were briefly listed with a special focus on droplet interface bilayer. Chapter 2 provides general methods describing all significant materials and procedures used in our works. Chapter 3 discusses our findings of differences in adsorption kinetics between lipid-in and lipid-out. Chapter 4 presents a new method to enable DIB formation using pure, unsaturated lipids. Chapter 5 presents a novel method to package DIB to make it more durable and portable. Chapter 6 provides results from our efforts to assemble lipid bilayers on 3D-printed microcaffolds. And lastly, Chapter 7 lists the overall conclusions and contributions from these research works.

Chapter 2

General Methods

2.1 Materials and Preparation

2.1.1 Lipid-in solution preparation.

To prepare lipid-in aqueous liposome solutions, lyophilized powder are suspended at a concentration of 2 mg/ml (2.4 mM) in an aqueous buffer (referred to simply as buffer) of 10 mM MOPS, 100 mM NaCl, pH 7 in deionized water (DI). This mixture is subjected to 4-5 freeze-thaw cycles to obtain multilamellar vesicles, and then extruded 11 times through a 100 nm-pore polycarbonate membrane (Avanti Polar Lipids) using an Avanti Mini-extruder or NanoSizer (T & T Scientific Corp.) to form unilamellar vesicles.[12] This solution is then diluted appropriately to achieve the required concentration.

2.1.2 Lipid-out solution preparation

To prepare lipid-out solutions of inverse micelles solutions in nonpolar solvent, lipid powder is dissolved in hexadecane ($C_{16}H_{34}$, 99%; Sigma Aldrich) at 10 mg/ml concentration and then diluted accordingly for further use. All the solutions are stored at room temperature. Hydrated lipid-out solutions are prepared by adding

1 μl of DI water into a vial containing 1 ml fresh lipid-out solution; this mixture is periodically vortexed. "Aged" lipid-out solutions are prepared by storing freshly prepared solutions at room temperature for 10 days prior to use.

2.1.3 Lipid-chloroform preparation for compression isotherm

For compression isotherm measurements, 1 mg/ml lipid solutions were prepared in chloroform according to the following procedure. 4 mL vials are pre-cleaned multiple times with chloroform and each vial is individually weighed until a stable weight is measured. Following this, appropriate amount of stock lipid-chloroform solution is added into each vial. After evaporating chloroform, vials containing lipid powder is weighed again to determine the accurate mass of lipid placed in each vial. Appropriate amount of chloroform is then added into each vial to make up 1 mg/ml solutions. Vials are immediately capped with septa caps (Thermo Scientific; Septa cap: Red PTFE/White Silicone) and are wrapped with parafilm for leak-proof seal. All compression isotherms measurements are performed within 24 hours of lipid/chloroform solutions preparation to ensure high accuracy of molecular area estimates.

2.1.4 SEBS-hexadecane organogel preparation

SEBS is purchased in powder form from Kraton (G-1650E; 10 kg mol⁻¹) and used without further purification. 10 mg ml⁻¹ (1 mM) SEBS/hexadecane solution is prepared in a glass beaker by mixing appropriate amounts of SEBS and hexadecane, followed by heating the mixture to 100°C until SEBS completely dissolves to produce a transparent solution. Following dissolution at 100°C, the mixture is cooled and stored for up to 3 weeks at room temperature (RT, 25 - 28°C). Molten organogel is obtained by reheating the organogel to 50°C.

2.2 Dynamic Light Scattering

Dynamic Light Scattering Measurement was performed using a 632.8 nm-wavelength Zetasizer (Malvern Instruments). A glass cuvette was filled with the sample solution and placed in the DLS machine. Appropriate refractive index (Water: 1.333; Hexadecane: 1.434) was used. All measurements were performed at room temperature.

2.3 Interfacial Characterization

2.3.1 Pendant Drop Tensiometer

A pendant drop tensiometer (Ramé-Hart Instrument Co. Model 590) and DROPImage Advanced software are used to measure the interfacial tension of an OW interface as described elsewhere. In this study, two very similar setups are used to measure interfacial tension for lipid-in and lipid-out cases at an OW interface. For lipid-out IFT measurements, a rectangular glass cuvette is filled with lipid-out solution and an aqueous pendant droplet is formed with buffer solution at the tip of a vertically oriented stainless steel, blunt needle as shown in Figure 2.1(b). For lipid-in measurements, the cuvette is filled with lipid-in solution and an inverted pendant droplet of oil is formed with pure hexadecane at the tip of a J-shaped, blunt needle as shown in Figure 2.1(a). This inverted configuration is incorporated because a hanging lipid-in pendant droplet consistently falls from the needle when the interfacial tension reduces below approximately 5 mN/m, making measurement of equilibrium tension impossible. Dynamic measurements of IFTs are found to be closely comparable between these two setups. In order to measure the equilibrium tension in both lipid-out and lipid-in cases, the droplet volume is maintained at 1 μ l (unless mentioned otherwise) so that the droplet does not detach from the needle. Consistent droplet size also enables direct comparison of the kinetics. All measurements are performed in constant-volume mode by using the dispenser's

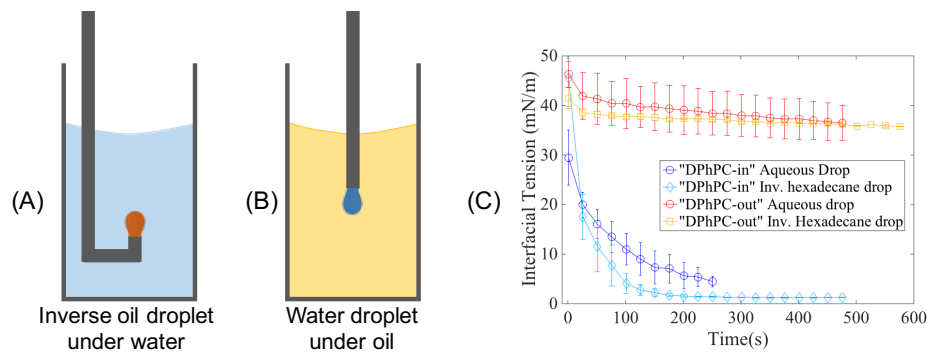


Figure 2.1: IFT measurement setup using a pendant drop tensiometer: (A) inverse oil drop formed at the tip of the needle placed under aqueous bulk, (B) pendant drop of water under oil bulk. (C) IFT data measured with pendant drop and inverse pendant drop approach for both DPhPC-in and DPhPC-out cases are compared.

feedback control feature. Measurements are taken at a rate of 60 samples per minute (1 Hz), and the IFT measurement is begun a few seconds before dispensing the droplet to enable recording of the complete dynamic change in interfacial tension. Prior to each measurement, the glass cuvettes are rinsed successively with isopropyl alcohol IPA and DI water and then dried in an oven at 80°C . About 3 ml of the bulk solution is then dispensed into the cuvette for a given test. A clean 23-gauge (1-1/2" length) (Ramé-hart) blunt tip stainless needle is then attached to the end of the dispenser tubing, and the tip of the needle is positioned in such a way that the pendant droplet remains completely submerged in the bulk solution and away from any other surfaces. A minimum of 5 measurements is taken for all cases, and all experiments are performed in a class (1000) clean room with an ambient temperature of $22 \pm 0.5^{\circ}\text{C}$ and relative humidity of $38.5 \pm 2.5 \%$.

Stirring of the bulk solution is performed in some tests using a magnetic stir bar (Sigma Aldrich) and a custom magnetic stirrer positioned below the glass cuvette. A 9 mm (dia.) cylindrical magnetic stir bar is placed in the cuvette before adding bulk solution. Because stirring affects the IFT measurement, the solution is stirred intermittently during tests and data points collected during stirring are disregarded.

The stir speed is limited such that the droplet does not detach from the needle due to agitation or excessive flow.

2.3.2 Langmuir Compression Isotherm

Surface pressure - Area (II-A) isotherms are measured using a KSV NIMA LB series (Model 1000UID) fitted with a platinum Wilhelmy plate following a standard procedure.[29] The trough and the barriers are thoroughly cleaned using ethanol and rinsed with DI water before every experiment. 20 μ l of 1 mg/ml lipid solution in chloroform is gently dispensed on to the subphase (DI water) using a Hamilton syringe (801RN, Sigma-Aldrich). The II-A isotherm measurement is started after waiting for 15 minutes to ensure that the chloroform in the monolayer is completely evaporated. The monolayer is compressed at a constant rate of 10 mm/min while the surface pressure is recorded at 1 second intervals. All measurements are performed at room temperature (20-23 °C) inside an acrylic housing to protect the monolayer from dust particles.

2.4 DIB formation and characterization

2.4.1 Liquid-in-liquid DIB formation

As shown in Figure 1.10, an open PMMA (polymethyl methacrylate) or PDMS (polydimethylsiloxane) substrate with an (height: 5 mm, width: 4 mm, depth: 8 mm each) open reservoir is filled with 250 μ l nonpolar phase. 200-500 nl (unless specified otherwise) aqueous droplets are dispensed on agarose-coated ball end of the wire-type silver-silver chloride (Ag/AgCl) electrodes that are mounted on micromanipulators (WPI). After appropriate incubation time, droplets are brought into contact to form a bilayer by manipulating the relative electrode positions. Upon contact, a DIB forms at the interface as excess solvent is spontaneously excluded from between the

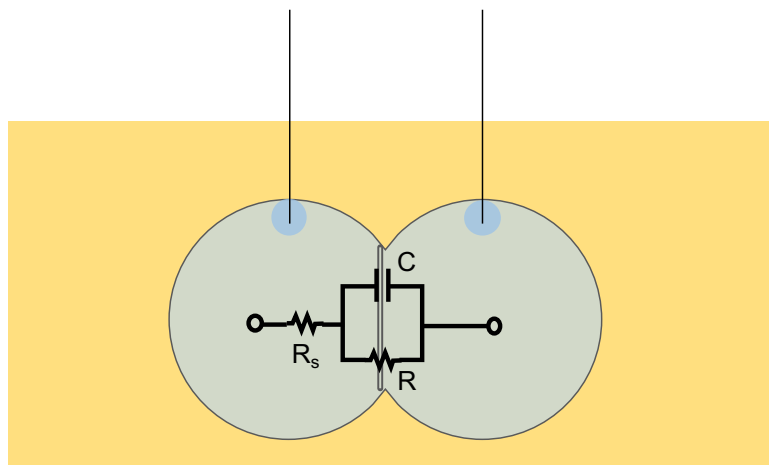


Figure 2.2: A droplet interface bilayer with an equivalent electrical circuit.

droplets. This event is recorded using a digital camera (QImaging) fitted to an inverted microscope (Olympus IX51).

2.5 Contact Angle Measurement

Images of successful DIBs are analyzed using MATLAB to extract the contact angle between the droplets (see DIB image in Figure 2.4). The bilayer tension and the energy of droplet adhesion is calculated based on the equations described elsewhere.[144, 145] A minimum of 10 trials is performed for each lipid condition.

2.6 Electrical Characterization

A DIB acts as a barrier to the transport of ions across them, and thus, can be considered as a resistor. At the same time, because of the charge storing capability of the DIB due to the dielectric property of the hydrophobic region, DIBs can be represented as a capacitor. Figure 2.2 shows a simple RC circuit that is used as a model for DIBs (BLMs), where a resistor, R is connected in parallel to a capacitor, C . The resistance offered by the aqueous solutions on either side of the bilayer (determined by the composition and concentration) is represented by an equivalent

resistor, R_s connected in series to the RC circuit. The complex impedance of this circuit and its frequency-dependent electrical response is derived and discussed in detail elsewhere.[146] Briefly, at low frequencies, the bilayer acts as a pure resistor while at very high frequencies, the resistance of the solution, R_s dominates. Between these two frequencies, the bilayer acts as a pure capacitor. This behavior of bilayer is exploited to characterize the DIBs formed in this work.

Electrical characterization of DIBs is performed in open PMMA substrates (described above) with droplets hanging on 125 μm wire-type silver-silver chloride (Ag/AgCl) electrodes that are mounted on micromanipulators (WPI). The electrodes are connected to an Axopatch 200B patch clamp amplifier (Molecular Devices) that allows the user to apply voltage and measure the induced pico-ampere range current. 500 nl droplets are placed on the two agarose-coated electrode tips. After the incubation time, the electrodes are then brought closer to each other to allow the droplets to come into contact with each other. Due to the capacitive nature of the bilayer, applying a triangular waveform voltage (10 mV at 10 Hz frequency) across the bilayer induces a square wave current whose amplitude is proportional to the nominal capacitance and area of the bilayer (see Figure 2.3(a & b)). This relationship is given by

$$I_s = 4A_v f_v C \quad (2.1)$$

where, C is the membrane capacitance and I_s is amplitude of the square wave produced as a result of an applied alternating triangular voltage with an amplitude (A_v) and frequency (f_v). For all cases tested, the square wave response is recorded during bilayer thinning, and the area of the bilayer is adjusted by manipulating the relative electrode positions to read an equivalent square wave current of about 100 pA ($4.17 \times 10^{-4} \text{ cm}^2$).

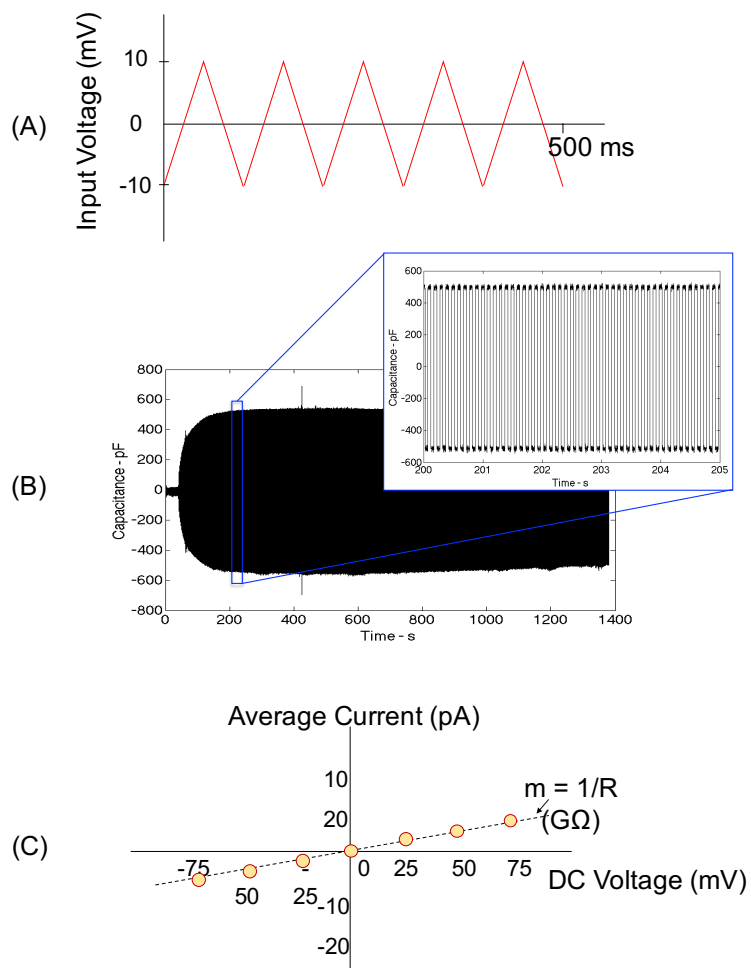


Figure 2.3: Electrical characterization. (A) shows the input triangular voltage to measure the membrane capacitance shown in (B). (C) shows a sample plot of current versus voltage that is used to calculate membrane resistance.

2.6.1 Resistance and Rupture Potential

To estimate the electrical resistance of the bilayer, DC voltage is applied across the bilayer in incremental steps of 25 mV, for about 60 seconds in each step, in alternating bias starting from 0 mV until the bilayer ruptures. The resultant current is digitized with a Digidata 1440A (Molecular Devices) at a sampling rate of 2 kHz and analyzed using MATLAB to determine the electrical resistance of the bilayer, extracted as the inverse of the slope of current-voltage data obtained between -75 mV and +75 mV (see Figure 2.3(c)). Finally, the voltage at which the bilayer ruptures is recorded as

the rupture potential. A minimum of 5 measurements is performed for every case discussed.

2.6.2 Specific Capacitance and Thickness

The nominal capacitance, C of a bilayer (calculated from electrical current measurement in response to an applied triangular voltage waveform) for different bilayer areas, A (estimated from optical images) are used to calculate the specific capacitance, C_m , of a DIB as given by

$$\frac{C}{A} = C_m = \frac{\epsilon_0 \epsilon}{d} \quad (2.2)$$

where ϵ_0 is the dielectric permittivity in vacuum (8.854×10^{-12} F/m), ϵ is the relative permittivity of the hydrophobic region of the membrane, and d is the thickness of the hydrophobic region.

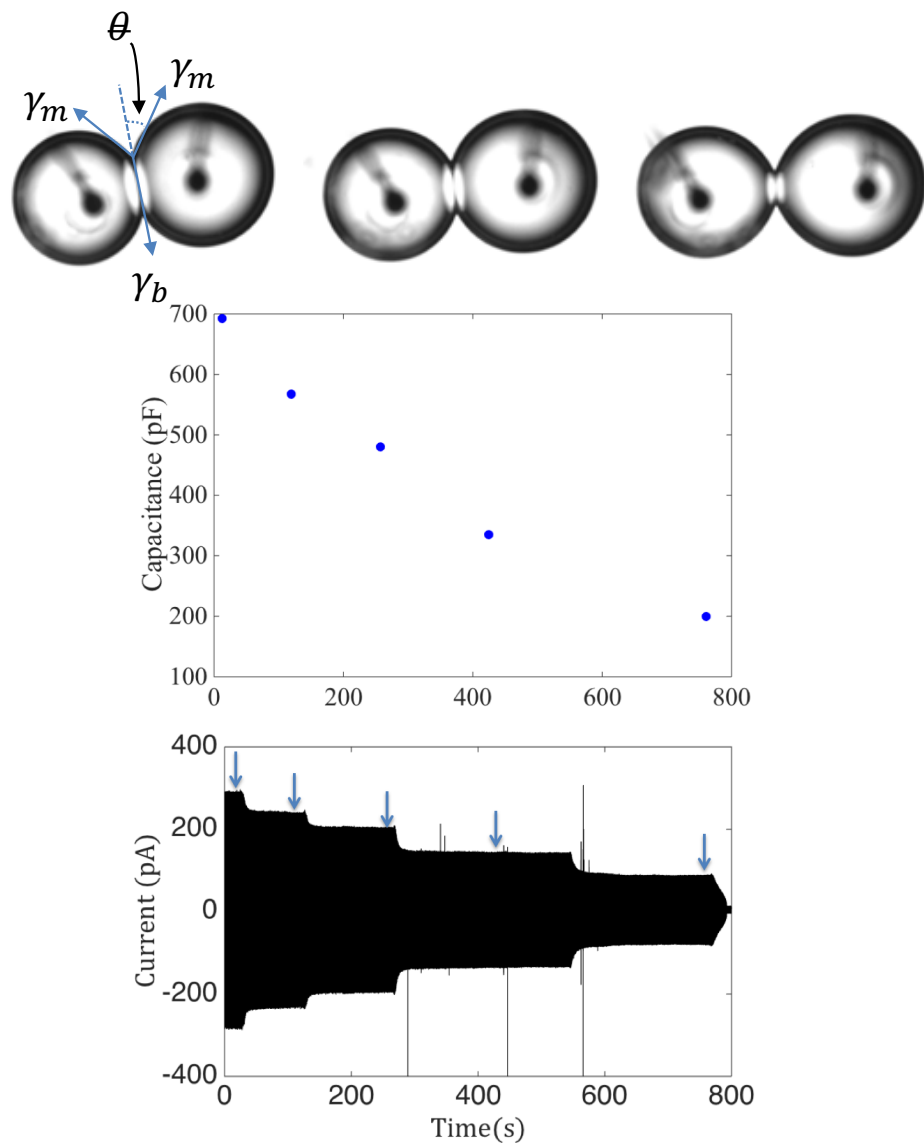


Figure 2.4: Specific capacitance measurement procedure.

Specifically, two droplets hanging from agarose-coated electrode tips are connected to form a DIB on an inverted microscope. Triangular wave is applied to the bilayer continuously and the resultant square wave is recorded. Length of the bilayer is varied in discrete steps by moving one droplet with respect to another by using a micromanipulator, which in turn alters the measured square wave. At every step, after the measured square wave reaches a steady state, an image of the interface is taken. These images are then processed to estimate the area of the bilayer with an assumption of circular interface. Figure 2.4 is plotted using the calculated capacitance values of the bilayers at the exact moments of image captures and the area of the bilayer estimated from the images.[147]

2.6.3 Alamethicin Ion-channel Gating

Alamethicin peptides purchased in powder form (A.G.Scientific) are dissolved in ethanol at 10 mg ml^{-1} and stored at -20°C . Alamethicin stock solution is then diluted in liposome solution to yield a final concentration of $1 \text{ }\mu\text{M}$. Ion-channel gating is recorded by applying a DC voltage above 70 mV and recording the resultant current at a sampling frequency of 10 kHz .

2.7 Nanoscribe 3D printing

Coating coverslips with ITO

Nanoscribe device uses an automated interface finding procedure to precisely find the surface of the substrate on which the parts will be printed. This procedure relies on the change in reflection properties at the surface. Therefore, glass coverslips, which are highly transparent, needs to be coated with a thin layer of reflective material such as ITO. $22 \times 22 \text{ mm}$ coverslips or $24 \times 25 \text{ mm}$ (Fisherbrand) are cleaned thoroughly by sequentially rinsing with DI water, Acetone and IPA, followed by air-drying. Clean

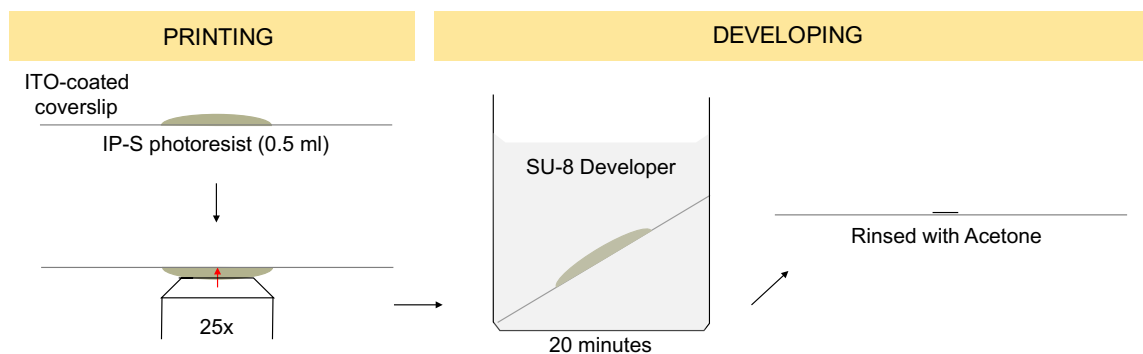


Figure 2.5: Schematics showing steps involved in printing and developing parts that are fabricated using Nanoscribe direct laser writing.

coverslips are placed in a vapor deposition chamber for 15 minutes at 30W power to deposit a \sim 100-150 nm thick ITO coating.

Designing and Printing

Various different scaffolds are designed using Autodesk Inventor 3D CAD software. During designing, the dimensions of the scaffold parts are set in millimeters. The completely assembled scaffold designs are then exported as .stl files. These files are then imported into DeScribe - a GUI software tool provided by Nanoscribe GmbH to create print jobs, which converts .stl files to .gwl files. DeScribe allows the user to position, orient and scale the scaffolds on the substrate as needed. Here, scaffolds are rescaled to microns from millimeters. After choosing the desired print settings and microscope objective, the job (.gwl file) is imported into NanoWrite that controls the laser lithographic system. As shown in Figure 2.5, a drop (0.5 ml) of IP-S photoresist (refractive index at 780 nm: 1.52) is dispensed on the surface of a ITO-coated coverslip and is placed on the automated substrate holder. The automated interface finder provided in NanoWrite software is then used to find the interface before starting the print job. No prebake is necessary for the photoresist used in this work.

Microscaffolds that are used in Chapter 6 are all printed in Dip-in laser lithography (DiLL) mode. In this mode, the substrate is placed upside-down where a 25x objective

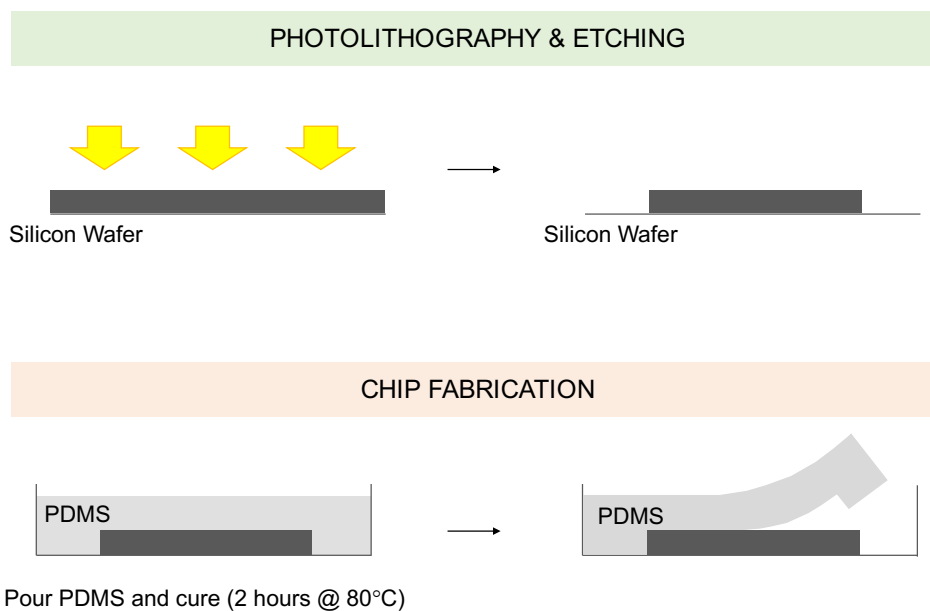


Figure 2.6: Schematics showing the steps involved in development of PDMS chip for microfluidics.

is dipped in the photoresist (see Figure 2.5). A typical print job can take from 10 to 30 minutes depending on the size of parts and other print settings. Higher resolution parts that are printed with 63x or 100x typically takes much longer time periods to print. For all parts printed in this work, 25x objective is used.

Once the printing process is complete, the IPL laden coverslip is carefully removed from the substrate holder and placed in a beaker containing SU-8 developer for 10-20 minutes (see Figure 2.5). This process removes the uncured IPL from the substrate, thus leaving behind the printed scaffold. Following this, the substrate is gently rinsed using Acetone and dried flowing compressed air.

2.8 PDMS Microfluidic Channel Fabrication

A standard soft-lithography procedure is implemented to make a simple microfluidic channel with the dimensions of 1000 x 2500 μm (see Figure 2.6 for schematics). Briefly, a mask containing the desired features is created using photo-lithography. Using this

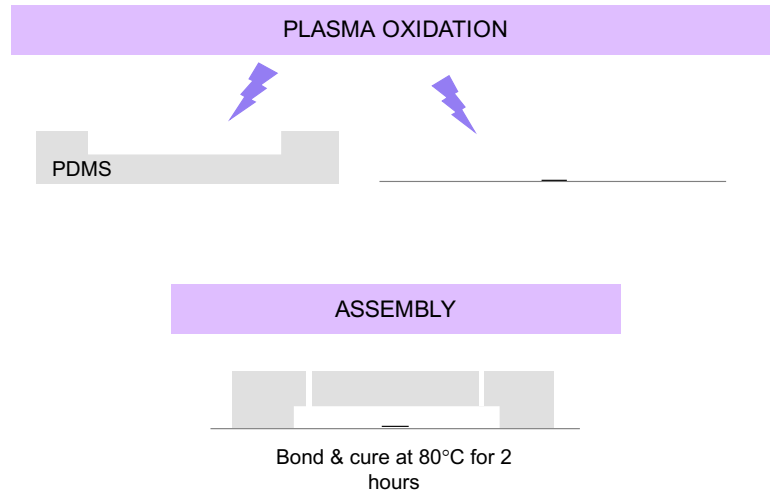


Figure 2.7: Schematic showing plasma oxidation and assembly steps involved to develop a microfluidic chip containing 3D printed scaffold in its liquid chamber.

mask, a silicon wafer is etched using deep reactive-ion etching process to create the required features with a height of $125 \mu\text{m}$. Developed wafers are then placed in a Petri dish and fresh PDMS is poured into it. After curing PDMS at $80 \text{ }^\circ\text{C}$ for 2 hours, the PDMS chip is peeled off.[98]

2.8.1 Plasma Bonding PDMS Chip on Glass Coverslip

Once the PDMS chip is cured, inlet and outlet through-holes are made by using a biopsy punch (dia.: 0.75 mm). In order create a leak-free microfluidic chip, the PDMS chip and coverslip (with printed scaffolds are printed) are then plasma treated using a plasma oxidizer for 30 seconds. Immediately after removing from the plasma chamber, the PDMS chip is bonded on to the coverslip as shown in Figure 2.7. Following this, the PDMS-coverslip assembly is placed in an oven to cure for 2 hours at $80 \text{ }^\circ\text{C}$ before using for experiments.

Chapter 3

Kinetics of Lipid Self-assembly at an Oil/Water Interface: Dynamic Interfacial Tension Measurements and MD Simulation

3.1 Introduction

In this work*, we study the self-assembly kinetics of phospholipids at an OW interface for both lipid-in and lipid-out water-in-oil systems to examine and quantify the fundamental differences in monolayer assembly. Here, we employ pendant drop experiments to measure the interfacial tension (IFT) at the OW interface and our results are compared to molecular dynamic simulations performed by our collaborators at University of Illinois at Urbana Champaign (UIUC) to predict the molecular arrangements of phospholipids in two-phase liquid environments. We also

*Results presented here are reproduced from our published work: Venkatesan, Guru A., et al. "Adsorption kinetics dictate monolayer self-assembly for both lipid-in and lipid-out approaches to droplet interface bilayer formation." *Langmuir* 31.47 (2015): 12883-12893.

MD Simulation's were performed by our collaborator's (and co-authors of this article) at University of Illinois at Urbana Champaign.

study the effect of advective flow around the aqueous droplet on the rate and extent of self-assembly by providing intermittent stirring instead of a continuous flow in lipid-out cases. DIBs obtained from these two techniques (lipid-in and lipid-out) are characterized based on their electrical properties, including resistance and rupture potential, to explore differences in the resulting interfacial membranes. To our knowledge, this is the first attempt to characterize and compare the conditions required to form stable DIBs using lipid-in and lipid-out techniques.

Two types of phospholipids that are widely used in the DIB community, namely 1,2-diphytanoyl-sn-glycero-3-phosphocholine (DPhPC) and 1,2-dioleoyl-sn-glycero-3-phosphocholine (DOPC) are considered in this study.[94, 148] We discuss the differences in monolayer formation rate for liposomes in water or inverse lipid micelles in hexadecane, the most widely used oil in DIB studies and identify reasons for slower monolayer formation in lipid-out cases. We identify that understanding the kinetics of lipid monolayer formation at an OW interface is important not only for DIB application, but also for other fields such as cosmetics, pharmacology and food science where such water-in-oil emulsions are commonly used.[106, 149]

3.2 Results

3.2.1 Interfacial Tension Measurements

The interfacial tension of the neat hexadecane/water interface in absence of phospholipids is first measured to be 44 mN/m, consistent with the literature.[150] Figure 3.1 shows average IFT data at the OW interface versus time for four different cases with phospholipids: DPhPC-liposomes (DPhPC-in) versus hexadecane, DOPC-in/hexadecane, DPhPC in hexadecane (DPhPC-out) versus aqueous buffer, and DOPC-out/buffer. In the cases of 2 mg/ml DPhPC-in and DOPC-in, the interfacial tension of a 1 μ l aqueous droplet decreases rapidly from >40 mN/m to an equilibrium value of 1.18 ± 0.2 mN/m and 1.99 ± 0.5 mN/m (Table 3.1), respectively, within

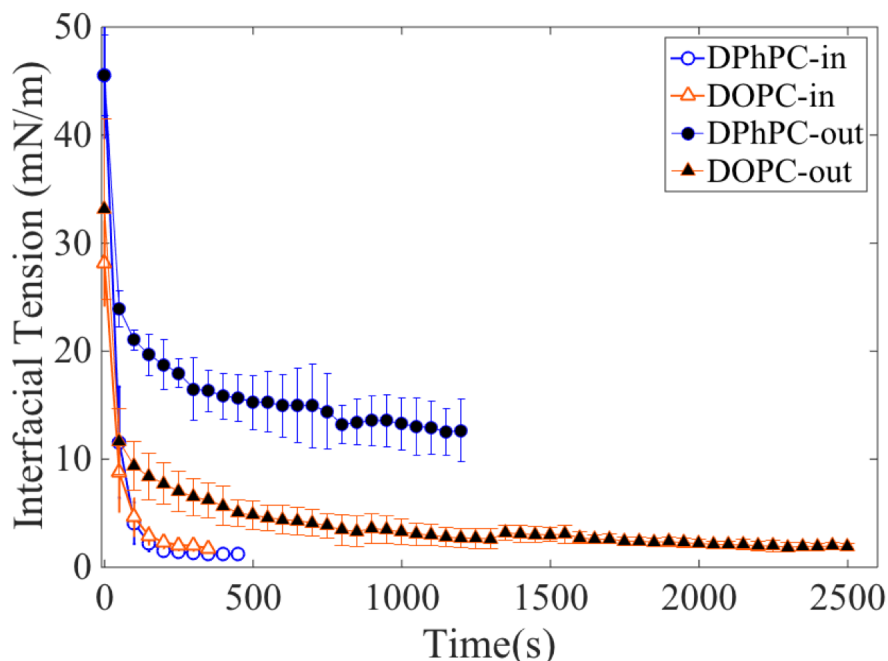


Figure 3.1: Interfacial tension versus time measured at an oil-water interface containing 2mg/ml of either DPhPC or DOPC lipids placed in the aqueous buffer or hexadecane.

~300 seconds. The saturation suggests that DPhPC and DOPC molecules have assembled to form fully packed monolayers with surface pressures >42 mN/m (Surface pressure = IFT of pure OW interface — IFT of OW interface with self-assembled lipid; $\Pi = \gamma_{O/W} - \gamma_{O/L/W}$). [16, 108] On the contrary, equilibrium tensions are not reached within 20 minutes for the cases of DPhPC-out and DOPC-out at the same lipid concentration and droplet size. After an initially quick drop in tension during the first 50-100 seconds, a slower reduction in tension at a rate of about 0.04 mN/m/s or lower is observed for both lipid-out cases. At the end of 20 minutes, the IFT falls to 12 ± 2.0 mN/m for DPhPC-out and 2.7 ± 0.8 mN/m for DOPC-out. Equilibrium IFT of 1.8 ± 0.3 mN/m is recorded for DOPC-out within about 30 minutes, though an equilibrium tension is not obtained for DPhPC-out even at 1 hour after droplet formation. These equilibrium tensions and rates for both lipid-in and lipid-out are in agreement with measurements of monolayer formation found in the literature. [108, 145]

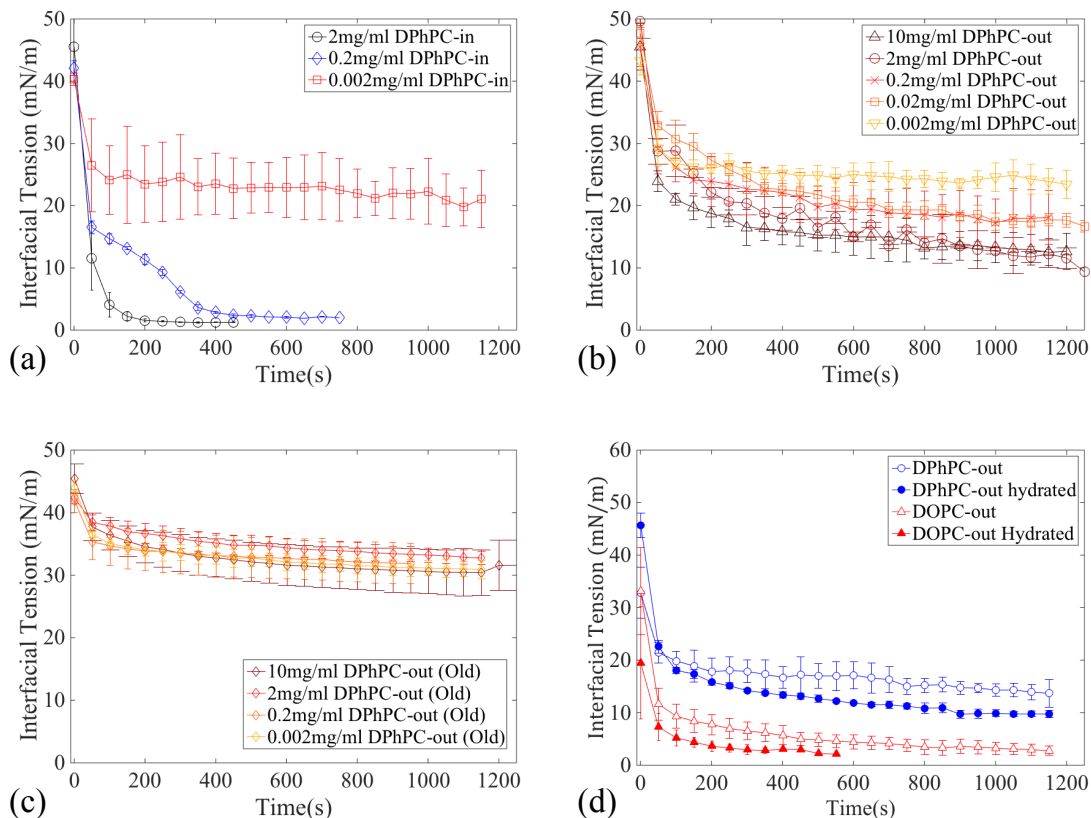


Figure 3.2: Interfacial tension versus time for: (a) 2, 0.2, and 0.002 mg/ml DPhPC-in concentrations; and (b) 10, 2, 0.2, 0.02 and 0.002 mg/ml DPhPC-out concentrations; (c) 4 different old DPhPC-out concentrations; (d) fresh DPhPC-out, hydrated DPhPC-out, fresh DOPC-out, and hydrated DOPC-out.

We performed a second series of experiments to examine the extent to which lipid concentration affects monolayer IFT for both lipid-in and lipid-out approaches. Figure 3.2(a) shows the change in interfacial tension as a function of time for three different concentrations of DPhPC liposomes (DPhPC-in) in the aqueous phase: 2, 0.2, and 0.002 mg/ml. All three concentrations are above the critical micelle concentration in water, which are in the ng/ml range for saturated phospholipids.[151] At 2 mg/ml concentration, an equilibrium tension of 1.5 mN/m is reached in less than 200 seconds, whereas at 0.2 mg/ml concentration, an equilibrium value of 1.86 mN/m is reached after only about 300 seconds. At a lower concentration of 0.002 mg/ml, the tension does not reach an equilibrium value even after 1000 seconds. Similarly, different

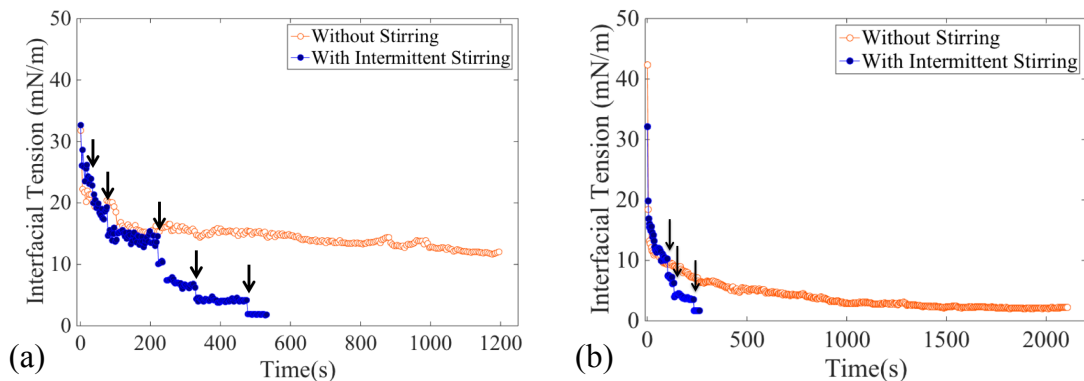


Figure 3.3: Interfacial tension versus time: (a) 2mg/ml DPhPC-out with and without stirring; and (b) 2mg/ml DOPC-out with and without stirring the lipid-out solution for a $1 \mu\text{l}$ droplet. Arrows mark the beginning of 30 s periods of stirring.

concentrations of DPhPC-out display different rates of IFT reduction (Figure 3.2(b)), where again none of the lipid-out concentrations result in surface pressures $>40 \text{ mN/m}$ indicative of a fully packed monolayer.

Because inverse micelles are known to swell and form complex networks in oil with the addition of water,[152] we also performed IFT measurements with intentionally aged and hydrated lipid-out solutions (0.1% v/v water content) to understand how these factors also may affect monolayer assembly. Results of the IFT measurements for fresh and freshly hydrated solutions of DPhPC-out and DOPC-out are compared in Figure 3.2(d) where no significant difference in rate of IFT reduction was noticed. In another set of experiments, intentionally aged lipid-out solutions were used to measure IFT (Figure 3.2(c)). A considerably lower rate of IFT reduction and much less dependence on concentration can be seen in case of the aged inverse micelle solutions compared to freshly prepared solutions.

As recently demonstrated by Thuttupalli, et al, incorporating advective flow of the lipid-out solution around the droplet results in a large and rapid reduction in the IFT to a value of about 5 mN/m . [116] This is attributed to the flow-induced supply of fresh DOPC inverse micelles to the droplet subsurface. Therefore, a final series of IFT measurements were performed with stirring of the lipid-out solution to explore

the effect of advective flow around the droplet on DPhPC-out monolayer formation. Figure 3.3(a) compares the IFT measurements of an aqueous droplet ($1 \mu\text{l}$) formed in still and intermittently stirred hexadecane containing 2 mg/ml DPhPC. An IFT value of 10 mN/m is reached after about 7000 seconds in a still bulk solution, while an equilibrium value of 1.9 mN/m is reached within 600 seconds with five periods of stirring (30 s each) of the bulk solution. Similar behavior is seen in DOPC-out solution (Figure 3.3(b)).

3.2.2 DIB Formation vs Lipid Type and Placement

DIB formation success rates under various conditions with a lipid concentration of 2 mg/ml are presented in Table 3.1. With DPhPC-in, a near 100% DIB formation success rate is seen when 500 nl droplets are placed in contact after a 5-minute incubation time in hexadecane. Meanwhile, tests with DOPC-in droplets in hexadecane rarely form stable lipid bilayers, usually rupturing immediately upon contact even when connected after 20 minutes of incubation time in oil. Interestingly, a significant increase in DIB formation success rate is observed for DOPC-in when smaller droplets ($<200 \text{ nl}$) are used.

In sharp contrast, aqueous droplets of buffer solution placed in DPhPC-out oil yield bilayers in only 5% of the trials after 20 minutes of incubation. This result holds true for lipid concentrations ranging from 0.2 mg/ml to 10 mg/ml in still oil; however, as many as 60% of trials with DPhPC-out lipid solution yielded stable lipid bilayers after only 10 minutes when the droplets are tossed back and forth in a tube containing the same lipid-out solution as reported elsewhere.[86] Comparable success rates (40%) are seen herein when a similar flow mechanism is implemented to prime the droplets. Separately, aqueous droplets placed in fresh DOPC-out and hydrated DOPC-out solutions are able to form DIBs with high success rates (70% and 80%, respectively) when connected within 20 minutes. Measured electrical properties

Table 3.1: Success Rates of DIB Formation and Measured Electrical Properties of the Bilayers

		DPhPC-in /Hexadecane	DOPC-in /Hexadecane	DPhPC-out /Buffer	DOPC-out /Buffer
Eq. Monolayer Tension (mN.m ⁻¹)		1.18 ± 0.2	1.99 ± 0.5	2.04 ± 0.15	1.8 ± 0.3
Bilayer Formation Success Rate	5 min	100%	0%	0%	40%
	20 min	100%	10%	5%	70%
	With flow	n/a	n/a	40%	100%
	Hydrated	n/a	n/a	5%	80%
Electrical Properties	Specific Resistance (MΩ-cm ²)	8.04 ± 3.6	0.55 ± 0.25	1.7 ± 0.8	0.7 ± 0.22
	Max. Rupture Potential (mV)	275	150	100	125

(Table 3.1), contact angles and calculated bilayer tensions and energies of adhesion fall in expected ranges as reported in the literature (Table 3.2).[145]

3.2.3 Electrical Measurements

Figure 3.4 shows the current-voltage plots from DIBs formed using lipid-in and lipid-out methods. As mentioned in Chapter 2, the slopes of these curves are used to calculate the bilayer resistance. The specific resistance calculated from these plots are reported in Table 3.1 along with the maximum voltage at which DIBs ruptured. Overall, DIBs formed with DPhPC-in method displayed highest specific resistance and workable voltage range.

3.2.4 Comparison to Simulation Results Performed at UIUC

First, the changes in free energy of an individual DPhPC micelle and, separately, a DPhPC inverse micelle near a pristine OW interface (without any pre-existing lipid molecules at the interface) are computed via MD. The calculated potential profile, based on the Jarzinsky relation,[153] is symmetrized about $z = 0$ (the OW interface) such that the potential is zero when the micelle (or inverse micelle) is in the bulk liquid environment (oil or water) on either side of the interface. The free energy

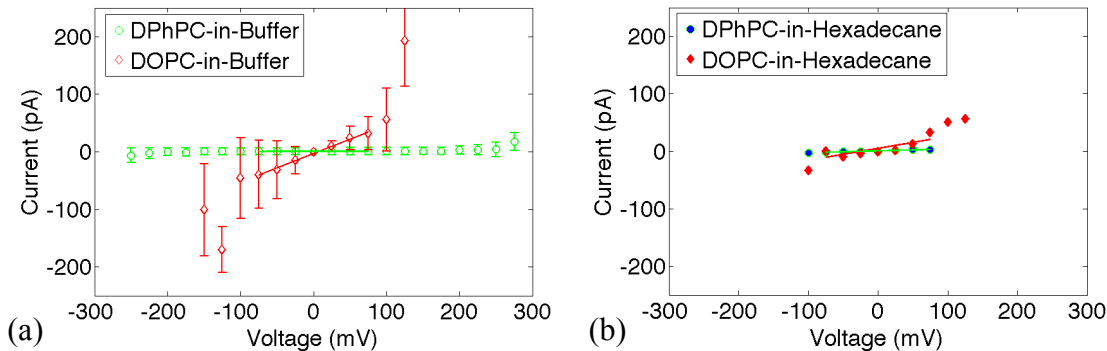


Figure 3.4: Current-voltage curves for DPhPC and DOPC (a) lipid-in; (b) lipid-out. Slopes are plotted between -75 mV and 75 mV to calculate resistance of the bilayers (inverse of slopes).

curves of the micelle (Figure 3.5(a)) and the inverse micelle (Figure 3.5(b)) indicate the relative favorability of lipid-in and lipid-out micelles to self-assemble at the OW interface. The potential of a 6-lipid micelle in water at the interface with respect to the bulk is -450 kJ/mol, while, for an inverse micelle (lipid-out) of the same size, the magnitude of the potential well at the interface is ~ 105 kJ/mol. This four times stronger potential field near the interface in DPhPC-in case compared to DPhPC-out assembly case gives rise to faster and more favorable self-assembly at a pristine OW interface. Comparable free energy curves are observed for DOPC-in and DOPC-out cases as well (Figure 3.5(c & d)).

In order to investigate the effects of pre-existing lipid molecules at the OW interface on the self-assembly (i.e. a partially packed interface), a second set of MD simulations are performed in which the OW interface is occupied by a sparsely packed monolayer. The population of pre-existing lipid molecules at the OW interface is controlled to establish various levels of defined initial configurations for the production runs. Four different packing density (area per lipid) cases of sparse lipid monolayers are examined: $2.54 \text{ nm}^2/\#$, $1.45 \text{ nm}^2/\#$, $1.02 \text{ nm}^2/\#$, and $0.79 \text{ nm}^2/\#$, where $0.79 \text{ nm}^2/\#$ corresponds to a surface pressure of 40 mN/m — maximum packing density reported in literature for DPhPC.[26] Represented in terms of percent coverage, $0.79 \text{ nm}^2/\#$ corresponds to 100% coverage, and $2.54 \text{ nm}^2/\#$, $1.45 \text{ nm}^2/\#$, and $1.02 \text{ nm}^2/\#$

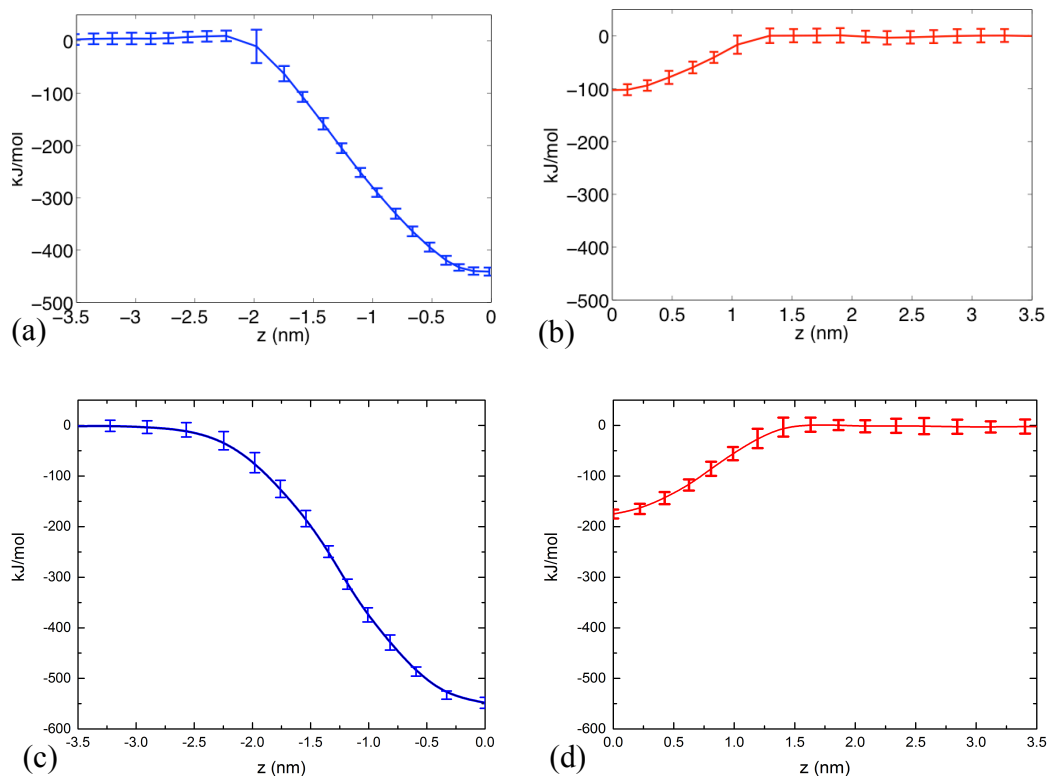


Figure 3.5: DPhPC and DOPC lipid assembly free energy curves as a function of the distance from the pristine OW interface. (a) & (c) shows free energy curves for DPhPC and DOPC micelle (lipid-in), respectively; (b) & (d) shows free energy curves for DPhPC and DOPC inverse micelle (lipid-out), respectively.

correspond to 31%, 54% and 77% coverage, respectively. The resultant free energy profiles for self-assembly process are compared in Figure 3.6. The potentials of the micelle at the OW interface are favorable (negative free-energy with respect to that of the bulk) for $2.54 \text{ nm}^2/\#$, $1.45 \text{ nm}^2/\#$, and $1.02 \text{ nm}^2/\#$, and unfavorable for $0.79 \text{ nm}^2/\#$ in the lipid-in case (Figure 3.6(a)). In other words, the micelles in water can spontaneously assemble at the interface to form a tightly packed monolayer until the maximum packing density is reached. On the other hand, inverse micelles in the lipid-out case display a positive potential (unfavorable) for a packing density as low as $1.02 \text{ nm}^2/\#$ despite the fact that there is enough space at the interface for more lipid molecules to insert (Figure 3.6(b)). These results indicate clearly that sparsely

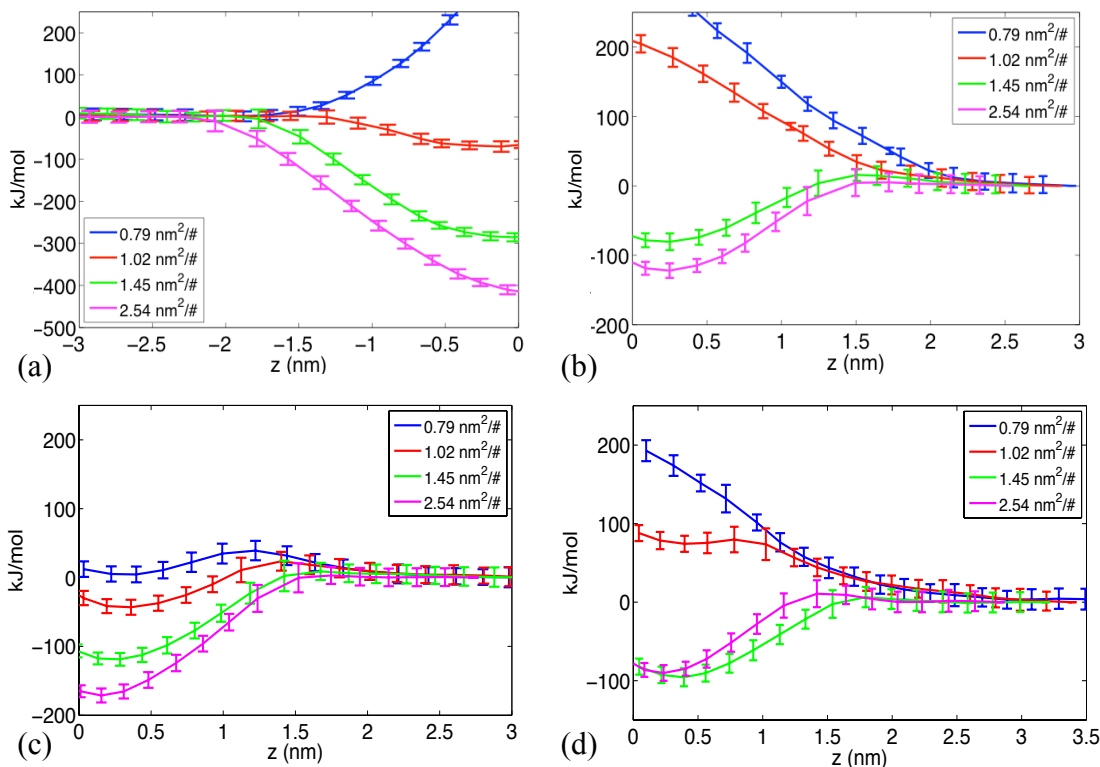


Figure 3.6: Free energy curves for (a) DPhPC-in micelles, (b) DPhPC-out inverse micelles, (c) DOPC-out inverse micelles, and (d) DPhPC-out swollen inverse micelles w.r.t. the distance from the OW interface with different packing density monolayers.

packed lipid monolayers with low area per lipid significantly hinder adsorption of lipid molecules assembling from the oil (lipid-out).

Additionally, the lipid-out self-assembly for the two types of lipid molecules (DOPC and DPhPC) are compared. The free energy curve of the DOPC-out (Figure 3.6(c)) shows stronger potential wells at the interface compared to the DPhPC case (Figure 3.6(b)), which indicates that the DOPC self-assembly is energetically more favorable than DPhPC-out assembly. These results explain the difference in the speed of the DPhPC-out and DOPC-out self-assembly that was observed in the experiments (Figure 3.2). Free energy curves for DOPC-in are not estimated as the IFT dynamics of DOPC-in are very much comparable to DPhPC-in. Therefore, drastic differences are not expected.

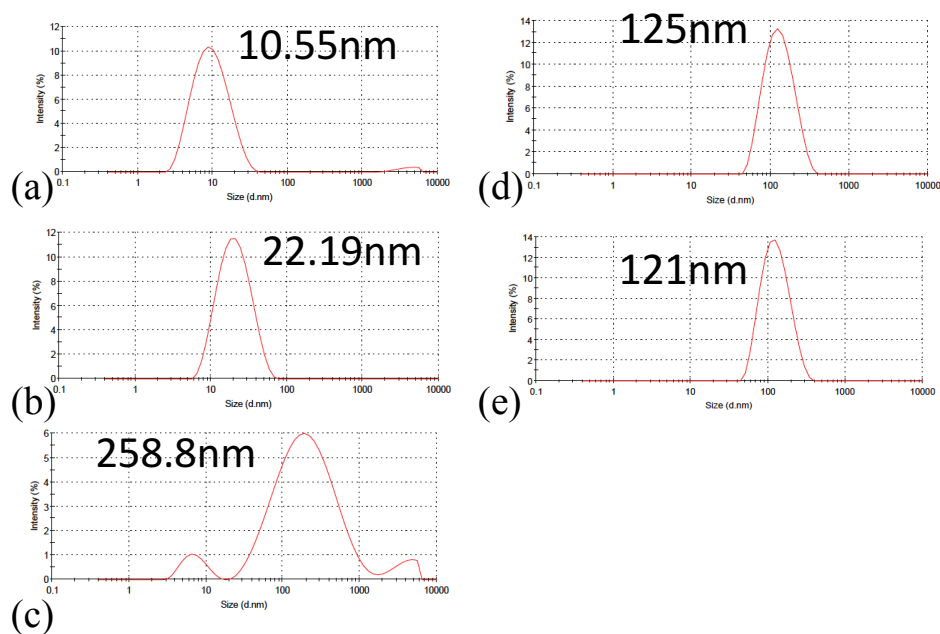


Figure 3.7: DLS measurements showing size distribution in terms of scattering intensity for a) fresh DPhPC-out sample, b) 10-day old DPhPC-out sample, and c) hydrated "swollen" DPhPC-out sample, d) fresh DPhPC-in liposome sample, and e) 10-day old DPhPC-in sample.

Finally, to understand the effect of hydrated (swollen) inverse micelles on the change in free energy during self-assembly, simulations are performed with 35 water molecules between the head groups of an inverse micelle. The free energy in the $1.02 \text{ nm}^2/\#$, $0.79 \text{ nm}^2/\#$ cases still exhibit positive values (i.e. unfavorable) near the interface as shown in Figure 3.6(d), but the magnitudes of the free energy barriers at the interface are reduced compared to the unhydrated case. Similarly, in the $1.45 \text{ nm}^2/\#$ case, self-assembly of a hydrated inverse micelle is slightly more favorable than its unhydrated form. This result is also in agreement with the experimental results (Figure 3.2(d)).

3.3 Discussion

When an aqueous droplet is placed in a non-polar solvent such as hexadecane, an interfacial tension is experienced at the droplet surface due to the relative strengths of attractive and repulsive van der Waals forces among oil molecules and water molecules. Lipid molecules, like other surfactants, self-assemble at the OW interface to reduce this interfacial tension, thereby lowering the surface free energy of the system. When these molecules form tightly packed monolayers, the IFT drops from ~ 44 mN/m ($\gamma_{O/W}$) to $\sim 1-2$ mN/m ($\gamma_{O/L/W}$), a minimum tension that corresponds to a maximum surface pressure ($\Pi = \gamma_{O/W} - \gamma_{O/L/W}$) value > 40 mN/m.[149] We measured the change in IFT over time at an OW interface caused by lipid self-assembly for two different lipids (DPhPC and DOPC) placed in two different liquid phases (water and hexadecane) using pendant drop tensiometry.

In general, we observed 5X and 10X slower rates of lipid monolayer formation for DOPC and DPhPC, respectively, when the lipids assemble at the interface from the oil phase versus from the aqueous side. Using MD simulations, we calculated a significantly higher (4X) decrease in free energy for DPhPC-in micelles compared to that for DPhPC-out inverse micelles. Similar magnitudes of energetic favorability are seen for DOPC-in when compared to DOPC-out as shown in Figure 3.5 (c % d), respectively.

The free energy includes different components, namely the lipid-water, lipid-oil and lipid-lipid interaction energies which are a function of the parameters for the Lennard-Jones (L-J) and Coulombic interactions. In the case of DPhPC and DOPC, the fact that the L-J parameters and the lipid charge distributions (DPhPC with 38 and DOPC with 24 charged atoms) are different gives rise to the differences observed in the free energy profiles. Note that the computed free energy includes both electrostatic and L-J contributions. When the lipid micelles in water (lipid-in) move towards the OW interface, they are surrounded by more water molecules than by oil molecules (and the opposite for lipid-out method). This results in stronger

lipid-water interactions for the lipid-in case resulting in a different energy profile from the lipid-out case. These results confirm that rates and energetics of assembly are not equal for lipids approaching the OW water interface from opposite sides, respectively.

In reviewing the literature, we found several studies[154–156] that examined the kinetics of monolayer formation at a polar-nonpolar fluid interface (e.g. water-air, water-oil) from liposomes distributed in the aqueous phase. These works contribute a basic understanding of the assembly process that consists of serial diffusion (liposomes diffuse from the bulk to the subsurface) and adsorption steps (vesicle structure in the subsurface disrupts and lipids assemble at the interface).[16, 157] The total rate of monolayer formation is thus limited by the slower of these two serial steps. When the concentration of liposomes in the bulk is quite low ($<2 \mu\text{M}$), the rate limiting process is reported to be the diffusion of liposomes into the subsurface (i.e. relatively fast adsorption acts to continually deplete the subsurface such that monolayer formation requires waiting on the next liposome to diffuse). However, when the bulk liposome concentration is high enough ($>0.2 \text{ mM}$),[151] diffusion is the faster of the two steps.

In our study, concentrations of lipids in the two liquid phases ranged from the typical concentration of $\sim 2 \text{ mM}$ used for forming DIBs down to $\sim 2 \mu\text{M}$. The computed values of the diffusion coefficients[154] of both 100 nm-diameter liposomes in water (1 cP viscosity) and 10nm-diameter inverse micelles in hexadecane (3 cP) are found to be quite similar: $4 \times 10^{-12} \text{ m}^2/\text{s}$ for the liposomes and $7 \times 10^{-12} \text{ m}^2/\text{s}$ for the inverse micelles. Therefore, we realize that the differences in kinetics of monolayer formation between lipid-in and lipid-out must not arise from the difference in diffusion of liposomes and inverse micelles. Instead, the differences must originate from differences in adsorption of lipid structures from subsurface.

Differences in lipid adsorption for the two approaches are quantified using a first-order irreversible reaction model to empirically extract short-term rates of adsorption. In this model, the concentration of lipids in the subsurface, C_0 ($\text{mol}\cdot\text{m}^{-2}$) is considered as the reactant while the surface density of phospholipids, Γ ($\text{mol}\cdot\text{m}^{-2}$), is the product

as shown in the following scheme, where k_a is considered to be a time varying adsorption rate constant (s^{-1}):



Due to high diffusion rates at high bulk concentration used in our system, C_0 is considered to be constant. For irreversible adsorption, the rate of increase in surface density of lipids in the monolayer is written as:

$$\frac{d\Gamma}{dt} = k_a(t)C_0 \quad (3.2)$$

For short time intervals (i.e. those much less than the time required for the surface tension to equilibrate) where the k_a is assumed to be a constant, integrating Equation 2 yields a linear temporal solution for the surface density of lipids in the monolayer. This solution can be rewritten in terms of the liposome (or inverse micelle) areal density in the subsurface, V_0 (liposomes. m^{-2} or inverse micelles. m^{-2}), and the number of lipids per unit structure, m , (i.e. 80,000 lipids/liposome or 100 lipids/invers micelle) as

$$\Gamma(t) = \frac{V_0 m}{A_v} k_a t \quad (3.3)$$

where A_v is Avogadro's number (6.02×10^{23} molecules/mole). At short times, Equation 3 shows a linear relationship between the time varying surface concentration and subsurface lipid concentration, adsorption rate, and time. Finally, an equation of state is required to relate surface density of lipids to surface pressure. Henry's surface equation of state relates equilibrium surface concentration to surface pressure, Π : [158]

$$\Pi(t) = nRT\Gamma(t) \quad (3.4)$$

where R is the ideal gas constant ($mJmol^{-1}K^{-1}$), T is the absolute temperature (K), and n is a factor that depends on the type of surfactant ($n=1$ for non-ionic

surfactants, $n=2$ for ionic surfactants). Thus, for neutral lipids like DPhPC and DOPC, $n=1$. Equation 4 is valid for low surfactant concentration systems where interaction between adsorbed surfactants is assumed to be negligible. As suggested by Bleys et al., the equilibrium Equation 4 can be applied to a dynamic system.[159] Thus, substituting Equation 3 into Equation 4 yields the following linear relationship for surface pressure versus time for irreversible adsorption at a fixed adsorption rate during brief intervals:

$$\Pi(t) = \frac{RT}{A_v} V_0 m k_a t \quad (3.5)$$

Yet, IFT measurements of phospholipids at an OW interface (Figure 3.1) clearly show that surface pressure does not increase linearly with time. To account for the fact that measured surface pressures are nonlinear, we consider that the favorability for lipid adsorption must decrease as surface density rises due to: 1) decreasing available area at the interface for new lipids, and 2) inhibiting interactions between adsorbed molecules and those in the subsurface.[160]

Empirically, this slowing of adsorption is described as a decrease in the adsorption rate constant, k_a , or in the lipid adsorption flux represented by the product $V_0 m k_a$. By letting the product $m k_a$ vary during the measurement, Equation 5 can thus be used to fit non-linear IFT data well in successive, 4 second time segments during which a constant local rate ($m k_a$) is computed from the slope (Figure 3.11(b)). The resulting dynamics of rates for both the lipid types placed in either phase are shown in terms of lipid adsorption flux, $V_0 m k_a$ (lipids.m⁻².s⁻¹) in Figure 3.8. After the first few seconds of fast adsorption, the lipid adsorption flux abruptly drops down and adsorption continues at a slower flux for DPhPC-out (Figure 3.8(a)). Such distinct change in lipid adsorption flux — a high initial flux followed by drastically slower flux until equilibrium is reached — is seen for both DPhPC-out and DOPC-out after about 75 s (Figure 3.8(d)). Dynamics of lipid adsorption flux for both DPhPC-in and DOPC-in does not seem to display such distinct regimes; rather, a single trend in

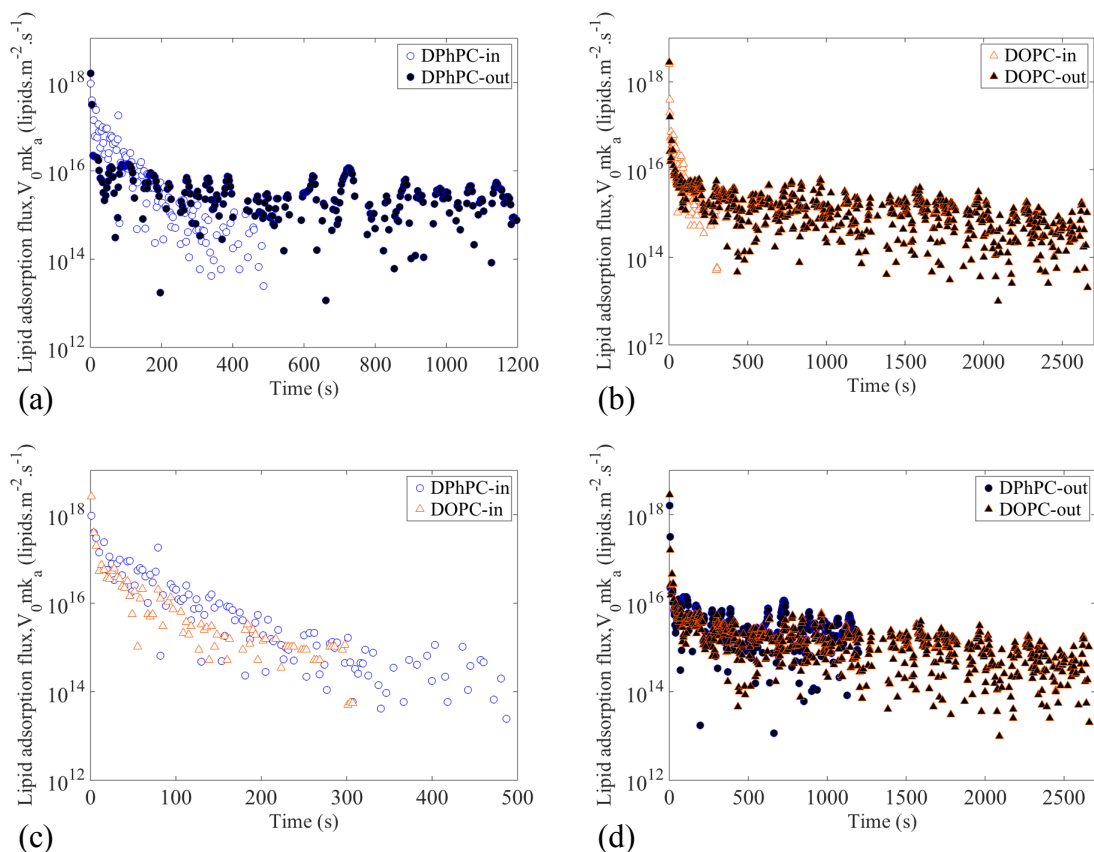


Figure 3.8: Estimated lipid flux rate versus time for a) DPhPC-in and DPhPC-out, b) DOPC-in and DOPC-out, c) DPhPC-in and DOPC-in, and d) DPhPC-out and DOPC-out at 2mg/ml concentration. Note: Only non-zero values are plotted.

decline of lipid adsorption flux (Figure 3.8(c)) is noticed. A noticeable difference in adsorption behavior for lipid-out suggests the possibility of the onset of an additional adsorption barrier leading to a changeover in regimes.

To further investigate the differences, data from Figure 3.1 and Figure 3.8 are combined in Figure 3.9 to cast the progression of lipid adsorption flux in terms of increasing surface pressure, which is proportional to surface density. As expected, in both lipid-in and lipid-out techniques, the lipid adsorption flux is highest during the first few seconds of monolayer formation when the surface pressure is the lowest as the lipid structures encounter a "clean" OW interface. During this phase, one could assume complete rupturing of liposomes or inverse micelles to deposit its

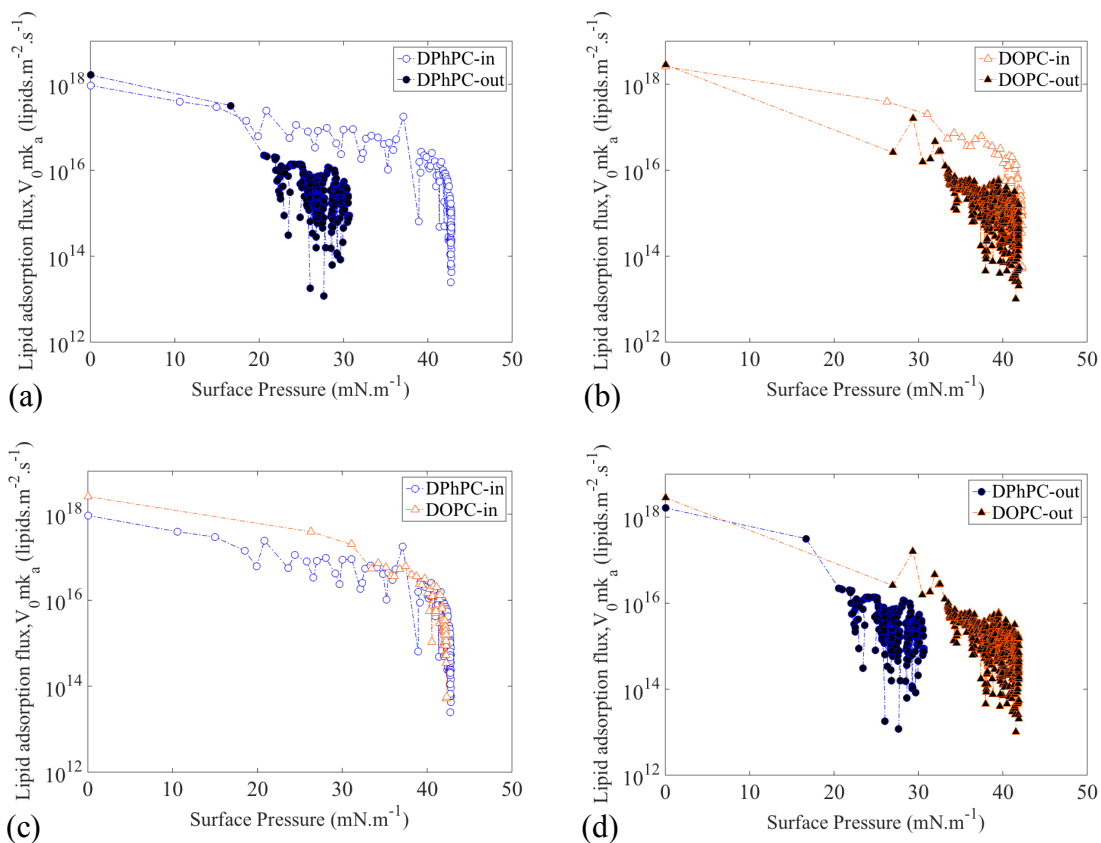


Figure 3.9: Estimated lipid flux rate versus surface pressure for, a) DPhPC-in and DPhPC-out, b) DOPC-in and DOPC-out, c) DPhPC-in and DOPC-in, and d) DPhPC-out and DOPC-out at 2mg/ml concentration. Note: Only non-zero values are plotted.

entire content at the interface. Walker and Richmond explained this as the "rupture mechanism" (Figure 3.10(a) & 3.10(c)).[16, 157] The higher initial values for lipid-in when compared to their lipid-out counterparts is possibly due to, a) the difference in the tendencies of liposomes and inverse micelles to break open at the interface, and b) the difference between the number of lipids per liposome ($\sim 80,000$ molecules) and an inverse micelle (~ 100 molecules).

As the surface concentration of lipids increases, the lipid adsorption flux starts to reduce due to the diminished exposed-OW interface and increasing repulsive interaction between the adsorbed lipids and the lipid structures approaching the interface. Figure 3.9(c) shows that, for DPhPC-in and DOPC-in, such hindrance

(quantified as low lipid adsorption flux) is minimal until the surface pressure reaches close to the maximum value (>40 mN/m) where the exposed-OW interface is minimal. On the contrary, for DPhPC-out, such an adsorption barrier intensifies at a much lower surface pressure (~ 23 mN/m) and hinders further adsorption (Figure 3.9(a)). Hence, a much slower reduction in surface tension is noticed after the initial quick drop in IFT (Figure 3.1). A similar adsorption barrier is seen in DOPC-out although only after a relatively higher surface pressure (~ 35 mN/m) is reached, which is possibly due to higher fluidity of DOPC tail groups when compared to DPhPC.[161, 162] We hypothesize that once this adsorption barrier has been established (2nd regime in Figure 3.9), adsorption takes place via an "extraction mechanism" (Figure 3.10(b & d)) — the process by which liposomes or inverse micelles deposit a fraction of its lipid content into the interface while remaining intact⁷⁴ — rather than by rupture mechanism. In agreement, the MD simulations show that an increase in free energy is observed when a DPhPC inverse micelle is placed near a partially packed interface with packing densities as high as 1.02 nm²/# (Figure 3.6(b)). In other words, adsorption of lipid molecules into the interface is hindered before the packing density of lipids at the interface reaches the maximum value of 0.79 nm²/# as seen in lipid-in. Therefore, we arrive at the conclusion that after a short period of simple adsorption-controlled process, such adsorption barriers limit the continued process of lipid self-assembly at the interface for lipid-out technique. In contrast, analysis of the lipid-in IFT data indicate that such adsorption barriers are not encountered for lipid-in until maximum packing density is achieved as the liposome-monolayer interaction is repulsive[163] — for comparison purposes, we call this a simple adsorption-controlled process. Furthermore, we conclude that diffusion is not a rate-controlling step due to the high concentrations used in our study for both lipid-in and lipid-out. In agreement, such mixed diffusion, adsorption, and adsorption-barrier controlled self-assembly have also been reported for phosphatidylcholine and other micelle forming surfactants at an OW interface.

One possible explanation for the onset of the adsorption barrier for inverse micelles is the formation of hydrated-inverse micelles and lipid-based organogels in the subsurface of the lipid-out solution. The incorporation of water (0.1% v/v) into a nonpolar organic solvent containing a high concentration of lipids is found to have substantial effects on both the nanoscale self-assembly of the lipids as well as the bulk properties of the solution.[152] For example, hydrating inverse micelles can result in the formation of worm-like structures that can overlap to form three-dimensional networks. Upon hydration, drastic increase in the size of lipid structures is measured using DLS (Figure 3.7). However, both experimental and MD simulation results show that there is no drastic, adverse difference in the rate of IFT reduction and energetic favorability for swollen inverse micelles over their un-swollen counterparts (Figure 3.2(d)). While these structures do not drastically affect the monolayer formation, these tangled micellar structures, may affect the bilayer formation. Although our MD simulations do not show evidence for aggregation of inverse micelle to the partially packed monolayer, the possibility of forming multi-molecular layers tethered to such interface should not be neglected.[151, 164, 165]

Our experiments and others have shown that stirring lipid-out solution increases the packing density of lipids at an OW interface by providing an advective flow of species around the aqueous droplets. In prior works, the enhanced rate of assembly was attributed to a reduction in the time required for the lipid species to reach the interface. Quicker self-assembly of lipids is seen in microfluidic devices than in a static system due to the convective motion of the droplet and the bulk that is found in the former system.[116] This difference was attributed to the advection-induced transport of lipids to the interface. Self-assembly studies using fluorescent surfactants in microfluidic devices displayed a decreasing concentration gradient of the adsorbed lipids from the rear to the front of the droplet that is in motion due to the presence of shear flow.[105] Proven the propensity of lipid-out systems to exhibit adsorption-limited kinetics, we believe that flow may actually have multiple roles: a) to crowd the assembled lipids at the interface due to shear flow, exposing bare OW interface

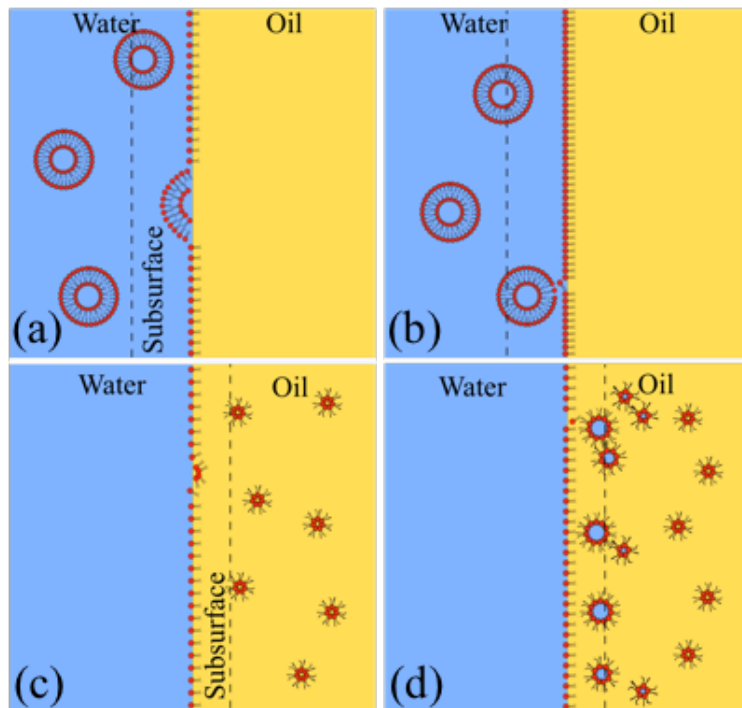


Figure 3.10: Schematic representation of lipid self-assembly at an oil-water interface following rupture mechanism (a: lipid-in, c: lipid-out) and extraction mechanism (b: lipid-in, d: lipid-out). Schematic (d) depicts the swollen inverse micelles through uptake of water.

where lipids in subsurface can get adsorbed (promoting rupture mechanism rather than extraction), and b) to perturb lipid assembly in the subsurface due to advective flow, allowing additional lipid insertion, thus reducing the IFT. Such stirring induced reduction in IFT is seen in both DOPC-out and DPhPC-out techniques (Figure 3.3). Stirring did not have drastic effects on "aged" or "hydrated" lipid-out solutions (data not shown) as presence of complex lipid structures in the bulk could affect the self-assembly process drastically.

Differences between DPhPC and DOPC IFT reduction rate could be due to the different innate shape of the lipids, the bulky methyl groups on the acyl chains of DPhPC, or the difference in phase of lipid at 20°C (phase transition temperature, t_m for DOPC: -18°C; t_m DPhPC: no transition between -120°C to 120°C).[162] DOPC-out inverse micelles, unlike DPhPC-out, do not exhibit an increase in free energy

when placed near a packed interface with area per lipid as low as 0.79 nm^2 . This is likely because DOPC molecules occupy a lower area ($\sim 65 \text{ nm}^2/\#$) at its maximum packing density.[166] Pre-packing the interface with a more tightly packed monolayer could produce a positive change in free energy.

To summarize, tightly packed monolayers are obtained within 5 minutes of droplet formation for both DPhPC-in and DOPC-in, and in about 30 minutes for DOPC-out. On the other hand, such tightly packed monolayer is not achieved with DPhPC-out even after 1 hour. We attribute this to the adsorption barrier established due to aggregated and/or hydrated inverse micelles on partially packed monolayer. Nevertheless, stirring of the bulk lipid-out solution are found to help achieve tightly packed monolayer quickly. We accredit this to the convection-induced relocation of interface-bound lipids and restoration of rupture mechanism based adsorption.

For bilayer formation, priming droplets with such flow techniques is not required for lipid-in solutions, since a tightly packed monolayer assembles within 5 minutes and monodispersed liposomes do not aggregate with one another or with the monolayer over time (see Figure 3.7). This favorability translates into a near 100% bilayer formation success rate is seen in case of DPhPC-in. While a similar behavior is expected from DOPC-in (as the IFT reduced to near 1.99 mN/m within 5 minutes), droplets ($>200 \text{ nl}$) with DOPC liposomes fail to form DIBs with high success rate even when connected after 20mins or longer. Nevertheless, smaller droplets ($<200 \text{ nl}$) seem to form DIBs even within 5 minutes with a drastically higher rate.[96] The reason for such droplet size-dependent behavior is unclear and requires separate investigation; varying Laplace pressures, droplet curvatures, and lipid shape factors may all be responsible.[43] As expected from the measured IFTs, low bilayer formation success rate is seen for DPhPC-out and DOPC-out when connected within 5 minutes, and higher success rate for DOPC-out after a 20-minute incubation time.

In accordance with the IFT data for hydrated DOPC-out (Figure 3.2(d)), a significantly higher success rate and reduced required incubation time is observed when connected just after 10 mins. On the other hand, hydrated DPhPC-out,

in stationary conditions, did not seem to improve the success rate. Employing a flow mechanism to prime the droplets before connecting improved the success rate for DPhPC-out considerably, which we explain by relocating the hydrated inverse micelles and other complex lipid structures away from the droplet subsurface, which can be found in stationary systems. In summary, near 100% DIB formation success rate displayed by DPhPC-in (that has the quickest monolayer formation with least IFT) and the dependence of success rate on droplet size for DOPC-in and hydration level for DOPC-out and DPhPC-out proves that while tightly packed monolayer is a fundamental precondition, it is not the only requirement.

High electrical resistance (gigaohm) allows detection and characterization of single-channel membrane proteins and peptides that are inserted in the bilayer. Bilayers with higher rupture potential (>125 mV) are favorable for studying voltage-regulated species such as alamethicin. DIBs formed with DPhPC-in are found to have both these desired properties. DIBs formed with other three cases seem to have low rupture potentials (<125 mV). Bilayers formed with DOPC in either phase appear to have lower resistance when compared to bilayers formed with DPhPC. This difference in bilayer resistance, again, could be because of the difference in shape factor and the fluidity of these two lipids at room temperature. Measured specific capacitance values (Table 3.2) for DPhPC and DOPC bilayers match the values reported in literature and no drastic difference is noticed between the bilayers obtained from the same lipid type placed in different phases.[5] This confirms that the hydrophobic thickness of bilayers obtained from the same lipid type is not affected by the phase in which the lipids are placed.[167] The consistency in contact angle (Table 3.2) across the various configurations is explained by the fact that contact angle is largely governed by the tendency for an oil to be excluded from the bilayer based on its size relative to the hydrocarbon chains of the lipids. Thus, little difference was expected or observed for DIBs consisting of 16-carbon DPhPC tails or 18-carbon DOPC DIBs in hexadecane, a 16-carbon alkane.

Table 3.2: Measured physical properties of DIBs

	DPhPC-in /Hexadecane	DOPC-in /Hexadecane	DPhPC-out /Buffer	DOPC-out /Buffer
Contact Angle (°)	20 ± 2	27 ± 5	18 ± 5	21 ± 5
Bilayer Tension (mN.m ⁻¹)	2.2 ± 0.4	3.5 ± 0.9	3.9 ± 0.3	3.36 ± 0.6
Energy of Adhesion (mN.m ⁻¹)	0.14 ± 0.001	0.43 ± 0.004	0.20 ± 0.01	0.24 ± 0.002
Specific Capacitance (μF.cm ⁻²)	0.685 ± 0.068	0.914 ± 0.274	0.638 ± 0.068	0.968 ± 0.072
Calculated Thickness (Å)	2.8 ± 0.3	2.1 ± 0.7	3.1 ± 0.3	2.0 ± 0.3

It is important to acknowledge the simplifications required for MD simulations. For instance, had we considered liposome with 80,000 molecules instead of a 6-lipid micelle, the free energy profile for the lipid-in cases presented in Figure 3.5 could change due the possible difference in favorability and the number of lipids supplied per adsorption. In addition, the MD model disregards interactions between neighboring micelles (or inverse micelles) either in the bulk or near the interface. Aggregation of inverse micelle due to aging or hydration could increase the stability of lipid structures in oil, thereby further reducing the rate of IFT reduction. The hydration level, which is defined as the number (#) of H₂O molecules inside an inverse micelle, and the number of lipids in a hydrated inverse micelle are also not considered. Finally, the curvature of the simulated oil-water interface is neglected since the droplets (ca. 1mm diameter) exhibit curvature radii orders of magnitude higher than those of the lipids. Despite these choices, the MD simulations capture well the sustained energetic favorability between a partially packed monolayer and lipid-in micelles and the increasing difficulty of oil-bound inverse micelles to adsorb to a sparsely populated monolayer. These trends are in direct agreement with the kinetic processes observed experimentally for both lipid-in and lipid-out.

Considering the complexity involved in the lipid self-assembly process at an OW interface, applying simple concepts of first-order reaction kinetics and Henry’s equation of state for ideal scenario may not be suitable for accurately capturing the kinetics of the entire process. However, with few valid assumptions, we demonstrate

Table 3.3: Qualitative determination of suitable minimum lipid concentration

Number of lipids required to cover a 1 μ l droplet surface: 6×10^{12} molecules (approx.)					
Concentration		2mg/ml	0.2mg/ml	0.02mg/ml	0.002mg/ml
Lipid-in	No. of lipid molecules present in 1 μ l aqueous droplet (approx.)	1.4×10^{15}	1.4×10^{14}	1.4×10^{13}	1.4×10^{12}
	% required for complete coverage (approx.)	0.4%	4%	40%	419% (More lipids required than available)
Lipid-out	No. of lipid molecules present in 10 μ l hexadecane solution (approx.)	1.4×10^{16}	1.4×10^{15}	1.4×10^{14}	1.4×10^{13}
	% required for complete coverage (approx.)	0.04%	0.4%	4%	40%

that this model could be used to determine the rate-limiting step involved in monolayer formation process, and to compare the kinetics for surfactants approaching from different phases. The validity and limitations of our model is analyzed below.

3.4 Validity and Limitations of the Proposed Model

Consider DPhPC-in: integrating Equation 3, an approximate estimate of total number of adsorbed lipids at equilibrium state, Γ^{eq} is obtained: 1.67×10^{-5} moles $^{-2}$. Using the equilibrium surface pressure value of 42.7 mN/m in Equation 4 leads to a Γ^{eq} value of 1.75×10^{-5} moles $^{-2}$, which is roughly equal to Γ^{eq} obtained from integrating equation 3. Figure 3.11(c) compares the experimental surface pressure to the back-calculated surface pressure from the model. The agreement found between these two curves validates the modeling approach.

The use of an exponential model, where adsorption is proportional to the surface density, to analyze experimental data is discussed in the Appendix (A.2). In short, a single exponent, exponential model fails to capture the evolution in surface pressure with respect to time. In addition, using a single exponential model to fit the lipid-out

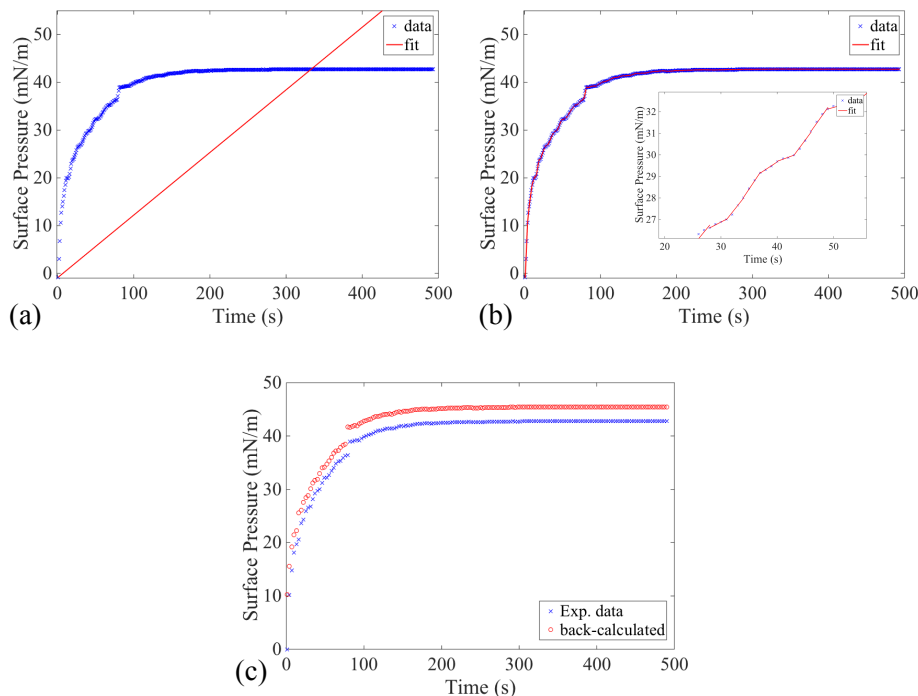


Figure 3.11: DPhPC-in surface pressure data and calculated fit using equation 5 for, a) the entire length of data with a single mk_a , and b) estimating mk_a values for 4s segments. Inset: A zoomed-in view of the same plot to show the short 4s data segments and its fit. c) Comparison of experimental surface pressure and back-calculated surface pressure from the model for DPhPC-in at 2 mg/ml.

data does not describe the two different modes of adsorption as is possible with the proposed linearized-model.

3.4.1 Limitations of the Model

The concentration range in which C_0 can be assumed to be constant must be determined (see Table 3.3) to determine the applicability of the proposed model. C_0 is assumed to be constant where the diffusion coefficient of lipid particles is high enough such that adsorbed lipids from the subsurface are constantly replenished by lipids originating from the bulk. For lipid-in cases, at high concentrations such as 0.2 mg/ml, just 4% of the total lipid content is required to completely cover the droplet surface. Thus, the concentration gradient between the subsurface and the bulk is

maintained, allowing C_0 to remain constant. However, at 0.02 mg/ml or below, C_0 may not be assumed to be constant as a significant portion (40%) of lipids are required to form a fully-packed monolayer. The calculation shown for a concentration of 0.002 mg/ml shows that an insufficient number of lipids are present to fully pack the interface, which explains why IFT only reduces to ~ 22 mN/m (Figure 3.2(a)).

Aside from the number of lipids present, the concentration gradient established between the interface and the bulk reduces for low lipid concentrations, which also prevents C_0 from remaining constant.

The bottom half of the Table 3.3 shows that even for a small lipid-out reservoir volume of 10 μ l, there exists an ample amount of lipids required for complete droplet coverage. Therefore, the calculation justifies that at reasonable concentrations, especially those higher than 0.02 mg/ml, depletion of lipids as a result of adsorption is minimal and our assumption that C_0 is constant is valid.

3.5 Conclusion

The results from this study answer some of the previously unanswered questions in regards to required incubation time for both lipid-in (lipid-in-water) and lipid-out (lipid-in-oil) techniques, and the reason for longer incubation time and reduced success rates for DIB formation using lipid-out technique. Results from interfacial tension measurements points to a simple adsorption controlled process for lipid-in assembly and predominantly adsorption-barrier controlled assembly for lipid-out techniques after an initial period of simple adsorption. For lipid-out technique, we identify that the adsorption limitation becomes prevalent in the later stages of monolayer formation due to a high potential barrier for inverse micelle structures near a partially packed monolayer. This interaction creates an environment favorable for inverse micelle aggregation in a way that is not seen in lipid-in technique due to the repulsive interaction between liposomes in water. Formation of organogel in the subsurface is determined as a possible reason for this adsorption barrier. Results presented

clarify that advective flow around the aqueous droplet helps achieve a tightly packed lipid monolayer by perturbing lipid structures in the subsurface and at the interface. IFT measurements, in general, are in consistent with DIB formation success rates in terms of a) minimum required incubation time, b) tighter packing i.e. lower IFT leads to higher DIB success rates. For the cases where aggregation and swelling of inverse micelle are noticed, application of advective flow around the aqueous droplet results in quickly achieving tighter packing and increasing the bilayer formation success rate, making lipid-out another successful technique for DIB formation in microfluidic devices.

Chapter 4

Evaporation-induced Compression of Monolayers to Enable Droplet Interface Bilayer Formation using Unsaturated Lipids

4.1 Introduction

In this chapter, we report a novel experimental methodology to enable DIB formation using unsaturated lipids. We demonstrate the implementation of a simple evaporation-induced monolayer packing technique that conditions the spontaneously self-assembled monolayers of two unsaturated lipids (that are in liquid-disordered state) namely, DOPC and POPC, and enable DIB formation with near 100% success rate. To understand how this method improves bilayer formation, the effects of lateral compression of DOPC and POPC monolayers are studied in comparison to DPhPC using pendant drop tensiometry and Langmuir compression isotherms. Electrical measurements of bilayer resistance, rupture potential and specific capacitance are also reported.

4.2 Approach

4.2.1 Description of Novel Procedure: Evaporation of Water Droplets to Compress Lipid Monolayer

Two Ag/AgCl electrodes are chlorided and ball-end tips are coated with Agarose gel. These electrode tips are then placed under an organic solvent contained in an open PMMA substrate. 300 nl aqueous droplets containing liposomes (lipid-in) are pipetted on to the agarose-coated tips and electrode are positioned in such a way that the droplets hang deep under the oil, far from the oil-air interface (see Figure 4.1). In a typical DIB formation experiment, after incubating the droplets for 5-7 mins to allow monolayer formation, the electrodes are repositioned gently to bring the droplets into contact. In the modified experimental procedure, an evaporation-assisted monolayer compression step is performed before bringing droplets into contact: after incubating the droplets for 5-7 mins, the electrodes are lifted upwards to bring the droplets close to/touch the oil-air interface for 10-15 seconds, where the droplets undergo shrinkage (see Figure 4.1(c)). Before shrinking, droplets are situated on the electrode in such a way that the agarose tip and the waist of the droplet are in the same xz-plane. Upon shrinkage, the droplets descend down the electrode such that the waist of the droplet is far below the agarose. During experiments, this change in xz-plane is used as the visual cue for monolayer formation and the electrodes are lowered deep under the oil and the droplets are brought into contact. In some cases, droplets fall off the electrode due to the very low IFT of droplets achieved by the shrinking step. In such cases, after droplets fall on to the PMMA substrate, they are brought into contact by gently pushing using a pipette.

In either procedure, the experiment is concluded successful if a DIB is formed — indicated both by visual confirmation of droplets "zipping" and by electrical measurement showing growth of square wave current for a triangular voltage input electrical measurement — and is found to be stable for at least 1 minute. The

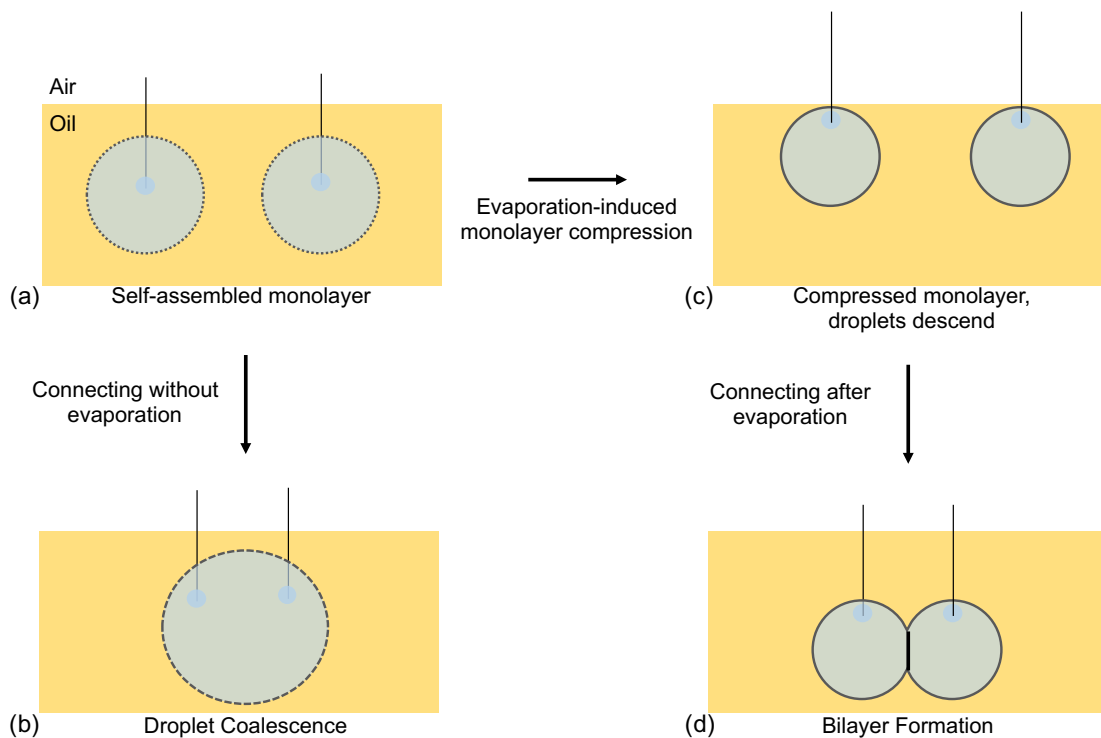


Figure 4.1: Schematic illustrating the steps involved in conventional procedure (a, b) and in proposed procedure (a, c and d) to form a DIB.

experiment is noted failure if the droplets coalesce before (i.e., immediately after contact), during or shortly after "zipping". Minimum of 5 trials were performed for each lipid-oil combination.

4.2.2 Pendant Drop Tensiometry with Step-wise Volume Reduction

Change in interfacial tension during monolayer formation is measured using a pendant drop tensiometer following a well-established procedure as reported in Chapter 2. In order to understand how the proposed evaporation-technique affects the monolayer packing, we performed another series of IFT measurements that emulates volume shrinking seen in DIB experiments. The automated volume control device used to

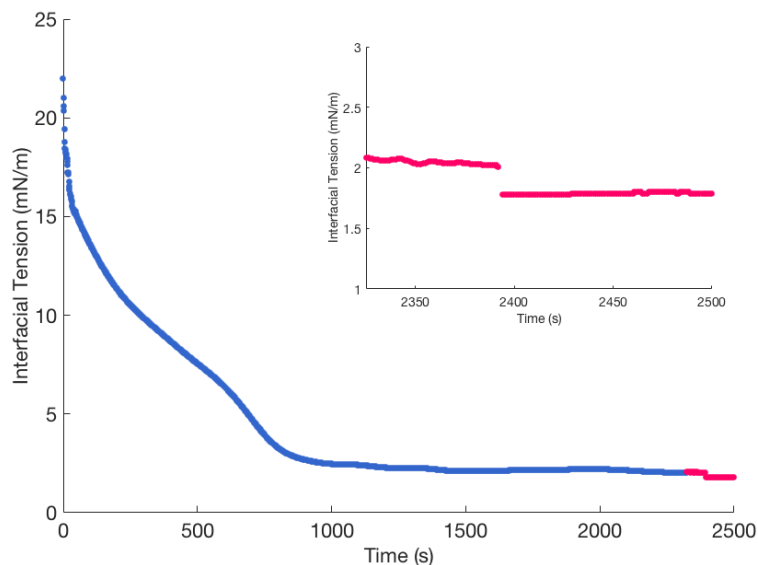


Figure 4.2: Representative data showing change in IFT due to spontaneous assembly of DOPC monolayer (blue; fixed-volume mode) and step-wise reduction in volume (red).

dispense pendant drops is used to reduce the volume of pendant drop in small steps (~ 0.08 to $0.50 \mu\text{L}$ per step) while measuring the IFT (see Figure 4.2).

4.3 Results

4.3.1 Improved DIB Formation Success Rate

We observe that when droplets are conditioned for a few seconds near the air-oil interface, we obtain drastically higher success rates in DIB formation, which are summarized for multiple lipids and oils in Table 4.1. As previously reported by researchers, DPhPC-in produced a near 100% DIB formation success rate in all organic solvents under consideration without any modification to the monolayer. Applying droplet shrinking procedure to the DPhPC coated droplets do not affect the success rate. DOPC and POPC, on the other hand, consistently fail to form DIB

Table 4.1: DIB Formation Success Rates

Lipid	Condition	DPhPC	DOPC	POPC
Hexadecane	without evaporation	10/10	2/20	0/10
	with evaporation	10/10	9/10	9/10
Dodecane	without evaporation	5/5	2/6	0/6
	with evaporation	3/3	7/7	9/12

under all organic solvents. However, application of shrinking procedure is seen to remarkably increase the success rate to near 100%.

Electrical Properties

Electrical resistance, rupture potential and specific capacitance measured for two lipid/organic solvent combinations are provided Table 4.2. DIBs formed with DOPC after shrinking exhibited a higher maximum rupture potential when compared to unconditioned monolayers while no change in rupture potential is observed for DPhPC. The specific capacitance of the bilayer follows a trend that is expected from previously published works; DIBs formed in shorter-chain alkane has a lower specific capacitance when compared to longer-chain alkane. This is due to higher amount of shorter-chain alkane partitioning between the two leaflets of the bilayer.[5]

4.3.2 Dynamic Interfacial Tension Measurements

Fixed-volume pendant drop tensiometer (PDT) is used to characterize the dynamics and the equilibrium IFT of monolayers formed with lipids at an oil-water interface. The decrease in IFT of hexadecane-water interface as a function of time measured using PDT for three different lipids is shown in Figure 4.3; data shown are average traces of 3 or more IFT measurements. DPhPC and DOPC self-assemble to form a monolayer within 500 seconds and result in an equilibrium IFT of 1.18 ± 0.2 mN/m

Table 4.2: DIB measured electrical parameters

Lipid	Resistance ($M\Omega.cm^2$)		Max. Rupture Potential (mV)		Specific Capacitance ($\mu F.cm^{-2}$)	
	Hexadecane	Dodecane	Hexadecane	Dodecane	Hexadecane	Dodecane
DPhPC	8.04 ± 3.6	6.47 ± 1.07	275	200	0.685 ± 0.068	0.386 ± 0.072
DOPC	1.99 ± 0.88	2.775 ± 0.71	150	100	0.652 ± 0.084	0.357 ± 0.074
POPC	1.03 ± 0.68	3.53 ± 2.21	100	125	0.626 ± 0.052	0.553 ± 0.130

and 1.99 ± 0.5 mN/m, respectively. In case of POPC, IFT does not reach a stable IFT value even after 15 minutes of self-assembly and a value of 12.68 ± 1.9 mN/m is recorded, indicating the presence of a partially-packed monolayer.

To investigate how droplet shrinking at the air-oil interface affects IFT of a pre-assembled monolayer, we performed successive step-wise reductions in pendant droplet volume. Figure 4.4(a & b) shows representative step-responses of IFT resulting from step-wise volume reduction performed after reaching an equilibrium tension for DPhPC and DOPC, respectively. In case of POPC, step-wise volume reductions are performed after 15 minutes of self-assembly (Figure 4.4(c)). In all cases, volume reduction steps result in instantaneous reduction in IFT. However, a notable difference in IFT step-response is seen between DPhPC and the other two lipid types. In case of DPhPC, after the instantaneous reduction, the IFT bounces back to a value (1.1 mN/m) close to the equilibrium (1.3 mN/m). Unlike DPhPC, a new, lower equilibrium IFT value is observed for DOPC monolayer. In case of POPC, as the volume reduction steps are performed before reaching an equilibrium value, IFT is reduced in steps until a minimum value (0.73 mN/m in Figure 4.4(c)) is reached. Below a certain IFT (<0.6 mN/m), further reduction in volume causes the interfacial tension to fall below a critical value needed to maintain a pendant drop at the tip of the needle. Figure 4.4(d) compares the step-responses of all three

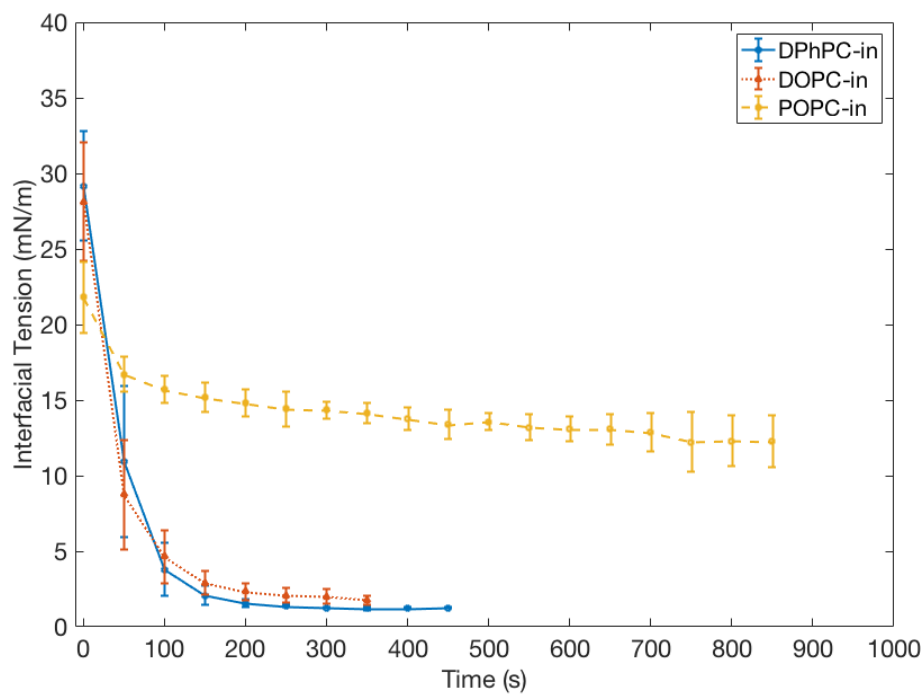


Figure 4.3: Change in interfacial tension with time measured using fixed-volume pendant drop tensiometer.

lipids w.r.t. droplet volume, indicating the minimal change in IFT for DPhPC when compared to DOPC and POPC upon shrinkage. Similar results are observed with other organic solvents (data not shown).

Figure 4.5(a) and 4.5(b) shows the change in IFT upon volume reduction performed on multiple droplets containing DOPC and POPC monolayer, respectively. From these figures, it is clear that volume reduction can consistently lead to reduction in IFT for both the unsaturated lipids.

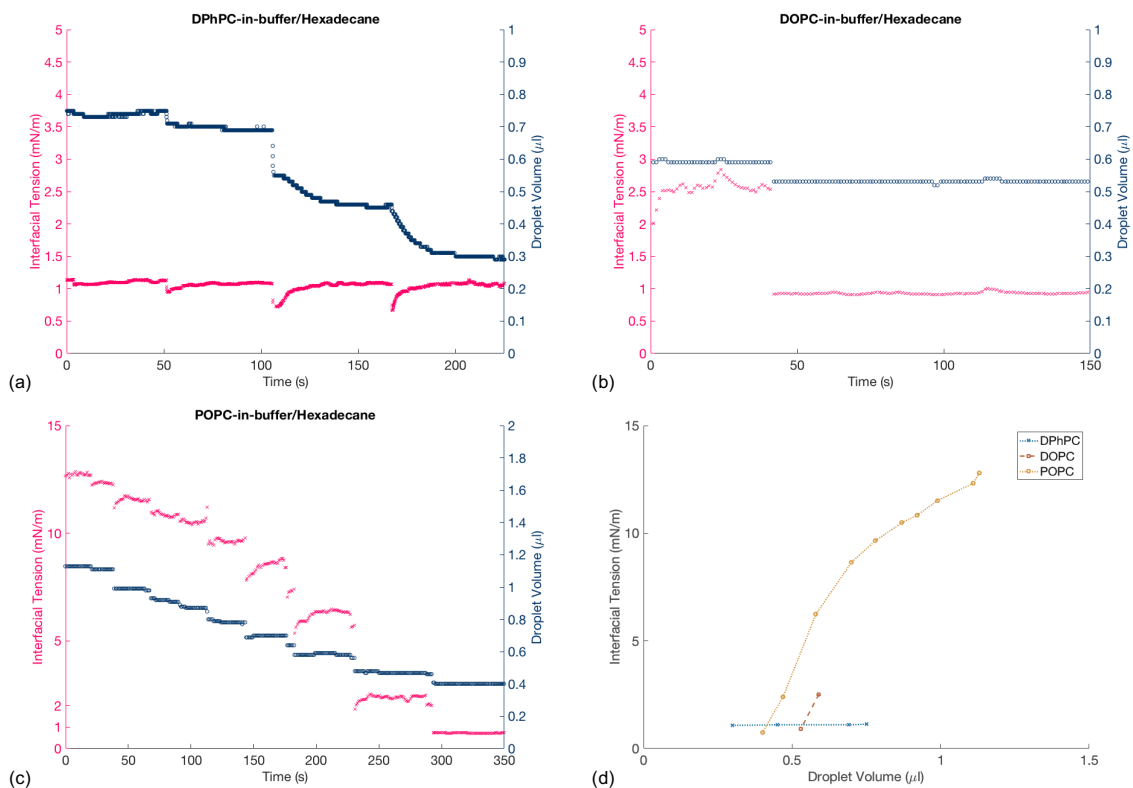


Figure 4.4: Representative IFT traces showing change in tension (blue) induced by step-wise reduction in droplet volume (red) for DPhPC (a), DOPC (b) and POPC (c). Change in IFT w.r.t. droplet volume for data shown in (a-c) is plotted in (d).

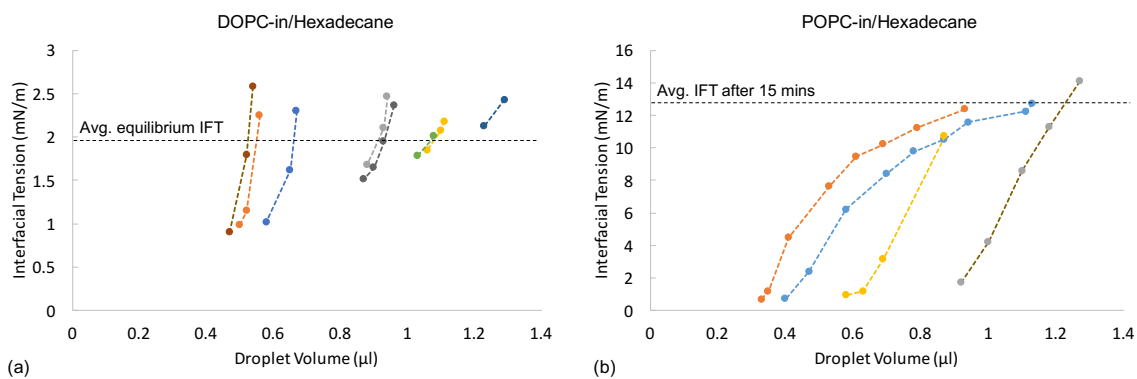


Figure 4.5: Change in IFT induced by step-wise volume change for multiple trials of DOPC (a) and POPC (b) monolayers. Dotted lines in the figure are only for guiding the eye.

Table 4.3: Compression isotherm parameters for pure monolayers.

Lipid	A_{35} (\AA^2)	A_{40} (\AA^2)	Π_c (mN/m)	A_c (\AA^2)	C_s^{-1} (mN/m)
DPhPC	70.2	67.3	42.1	63.9	122.8
DOPC	62.5	57.8	41.7	53.6	64.9
POPC	55.5	52.5	42.7	50.3	93.2

4.3.3 Langmuir Compression Isotherm

To quantify the lateral compressibility of these monolayers and identify differences in area per lipid at the bilayer-monolayer equivalence pressure, we performed monolayer compression isotherm measurements for the three lipids under consideration. Figure 4.6(a) shows the compression isotherms of pure DPhPC, DOPC and POPC monolayers formed at an air-water interface. Surface pressure for DPhPC, DOPC and POPC monolayers begin to increase around 120 \AA^2 , 125 \AA^2 and 107 \AA^2 , respectively. Upon further compression, all three monolayers go through a liquid-expanded state and reaches collapse pressure without going through a LE-LC coexistence state as seen with other lipids such as DPPC. Collapse pressures and area per lipid molecule at three different surface pressure values including at monolayer-bilayer equivalence point of 40 mN/m is provided in Table 4.3.[26] These measured isotherm parameters are in good agreement with previously reported values. At collapse pressure, a single DPhPC molecule takes up a larger area (63.9 \AA^2) when compared to DOPC (53.6 \AA^2) and POPC (50.3 \AA^2).[121, 168, 169] Figure 4.6(b) shows the change in inverse of compressibility modulus (stiffness) as the monolayer is compressed. Highest stiffness was noticed for DPhPC monolayer (122.8 mN/m) while lowest stiffness (highest compressibility) was observed for DOPC monolayer (64.9 mN/m).

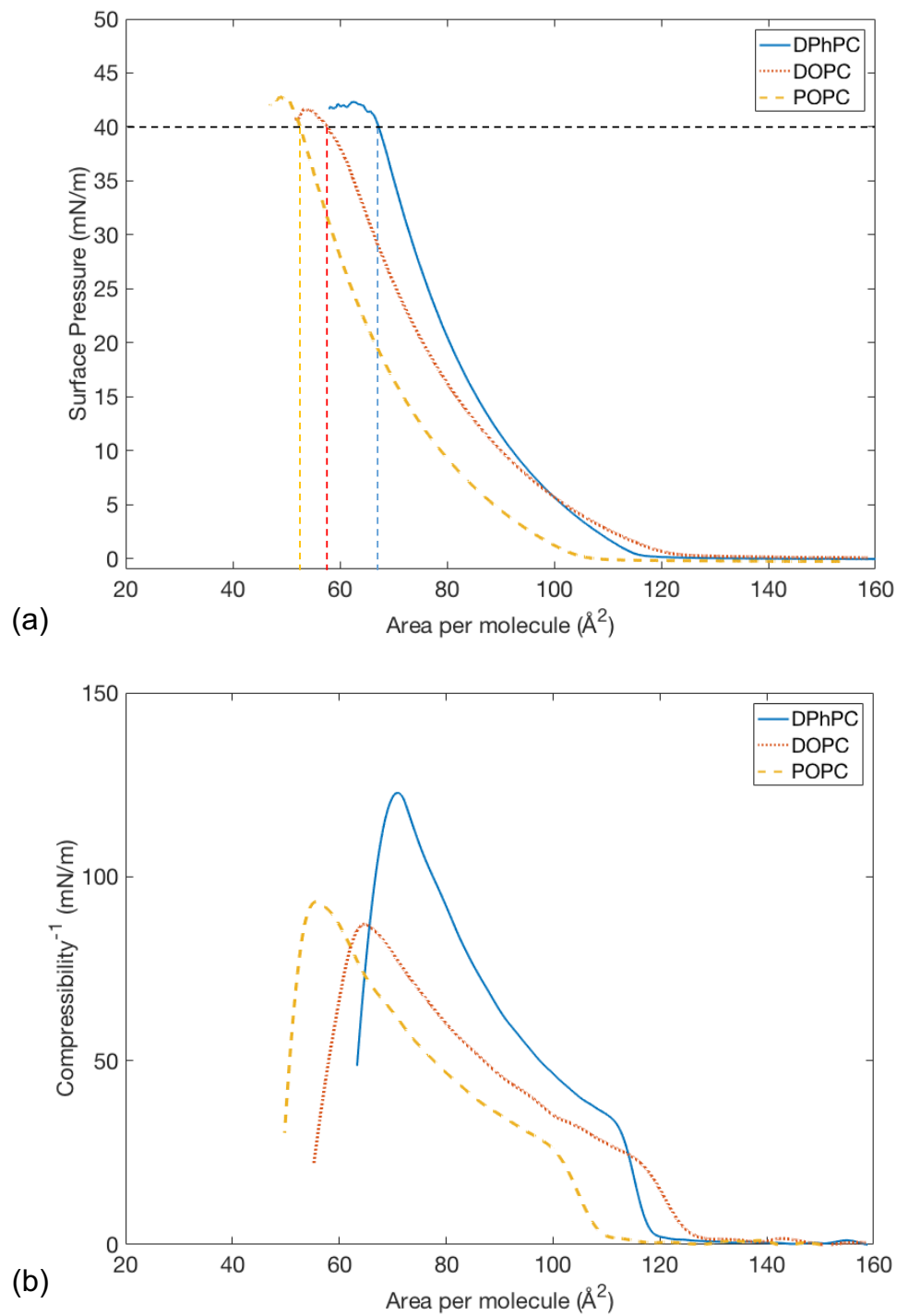


Figure 4.6: Compression isotherm (a) and inverse compressibility modulus (b) for DPhPC (blue solid line), DOPC (red dotted line) and POPC (yellow dashed line). Each curve is average of 3 or more measurements. Black horizontal dashed line corresponds to the bilayer-monolayer equivalence pressure of 40 mN/m.

4.4 Discussion

It is well known that many amphiphilic lipid molecules spontaneously assemble to create a monolayer at an oil-water interface with head groups facing the aqueous phase and tail groups facing the oil phase.[18] Such self-assembled monolayers are essential for the creation of droplet interface bilayers (DIBs).[84] To create a DIB, two or more aqueous droplets each coated with a lipid monolayer are connected under a suitable solvent. If the droplets are not coated or poorly-coated with lipids, the interfacial tension between the OW interface remains high (as high as 44 mN/m). This high interfacial tension creates a thermodynamic drive to fuse the droplets in order to minimize the total surface area; surface area (and, in general, surface energy) of fused droplet is lower than the total surface area of two separate droplets. In DIBs, using a solvent that is "not suitable" also leads to droplet coalescence due to reasons such as high IFT or due to large solvent molecular size.[170] In this chapter, we successfully demonstrate an evaporation-induced monolayer compression technique to improve and, in some cases, enable DIB formation with lipids that were previously known to be unsuitable under three commonly used organic solvents. It is clear from Table 4.1 that a remarkable increase in DIB formation success rate can be realized under all solvents considered by employing the proposed evaporation-technique for DOPC and POPC lipids. In this following discussion, we use results from DIB formation, IFT and compression isotherms to explain the reason for improved success rate attained by evaporation-technique.

Dynamic interfacial tension measurements performed using pendant drop tensiometer reveals that DPhPC lipids, when placed in aqueous droplets as liposomes (lipid-in), self-assemble at a hexadecane-water interface to form a monolayer with an equilibrium IFT (γ_{eq}) of 1.18 ± 0.2 mN/m within 5 minutes (Figure 4.3). As expected, when DPhPC-coated 300 nl droplets are connected under hexadecane after a 5-minute incubation time, the droplets consistently (100% success rate as presented in Table 4.1) zip to form a DIB. On the other hand, same size droplets coated with DOPC

monolayer fail to form DIBs consistently (10% success rate) despite the comparably low equilibrium IFT achieved in under 5 minutes. Longer incubation time does not seem to improve the DIB formation success rate, suggesting that DOPC monolayers with an IFTEq of 1.99 ± 0.5 mN/m is not suitable (not packed enough) for DIB formation.[23] Lastly, as expected from such slow monolayer formation for POPC lipids characterized by a slow reduction in IFT (see Figure 4.3), DIB formation with POPC-coated droplets is unattainable even after 20 minutes of incubation.

If poor DIB formation success rates observed for DOPC and POPC lipids is attributed to poorly- or partially-packed monolayers, increasing the monolayer packing density should improve the success rate. The proposed mechanism for the droplet evaporation technique to improve the success rate of DIB formation is that reducing the surface area of a droplet (by shrinking its volume) that is pre-coated with a partially-packed monolayer will result in lateral compression and tighter packing of phospholipids at the interface, which in turn, should aid/enable bilayer formation.

IFT data presented in Figure 4.5 proves that step-wise volume reductions performed on pendant drops result in a decreased IFT for both POPC and DOPC. Volume reduction steps performed on POPC monolayer at the end of 15 minutes results in reduction in IFT resulting from tighter packing due to the decreased available surface area for each molecule pre-adsorbed in the monolayer at each step. Eventually, a minimum value less than 1 mN/m is consistently observed as shown in Figure 4.5(b). Further reduction in volume causes the drop to fall off the needle, possibly due to further reduction in IFT thus, terminating the measurement. In case of DOPC, although the volume reduction step is performed after reaching an equilibrium IFT, a steady, lower value below 1 mN/m is realized (i.e., $\gamma_{spontaneous} > \gamma_{saturation}$), suggesting a possible packing state that is tighter than equilibrium packing achieved by spontaneous assembly alone. In case of DPhPC, volume reduction steps performed after reaching equilibrium does not result in further decrease in IFT, indicating that the monolayer is already in its tightest packing configuration (i.e., $\gamma_{spontaneous} \approx \gamma_{saturation}$). After the transient reduction in IFT seen immediately after

volume reduction, the tension rises back to its equilibrium value due to the exclusion of excess lipid molecules from the compressed monolayer through buckling. In essence, results from Figures 4.5(b & c) prove that spontaneously assembled monolayers of DOPC and POPC can be compressed to a tighter packing state with lower IFT than that is achieved by self-assembly alone by artificially reducing drop volume. Comparing results from Table 4.1, we find that volume reduction after monolayer formation results in monolayers that are remarkably more suitable for DIB formation than that is achievable by uncompressed, self-assembled monolayers.

4.4.1 Explanation for improved DIB formation success rate

All lipids under consideration are made up of identical phosphatidylcholine (PC) head groups. However, their tail groups vary in length and in composition (see Figure 4.7 inset). DPhPC has two fully saturated 16C fatty acid chains with 4 methyl groups attached to each chain. DOPC is made up of two 18C fatty acid chains with a single double-bond ($\Delta 9$ -Cis) in each chain. POPC, on the other hand, is a hybrid-monounsaturated lipid that is made up of a fully saturated 16C chain and a monounsaturated 18C ($\Delta 9$ -Cis) fatty acid chain. These double bond(s) found in the tail groups of DOPC and POPC are known to induce a bend (often referred to as "kink") in the tail.[40] These kinks weaken the tail-tail interactions between neighboring lipids in the same layer, thereby lowering its gel-to-liquid phase transition (DOPC: -17°C & POPC: -2°C) when compared to their saturated counterparts (DSPC: 55°C & PSPC: 49°C).[171] On the other hand, due to reduced short-range intermolecular interactions caused by the bulky tail groups, DPhPC lipids do not exhibit a clear transition temperature between -120°C and 120°C . [162]

While all three lipid types are expected to be in liquid-disordered phase at RT,[171, 172] the shape and the area occupied by these molecules varies significantly. In a natural membrane, DOPC and POPC molecules are known to induce packing defects due to their conical shapes caused by the kinks in their tail groups. On the other

hand, DPhPC molecules take up a cylindrical shape and thus pack well to form a defect-free planar membrane.[7, 40, 173, 174] Results from monolayer compression isotherm show that at the bilayer-monolayer equivalence pressure of >40 mN/m, the area per lipid molecule is about 67.3 \AA^2 , 57.8 \AA^2 and 52.5 \AA^2 for DPhPC, DOPC and POPC, respectively.

Presence of other types of lipids and biomolecules in the monolayer assembly can lead to change in the packing properties of the membrane. Previously reported compression isotherms of DOPC and POPC monolayers in the presence of cholesterol have shown that cholesterol molecules impose a spatial restriction on the tail groups and drive the lipid molecules to pack closer (reduced area per molecule), thereby reducing the extent of packing defects.[31, 175] For instance, addition of 0.25 molar fraction cholesterol in a monolayer has been shown to reduce the area/lipid by about 10 \AA^2 . [171] X-ray diffraction studies have revealed that even non-surface active molecules such as alkanes partition in between the hydrocarbon tail groups in a monolayer and change its packing and thermodynamic properties.[115, 176–179] Compression isotherm experiments by Thoma et al reveals that higher amounts of alkanes can be found partitioned among the DPPC tail groups if the length of hydrocarbon chains match the length of lipid tails.[113]

Now, combining our understanding of lipid monolayers at an oil-water interface with compression isotherm and IFT measurements, we conclude that due to the conical shape of DOPC, the self-assembled monolayer is, a) not packed to its maximum packing density and contains great degree of packing defects, and b) incorporates solvent molecules in the defects found in between its tail groups (see schematic in Figure 4.7(b)). Reduction in area available for each lipid, brought about by decreasing droplet volume, forces the molecules to come closer and pack in a state that is not achieved with spontaneous assembly alone. Upon lateral compression, the increased spatial restriction reduces the defects caused by the kinks in tail groups by packing the lipids tighter and, in addition, squeezes out the solvent molecules from the monolayer into the bulk.[113] This in turn, leads to a decreased IFT as

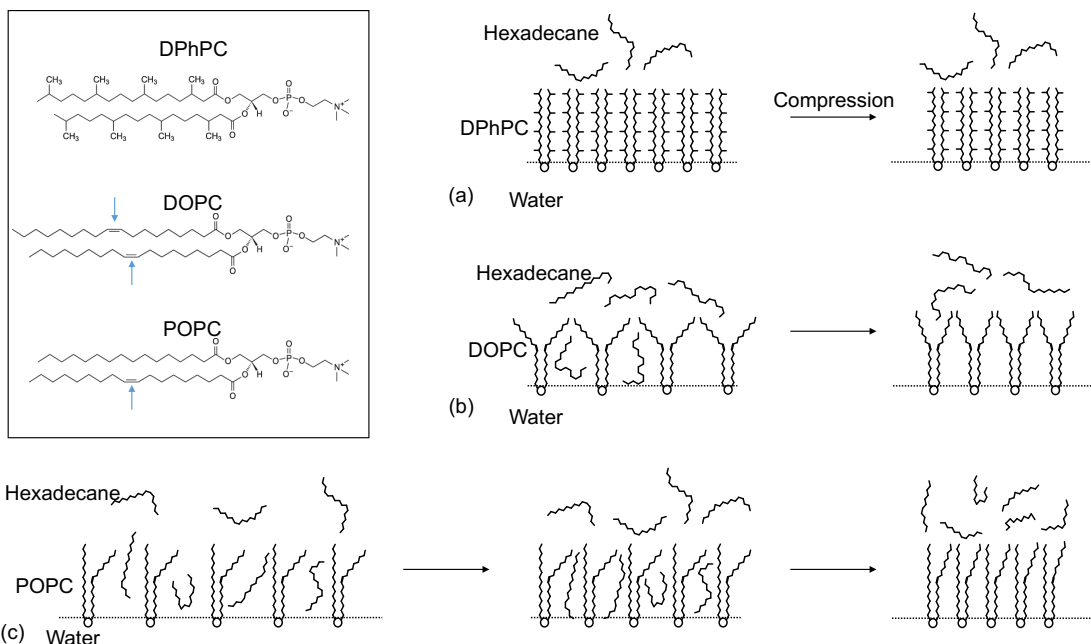


Figure 4.7: Sketch showing organization of DPhPC (a), DOPC (b) and POPC (c) molecules and hexadecane molecules in a monolayer formed at a hexadecane-water interface before and after compression. The chemical structures of lipids are provided in inset with arrows pointing at the double-bonds found in the fatty acid chains.

shown in Figure 4.4(a). In case of POPC at the end of 15 minutes, the monolayer bares poorly-packed lipids with solvent molecules interdigitated in between the tails. Upon compression, the packing density is increased, and eventually the tail groups are compressed together, thereby forcing the solvents molecules to exclude from the monolayer (see Figure 4.4(c)). We believe that the improved DIB formation success rate is due to the combination of increased lipid packing density and a monolayer that is free of solvent. Lastly, in case of DPhPC, which are cylindrically shaped with bulky tails, the lipid molecules are in its tightest packing state at equilibrium with minimal defects, thereby leaving very little free volume for organic solvent to partition into the monolayer. Laterally compressing this monolayer leads to exclusion of DPhPC molecules into the bulk phase with no change in packing density, hence the unchanged IFT (in Figure 4.4(a)) and success rate.

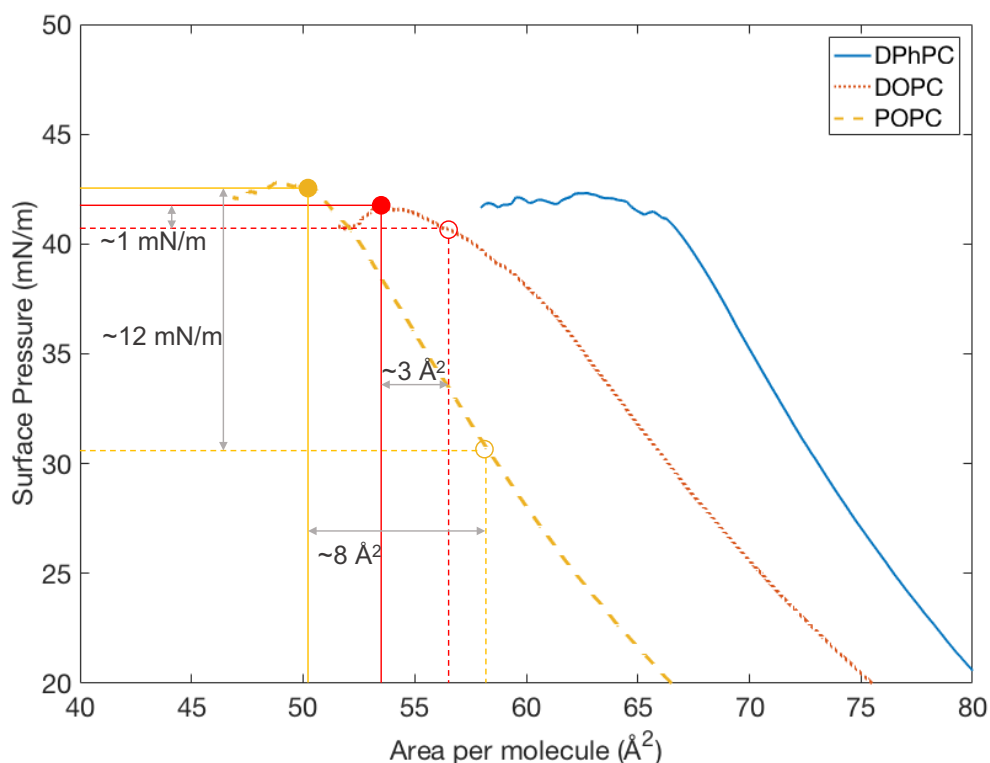


Figure 4.8: Compression isotherms indicating collapse pressures (shaded circles) and estimated pressure corresponding to spontaneously assembled monolayer (unshaded circles).

4.4.2 Decrease in Area/lipid: comparing compression isotherm with IFT

As direct comparison of IFT that is measured at OW interface (using PDT) and surface pressure that is measured at WA interface (using Langmuir trough) is not feasible, we make the comparison by equating the change in IFT with change in surface pressure. Assuming the minimum tension reached in PDT measurements (Figure 4.5) corresponds to the maximum (collapse) pressure in compression isotherm (Figure 4.6(a)) for the given lipid type, we estimate the change in area per lipid induced by the volume reduction steps. Shaded circles in Figure 4.8 represents the collapse surface pressure of each monolayer and now assumed to correspond to the average lowest IFT in PDT measurements (0.97 mN/m for DOPC and 1.02 mN/m

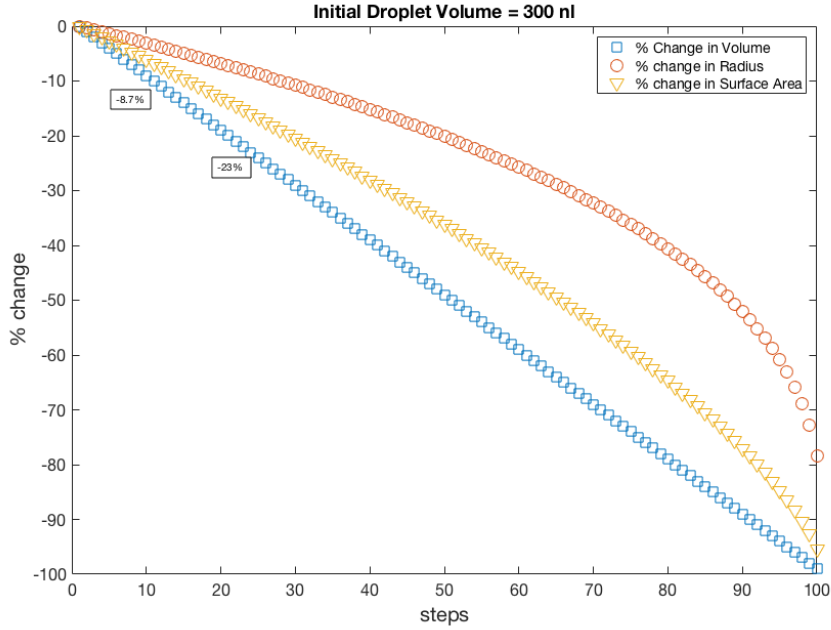


Figure 4.9: Comparing percentage change in Volume, Surface Area and Radius of 300 nl droplet.

for POPC). The total change in IFT, $\Delta\gamma$ attained by volume reduction steps is given by $\gamma_{spontaneous} - \gamma_{min}$. Subtracting $\Delta\gamma$ from collapse pressure (Π_c), should give us the surface pressure that is achieved by spontaneous assembly ($\Pi_{spontaneous}$) alone. These estimated $\Pi_{spontaneous}$ for DOPC and POPC is marked by unshaded circles in Figure 4.8. Making this calculation enables us to a) estimate the area per lipid molecule in the monolayer that is attained by spontaneous assembly alone, and b) calculate the change in area per lipid molecule that is brought about by the step-wise volume reduction. According to this, Figure 4.8 suggests that each DOPC molecule in a spontaneously assembled monolayer takes up about 50.6 \AA^2 , which is $\sim 3 \text{ \AA}^2$ (5.6%) more than area at collapse pressure. In case of POPC, each molecule in the monolayer attained at the end of 15 mins takes up about 42.3 \AA^2 , which is $\sim 8 \text{ \AA}^2$ (16%) more area than at its collapse pressure i.e., maximum packing.

4.4.3 Required Volume Reduction and Period of Evaporation

The above analysis is used to estimate the amount of shrinkage in droplet volume required to achieve the tightest packing before connecting them to droplets to successfully form a DIB. Assuming a lipid-coated aqueous droplet to have a spherical shape, a 300 nl droplet has a surface area of 2.17 mm². A 6% and 16% reduction in area per molecule required for DOPC and POPC requires a final surface area of 2.04 mm² and 1.82 mm², respectively. In terms of volume, the final volume is about 274 nl (8.7% shrinkage) and 231 nl (23% shrinkage) (see Figure 4.9). In case of POPC, we experimentally find that the volume reduction required is about 20% even with a 5-minute incubation time. In other words, droplets with POPC liposomes does not require a 15-minute incubation before performing evaporation-induced shrinking. This is probably due to the fact that a) droplets used in DIB experiments are 300 nl as opposed to 1-2 μm droplets used in pendant drop IFT measurements, and b) self-assembly of lipids and evaporation can take place simultaneously and collectively reduce the required incubation time.

The above analysis, in conjunction with an independent study to measure the rate of evaporation of DI water droplets held at OA interface, can be used to estimate the period of time a lipid-coated droplet is required to be held at the OA interface. We estimate a 0.4 nl/s evaporation rate of DI waters placed at the OA interface (see Appendix A.3). Therefore, we conclude that holding aqueous droplets at OA interface for 15-20 seconds after 5 minutes of incubation time should compress the monolayer enough to pack the lipids to its tightest state and condition the monolayers to be suitable for DIB formation.

It is important to note that the low IFT data measured using pendant drop tensiometer is measured using droplets sized (1-2 μl). While the accuracy of tension values may be compromised by small droplet size, the deformation seen in these droplets with very low IFTs are significant enough to make accurate measurements. Quantitatively, the Beta value — a value corresponding to the shape factor of

the droplet, is found to be within the recommended range (recommended Beta = 0.2 to 0.4). It is also important to note that the comparative analysis of IFT and compression isotherm data in Figure 4.8 is performed only to get an estimate of possible area change obtained by lateral compression. The true values of the estimated change in area is subjected to high variability based on the accuracy of either measurements; area per molecule values in compression isotherm are affected drastically by experimental procedures and are found to be highly variable in literature.[180]

4.5 Summary

In Summary, we demonstrated a simple evaporation-induced monolayer compression technique to condition monolayers that are made up of unsaturated lipids in order to enable DIB formation. To understand the change in physical state of monolayer, we utilized pendant drop tensiometer and Langmuir trough compression isotherm to estimate the steady-state interfacial tension and area per lipid in a monolayer, and how these physical parameters change upon lateral compression. Lastly, we report electrical properties of DIBs formed with DOPC and POPC, under three different organic solvents, that were previously unable to determine due to their inability to form stable bilayers.

Chapter 5

Improving Bilayer Stability and Portability Using Polymer Encapsulation

5.1 Introduction

Conventional DIBs are formed with two immiscible liquid phases placed in an open substrate, consequently making it prone to spillage, contamination and requires delicate handling with very limited portability. Thus, a convenient and robust DIB platform with an significantly improved durability and portability without compromising the basic functionalities of a lipid bilayer is still needed. In this chapter we present results from our efforts to fulfil this need. *

*Results presented here are reproduced from our published work: Venkatesan, Guru A., and Stephen A. Sarles. "Droplet immobilization within a polymeric organogel improves lipid bilayer durability and portability." *Lab on a Chip* 16.11 (2016): 2116-2125.

5.2 Objective and Approach

The objective of this work is to improve to transform DIBs, a lab-based technique, into a more portable and durable material system that is easier to handle without compromising membrane integrity or functionality or losing advantages of a conventional DIB system. We study the use of a phase-changing poly[styrene-*b*-(ethylene-co-butylene)-*b*-styrene] (SEBS) organogel that solidifies from a molten liquid to a soft elastic gel at $\sim 40^\circ\text{C}$ for developing a novel liquid-in-gel encapsulated DIB system that has improved portability and durability as compared to DIB systems that have been studied thus far. This temperature-sensitive organogel material is made by dissolving SEBS, a triblock copolymer and thermoplastic elastomer, in hexadecane and heating the mixture to $>40^\circ\text{C}$; we use this molten mixture to replace the bulk organic phase that surrounds the lipid-coated aqueous droplets. To properly examine this substitution, we perform experiments on DIBs formed in the presence and absence of SEBS at both 50°C and near room temperature to confirm that both lipid monolayer self-assembly and bilayer thinning between droplets are unobstructed by the presence of SEBS polymer molecules in the oil. We also record alamethicin ion channel gating in liquid-in-gel DIBs to demonstrate that the basic structural and functional properties of the lipid bilayer are retained, and we demonstrate that droplet encapsulation using organogel successively immobilizes droplets in place and cushions them during accelerations, thereby achieving increased DIB durability and portability.

5.2.1 Liquid-in-gel DIB formation

In addition to the experimental setup required for forming conventional DIB as mentioned in Chapter 2, a heating module consisting of a heating pad and a thermocouple are used to assemble organogel-encapsulated DIBs. A 30 mm x 30 mm resistive heating element (Omega, KHLV-101/10) is placed underneath a PMMA or PDMS substrate and connected to a BK Precision 1788 digital power supply. The tip of a thermocouple (Omega, P/N:JMTSS-020U-6)) probe is placed under

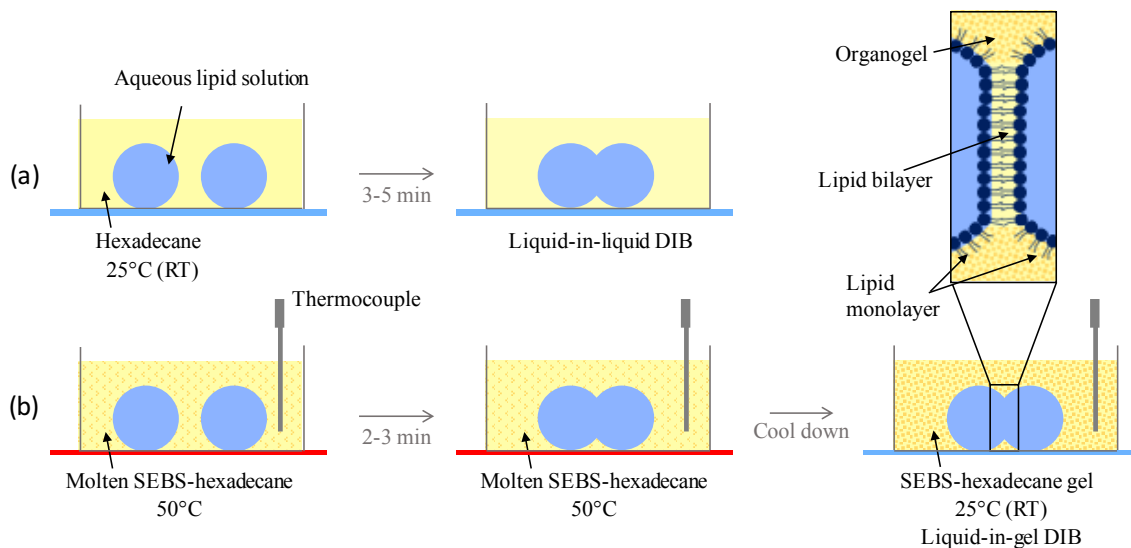


Figure 5.1: Procedure for assembling a single DIB using: A) the liquid-in-liquid method, and B) the liquid-in-gel method. Note: electrodes not shown for clarity.

the bulk solvent, adjacent to the aqueous droplets as shown in Figure 5.1(b). This allows close monitoring of the temperature of the external phase that surrounds the droplets. First, about 250 μl of molten SEBS/hexadecane solution is dispensed into the droplet compartment and the heater is turned on such that the temperature in the droplet compartment reaches 50°C. At this temperature, the SEBS/hexadecane mixture remains in the molten phase with a viscosity of $\sim 16\text{mPa}\cdot\text{s}$. In comparison, hexadecane and AR20 silicone oil (Sigma Aldrich), which have both been used as the oil phase for DIB formation at room temperature, have viscosities of 3 mPa.s and 20 mPa.s, respectively. 200-500 nl aqueous droplets are then pipetted into the substrate and are brought together after 2-3 minutes to form a DIB. Once the bilayer is formed, the heater is turned off to passively cool ($\sim 2^\circ\text{C}/\text{min}$ maximum cooling rate) the system to room temperature. The molten SEBS/hexadecane mixture starts to gelate upon cooling below 40°C where it turns into a weak gel at room temperature with a storage modulus of $\sim 11\text{ Pa}$ at 1 rad/s (liquid to gel transition can be observed as cooled below 40°C).

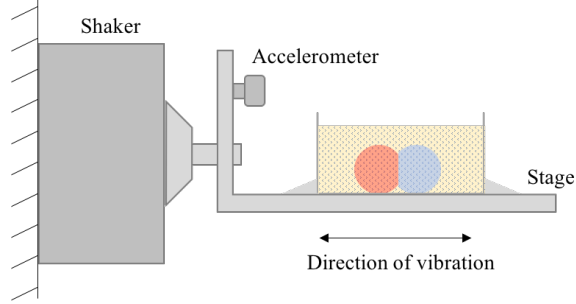


Figure 5.2: Schematic of experimental setup for durability test.

5.2.2 DIB Durability Test

The durability of DIBs is quantified by performing vibration experiments in which the DIB embodiments are vibrated horizontally in a direction perpendicular to the bilayer as shown in Figure 5.2. The DIB systems are vibrated at multiple frequencies ranging from 10 Hz to 60 Hz and varying displacements in order to impose a range of accelerations. An L-shaped stage made of aluminum is fixed to an electromagnetic shaker (Brüel & Kjaer 4810), which is mounted firmly on a vibration isolation table. The shaker is driven by a sinusoidal voltage waveform output by a custom LabVIEW program. A KEPCO BOP 20-5D power amplifier is used to deliver the required current to the shaker. An accelerometer (PCB Piezoelectronics; model 480E09) is mounted on the aluminum stage in the direction of the vibration to measure the amount of applied acceleration. The voltage output from the piezoelectric sensor is digitized using the Digidata 1440A and the acceleration is computed using AxoScope software. In addition to the vibration experiment, the durability of the liquid-in-gel DIB is also investigated by performing a simple drop experiment in which a PDMS substrate containing a liquid-in-gel DIB is dropped from varying heights onto a table until the bilayer ruptures and the droplets coalesce. Visual detection of droplet coalescence is aided by adding water-soluble food coloring into one of the two droplets.

5.3 Results and Discussion

5.3.1 Rheology Measurement

Rheometric measurements were performed by using a parallel plate rheometer (TA Discovery Hybrid Rheometer). Experiments were run from 25°C to 55°C with 5°C steps from angular frequencies 0.25 rad/s to 100 rad/s.

5.3.2 Encapsulation of DIB

SEBS triblock copolymer consists of glassy polystyrene (PS) endblocks and a rubbery poly(ethylene-butylene) (PEB) midblock. The SEBS (Kraton G1650) used in this work is 31% polystyrene with a fractional molecular weight of 27 900 g mol⁻¹ and 69% poly(ethylene-butylene) with a fractional molecular weight of 62100 g mol⁻¹. [181] When mixed with a midblock-selective solvent such as hexadecane at elevated temperature (>100°C), a clear homogenous solution is obtained in which the polymer molecules exist in disordered state. When cooled below the order-disorder transition temperature (~45°C; see Figure 5.3(A-C) for rheology data), SEBS triblock molecules microphase segregate to form a weak gel in which the polymers are present in an ordered state. During this microphase segregation (order-disorder transition), the PS-endblocks that are insoluble in hexadecane cluster together to form nanoscopic micelle cores, while the soluble PEB-midblocks either loop into the same PS core or span between adjacent PS cores in a hexadecane-filled inter-micellar space to form a continuous organic gel. [182, 183] At high concentrations of SEBS/hexadecane (≥ 50 mg ml⁻¹), the organogel shows flexibility and retains its shape (see Figure 5.5(D)); at 10 mg ml⁻¹ used herein for encapsulation, the gel does not hold shape very well and is considerably more viscous. While this process requires heating to ~45°C, we note that this temperature is below the denaturation temperature of many peptides and proteins, including that for alamethicin, α -hemolysin, and bacteriorhodopsin, which denature above 65°C, [184, 185] which have been frequently incorporated into DIBs

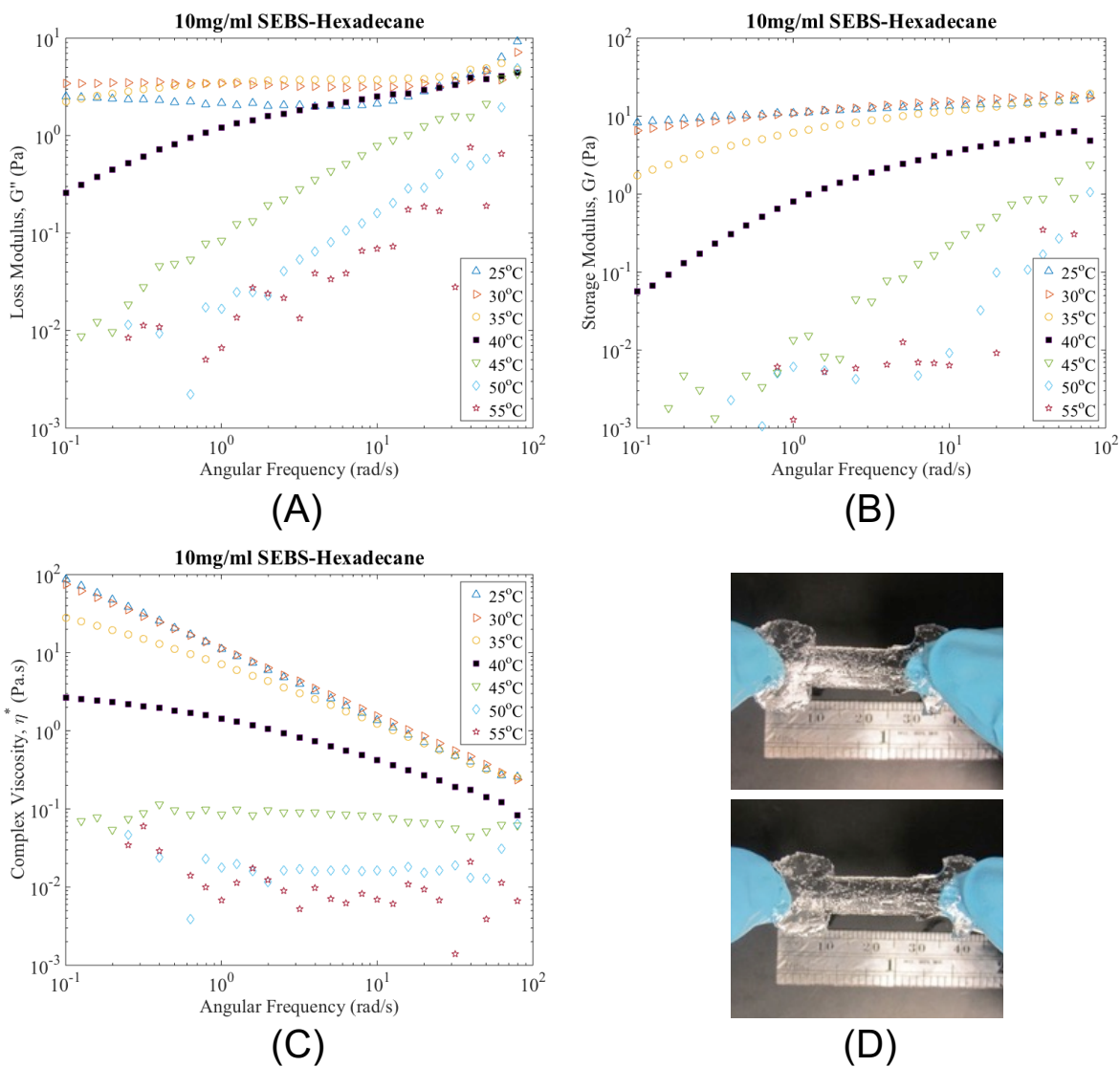


Figure 5.3: Loss modulus (A), storage modulus (B), and complex viscosity (C) of 10 mg/ml SEBS/hexadecane mixture plotted with respect to angular frequencies at various temperatures (25-55°C). A dog-bone shaped specimen made from 50 mg/ml SEBS/hexadecane shows flexibility and shape retaining property of the organogel (D).

to provide stimuli-responsive functionality or enhance transport. Therefore, this material should be compatible with many types of functional biomolecules.

It has been shown previously that connecting aqueous droplets containing DPhPC liposomes after incubating them in hexadecane for 5 minutes at room temperature yields DIBs nearly 100% of the time. For the same sized droplets placed under molten SEBS/hexadecane at 50°C, we observe that droplets in contact spontaneously form a stable adhesive interface at a rate of ca. 80% ($n = 40$ trials) when they are joined after 2 to 3 minutes for monolayer assembly. In contrast, droplet coalescence occurs when the incubation time is shorter than 1 minute. Yet, longer incubation time does not improve the success rate of DIB formation. In fact, connecting droplets after more than 5 minutes of incubation results in neither coalescence nor spontaneous bilayer thinning. The observation that droplets simply remain separate instead of forming an adhesive connection suggests either that SEBS triblocks interact with the lipid monolayers or multiple layers of lipids assemble at the oil-water interface,[151, 165] both which make bilayer formation unfavorable. Compared to assembly of lipids in the absence of SEBS and at room temperature, we attribute the shorter incubation time required for droplets placed in molten organogel versus hexadecane to the increased rate of monolayer assembly expected at an elevated temperature. DIBs formed in molten gel are found to be stable for several minutes. However, we observe that usually within 10 minutes, the droplet pair fall off the suspended wire-type electrodes, which is likely due to accelerated droplet shrinkage at an elevated temperature which we believe leads to a decreased interfacial tension and poorer adhesion to the electrodes caused by tighter packing of lipids in the monolayer. Cooling the system to room temperature causes the organic phase to gel. Similar to the use of microfluidic methods for DIB encapsulation,[186] this transformation restrains the droplets in place and preserves electrical contact with the droplets without disturbing the bilayer formed at the interface. Once cooled, the bilayer is found to be stable for a minimum of 12 hours, similar to that observed for conventional DIB. Figure 5.4 shows bright-field images of a DIB in molten and cooled SEBS gel. Unlike prior studies which yielded

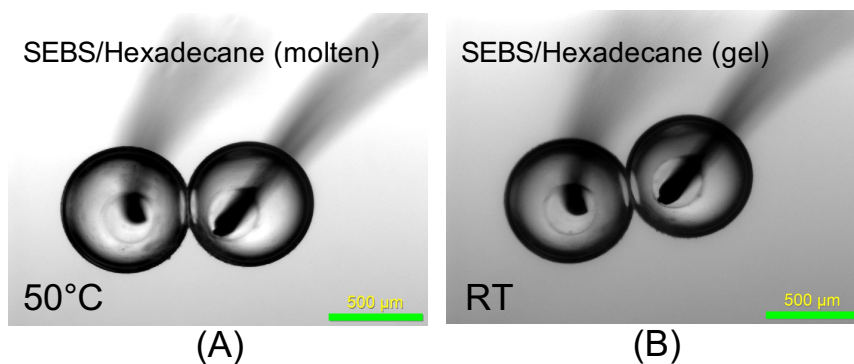


Figure 5.4: Micrographs of a DIB formed in molten 10mg/ml SEBS-gel (A) and cooled to room temperature (B). Scale bar represents 500 μm .

membranes that were sandwiched between hydrogels,[125] this approach results in a liquid supported bilayer between organogel-encased droplets. The system can also be reheated to re-melt the SEBS gel without rupturing the bilayer (Figure 5.5(A & C)). Attempts to assemble DIBs in higher concentration SEBS/hexadecane ($>30 \text{ mg ml}^{-1}$) requires heating the system to higher temperatures ($>60^\circ\text{C}$) which lowered the success rate for DIB formation.

5.3.3 Capacitance vs temperature

An important aspect of this work is to determine if SEBS copolymers present in the external medium can stabilize the interface between droplets in the absence of lipids. As a control experiment, aqueous droplets devoid of lipids are placed in molten SEBS/hexadecane solution and brought into contact after 20 minutes of incubation. These experiments ($n = 5$) repeatedly show that droplets coalesce when placed in contact under molten SEBS/hexadecane without lipids present. This finding affirms prior interfacial tension measurements,[187] which showed that, despite being amphiphilic, these polymer molecules do not self-assemble at an oil-water interface like lipid molecules to form a monolayer. As a result, we would not expect, nor do we find, that SEBS molecules can stabilize the interface between two droplets.

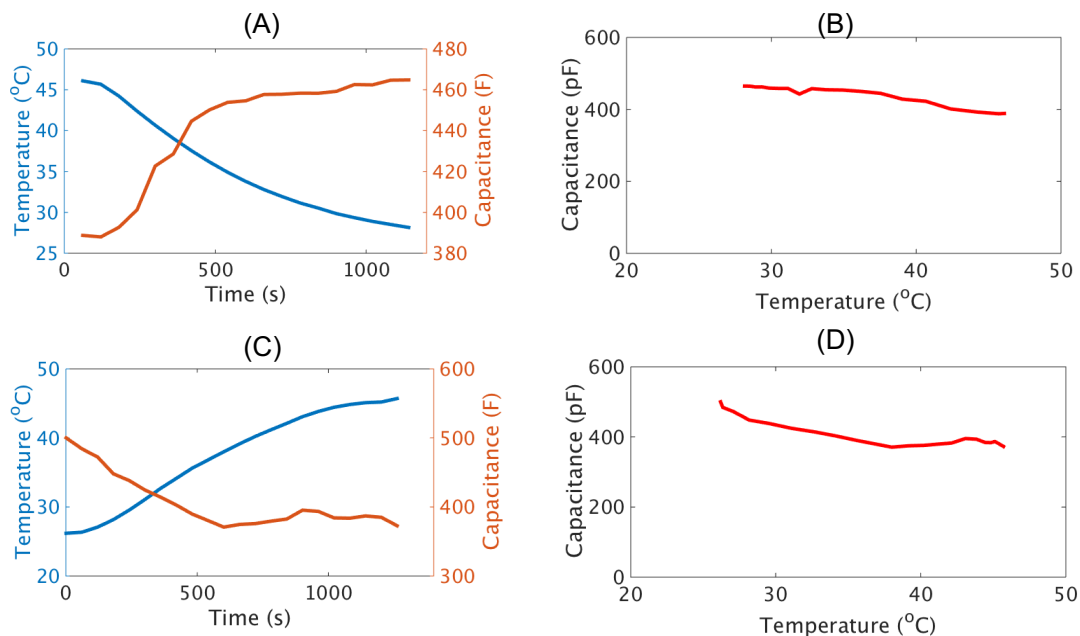


Figure 5.5: Change in nominal bilayer capacitance and temperature with time as a DIB formed in SEBS-gel is cooled (A) and heated (C). Change in capacitance of the same bilayers plotted w.r.t. temperature as the system is cooled (B) and heated (D).

5.3.4 Characterization of encapsulated DIB

Thickness Estimation

Thickness of the interface formed between the droplets is measured to determine if SEBS polymer molecules are trapped in the bilayer or not. This is done by measuring and comparing specific capacitance, C_m of interfaces formed in the presence and absence of SEBS. Unfortunately, the C_m -measurement technique described in Chapter 2 is inapplicable for the liquid-in-gel system at room temperature since the positions of droplets are severely constrained in gel-encapsulated DIBs. Instead, C_m measurements are only performed on molten gel encapsulated DIBs (at 50°C) for which droplet manipulation is not inhibited by solidified organogel.

Specific capacitance, C_m of liquid-in-liquid DPhPC DIBs in hexadecane is found to be $0.75 \pm 0.07 \mu\text{F}\cdot\text{cm}^{-2}$ (Table 5.1). Using the same measurement technique, Taylor, et al recently reported C_m values of $0.708 \pm 0.02 \mu\text{F}\cdot\text{cm}^{-2}$ for DPhPC bilayers

Table 5.1: Electrical and physical properties of liquid-in-liquid and liquid-in-gel DIBs

Property	Liquid-in-liquid		Liquid-in-gel	
	RT		RT	50°C
Specific Capacitance, C_m ($\mu\text{F}\cdot\text{cm}^{-2}$)	0.75 ± 0.07		-	0.72 ± 0.05
Estimated Bilayer Thickness, d (nm)	2.6 ± 0.2		-	2.7 ± 0.2
Resistance ($\text{G}\Omega$)	218.9 ± 72.3		257.6 ± 68.9	99.3 ± 69.8
Rupture Potential (mV)	219 ± 24		196 ± 34	161 ± 32
Electro-wetting constant, α (V^{-2})	11.82 ± 1.6		8.2 ± 2.2	18.7 ± 3.5

formed in hexadecane at 50°C.[94] Note that the reduced C_m at higher temperature is due to the increase in the amount of hexadecane present in the bilayer region. In comparison, the interface formed between aqueous droplets encapsulated in molten SEBS-gel at 50°C is found to have a specific capacitance of $0.72 \pm 0.05 \mu\text{F}\cdot\text{cm}^{-2}$, which is not significantly different ($t(10)=0.542$, $p=0.599$) from that of liquid-in-liquid DIBs formed in hexadecane at the same temperature. Using Equation 1, we see that these values for C_m yield estimates of ca. 2.6-2.7 nm for the hydrophobic thickness of the membrane in the presence and absence of SEBS in the surrounding medium at 50°C. These statistically similar values, which match well with the literature, thus prove that the interface between droplets is that of a single lipid bilayer and that it does not contain any trapped SEBS in the molten state.[5, 147]

It is well established that small hydrophobic molecules, like those of n-alkanes of equal or lesser length than that of the phospholipid acyl chains,[188] can remain trapped in a planar lipid bilayer. More specifically, the presence of solvent in a bilayer can increase membrane thickness (and thus decrease specific capacitance) as well as increase the lateral tension of bilayer due to increasing spacing between neighboring lipids. In DIBs, where the volume of the aqueous phase is conserved, increasing the bilayer tension relative to that of the monolayers results in a decrease in the area of adhesion between adhesive droplets. For example, a DIB in decane ($142 \text{ g}\cdot\text{mol}^{-1}$) has more solvent in the bilayer region leading to higher bilayer tension and a smaller

bilayer area than is obtained with hexadecane ($226 \text{ g}\cdot\text{mol}^{-1}$) as the oil. Conversely, a larger-molecule solvent such as squalene ($411 \text{ g}\cdot\text{mol}^{-1}$) yields a more "solvent-free" DIB with a larger contact area due to the poorer solubility of the oil in the acyl chains of the monolayers.[189] The SEBS copolymers used in this work are significantly larger ($90 \text{ kg}\cdot\text{mol}^{-1}$) than solvents such as hexadecane and squalene used to form DIBs to-date. Therefore, SEBS molecules are expected, and found (at 50°C), to be completely excluded from the hydrophobic region of the bilayer, but not necessarily change how much hexadecane remains in the membrane ($<10\%$ for DPhPC bilayers at RT).[5] As a result, the estimated hydrophobic thicknesses of bilayers formed in liquid-in-gel system in the molten state are very similar to those of liquid-in-liquid DIBs formed in hexadecane alone.

Achieving a polymer-free DIB in the molten state for the organogel mixture also means that it is highly unlikely for polymer species to enter the membrane upon cooling to the gelled state, where triblocks integrate into a gel network that has an even higher molecular weight. Specifically, at room temperature, the interconnected polystyrene cores in this gel matrix are found to be about 7 nm wide,[181] which makes it highly unlikely for SEBS polymers or aggregates to enter the hydrophobic region of the bilayer. Note that the slight reduction in nominal membrane capacitance during cooling process (Figure 5.5(B)) is due to the reduction in the amount of hexadecane trapped in the bilayer region. This further supports our claim that polymer molecules do not incorporate into membrane upon cooling (or reheating).

Electrical Characterization

The electrical properties of liquid-in-liquid DIBs and liquid-in-gel DPhPC DIBs are also compared in Table 5.1. A high bilayer resistance is indicative of a desirable leak-free membrane. Figure 5.6 shows the current-voltage response from which resistance is calculated as described in Chapter 2. Rupture potential gives information regarding the practical voltage range that can be applied to the bilayer before complete breakdown of bilayer takes place, causing droplet coalescence. Resistance

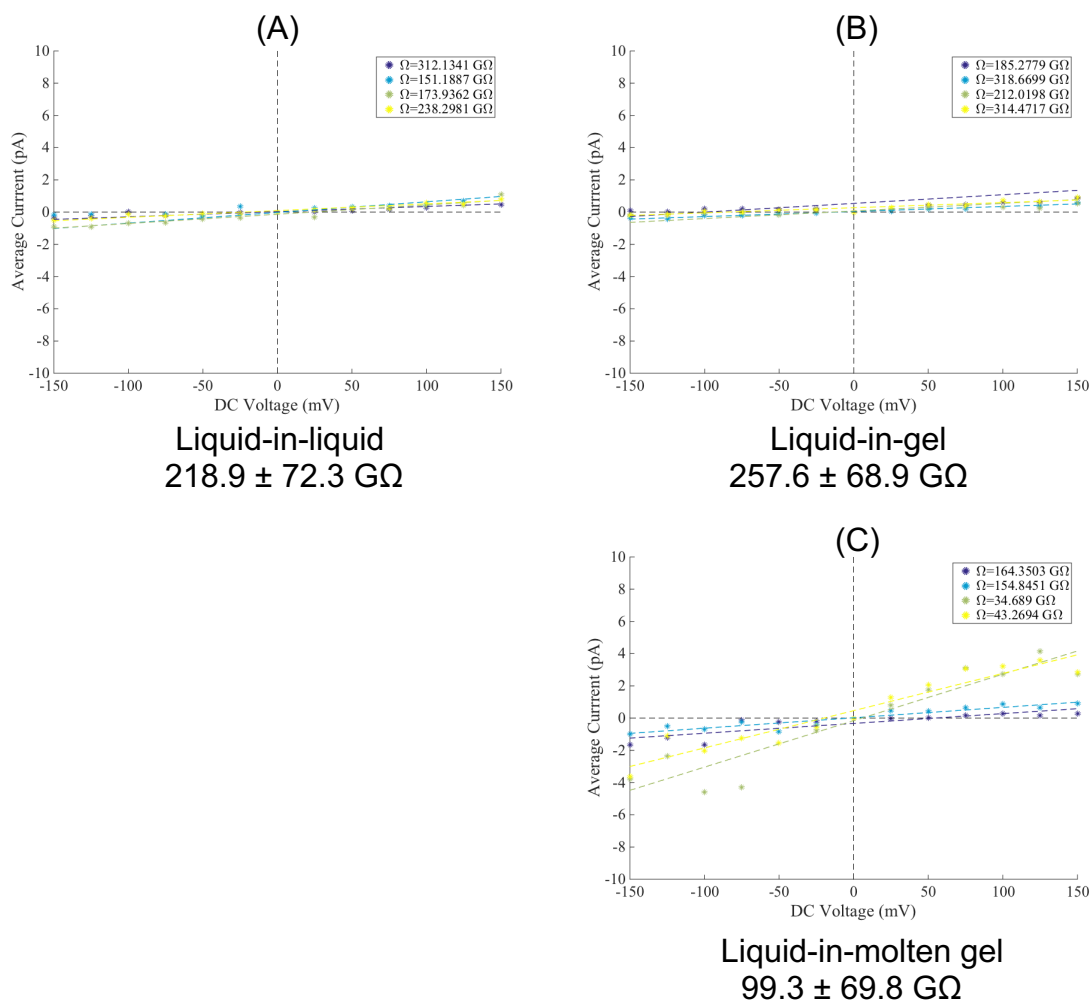


Figure 5.6: Electrical resistances of A) liquid-in-liquid, B) Liquid-in-gel (20°C), and C) Liquid-in-molten gel (50°C) are calculated by finding the slope of the current versus voltage plot.

and bilayer rupture potential of liquid-in-gel DIBs ($257 \pm 68.9 \text{ G}\Omega$; $196 \pm 34 \text{ mV}$) are found to be not significantly different from that of liquid-in-liquid DIBs ($218.9 \pm 72.3 \text{ G}\Omega$; $219 \pm 24 \text{ mV}$); unpaired t-test values for resistance ($t(6)=0.77$, $p=0.468$) and rupture potential ($t(6)=1.105$, $p=0.311$) further prove that these membrane properties are statistically similar (i.e., $p>0.05$). However, the electrical resistance of liquid-in-molten gel DIBs are found to be significantly lower than liquid-in-gel DIBs; a calculated t-test value of $t(6)=3.228$, $p=0.018$ is obtained, which shows that the

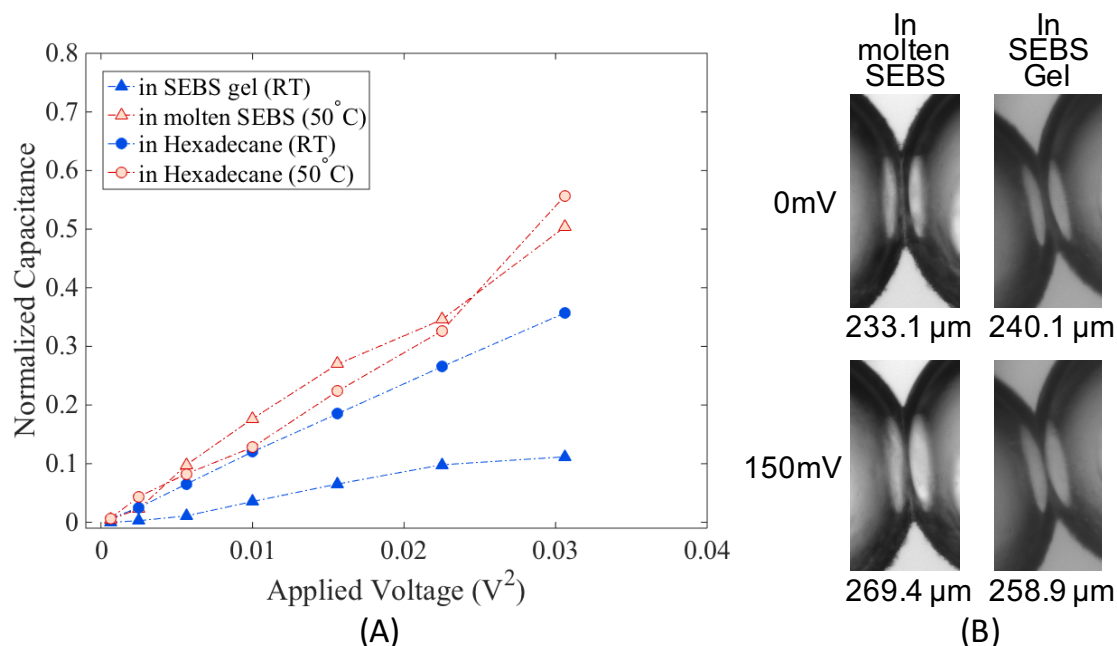


Figure 5.7: Electrowetting behavior of DIB SEBS-gel and liquid-in-liquid DIB at RT (blue) and 50°C (red); the increase in capacitance of bilayer with applied voltage is plotted according Equation 1 (A). (B) Bright-field microscopic images of a single DIB at 0 and 150 mV applied voltage in molten and gelled SEBS.

membrane resistance is statistically higher once the system is cooled. A decrease in bilayer resistance at elevated temperatures has been reported in previous works.

Electrowetting Responses to Assess Gel Confinement of DIBs

Application of a voltage across a lipid bilayer reduces its lateral tension due to the electrowetting of the dielectric between droplets, which increases the contact angle between the pair and the interfacial area, due to the conservation of droplet volume.[91] This increase in bilayer area causes nominal membrane capacitance to increase with the magnitude of the applied voltage. In oil-rich membranes, an applied voltage can also increase the capacitance per unit area of a membrane as a result electrostriction that reduces the hydrophobic thickness of the bilayer. However, this increase in specific capacitance was found to be relatively insignificant ($<1.5\%$

for $\pm 100\text{mV}$) for DPhPC bilayers formed in hexadecane. Therefore, the nominal capacitance of a DIB in hexadecane is expected to increase as given by

$$C(V) = C_0(1 + \alpha V^2) \quad (5.1)$$

where, $C(V)$ is the bilayer capacitance at applied voltage, V , C_0 is the capacitance at zero volts, and α is the electrowetting proportionality constant with a value ≥ 0 .

We aim to qualitatively evaluate differences in DIB confinement caused by the organogel by comparing the amount by which the membrane can increase in area due to electrowetting. The electrowetting responses of DIBs formed in liquid and in gel are quantified by measuring nominal bilayer capacitance at varying DC biases from 0 to +150 mV. Figure 5.7(a) shows the normalized capacitance, $(C(V) - C(0))/C_0$, versus the square of the voltage for representative measurements on these DIB systems. In this representation, we see that all conditions exhibit a fairly linear relationship between normalized capacitance and voltage squared, where the slope of each represents α .

Liquid-in-liquid DIBs whose boundaries are not constrained by the surrounding medium exhibit an average α value of $11.82 \pm 1.6 \text{ V}^{-2}$ at RT and $17.02 \pm 3.0 \text{ V}^{-2}$ at 50°C . Liquid-in-molten gel DIBs are found to produce a comparable α value of about $18.7 \pm 3.5 \text{ V}^{-2}$. Liquid-in-gel DIBs, on the other hand, display a reduced α value of $8.2 \pm 2.2 \text{ V}^{-2}$, suggesting that the gel imposes a geometric constraint on the bilayer. Figure 5.7(b) shows microscopic images of bilayers and the measured bilayer size under 0 mV and +150 mV applied voltage for liquid-in-gel system at molten state (50°C) and at gel state (room temperature). The difference in bilayer size between the molten and gel states at 0 mV is due to a small drift in the relative electrode positions during the cooling process. Nevertheless, the constriction of electrowetting-induced bilayer growth at gelled state is evident from the difference between the measured bilayer sizes at 150 mV: a $\sim 36 \mu\text{m}$ increase in equivalent bilayer diameter for molten state as opposed to $\sim 19 \mu\text{m}$ for gel state. Similar magnitude of bilayer growth was

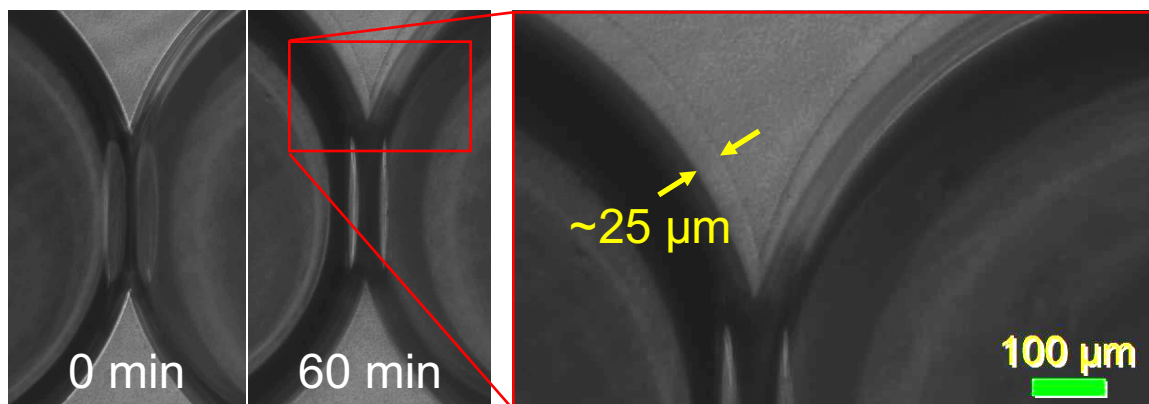


Figure 5.8: Appearance of hexadecane-filled gap between the droplet phase and SEBS-gel phase due to the evaporation of droplet phase.

reported for liquid-in-liquid DIBs in prior literature.[91] While the reduced α value can be attributed to the constrained annulus, it is important to note that α is not zero. This finding could be due to: a) a thin layer of liquid hexadecane separating the water droplets from the gel, allowing for some bilayer expansion, b) the low stiffness of soft gel, which allows electrowetting to compress the organogel in the annulus region and allow bilayer expansion, or c) combination of both a & b (see Figure 5.8).

It is well known that aqueous droplets placed under hexadecane are known to shrink over time due to the evaporation of water molecules. As a result of this effect, bilayer buckling was observed when femtoliter droplets are used to form DIBs using DOPC lipid in soybean oil.[96] Figure 5.8 shows a phase contrast images of a bilayer taken at $t=0$ min and 60 min. Image taken after 60 min shows a clear $\sim 24 \mu\text{m}$ gap between the aqueous volume and the SEBS-gel that is not present initially (at $t=0$ min). This gap, which grows at a rate proportional to that of droplet shrinkage, is presumed to be filled with liquid hexadecane as macrophase separation of hexadecane from a SEBS-gel matrix is expected.[190] Careful analysis of phase contrast images have shown that the SEBS-gel boundary does not change even after longer periods of time. The increasing gap between the SEBS-gel boundary and the aqueous droplets is expected to exhibit a higher electro-wetting constant than that is seen during first

few minutes. Therefore, all the electro-wetting measurements conducted at room temperature are done immediately after the gel is cooled to room temperature.

Verification of Functional Properties of Membrane-Bound Peptides

Alamethicin is a voltage-activated, pore-forming peptide that forms ion channels in fluid lipid bilayers.[191] To further validate that the interface between gel-encapsulated droplets is in fact a lipid bilayer and not a polymeric interface, we added 1 μM alamethicin to the liposome solutions that comprise the droplets. Figure 5.9 shows the ion currents through alamethicin channels contained in a liquid-in-gel DPhPC bilayer at 25°C in response to an applied voltage of +175 mV. The corresponding histogram of conductance levels (i.e. current divided by applied voltage; unit: pS) shows multiple discrete conductance levels and sub-conductance levels that are characteristic of alamethicin channels in a fluid lipid bilayer.[192] In comparison, measurements of alamethicin gating in a DIB surrounded by molten gel at 50°C shows shorter channel dwell times ("flicker") when compared to its activity at room temperature (Figure 5.10). This channel activity at both temperatures confirms that the membrane retains its fluid environment across the temperature range, which enables channel insertion, and, at least for alamethicin, we observe that the heating required to assemble the DIB within a molten gel does not prevent functional channel activity upon cooling to room temperature.

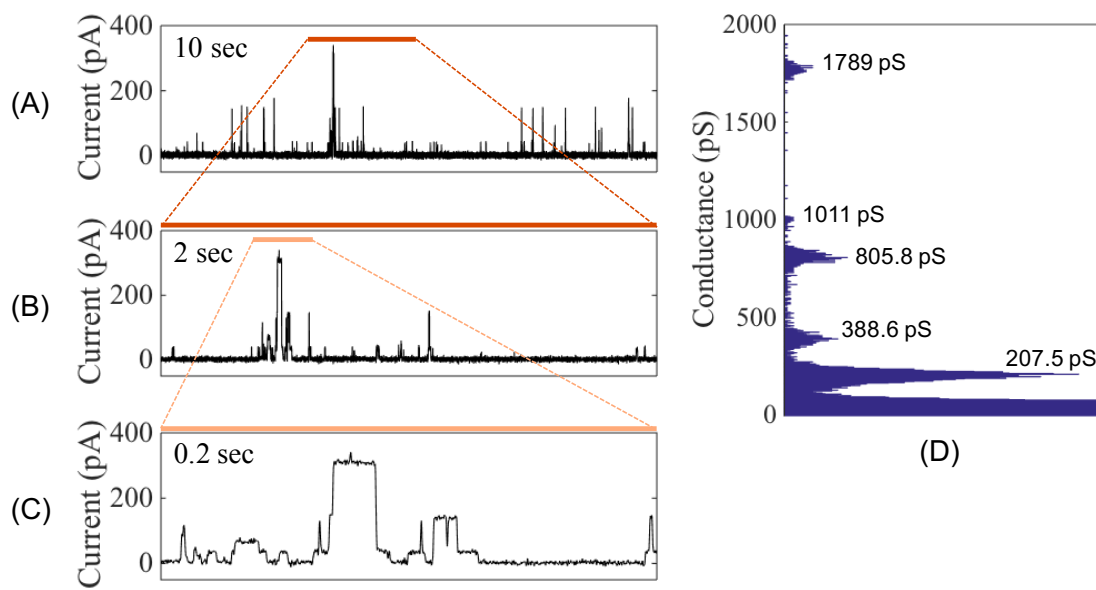


Figure 5.9: Single-channel alamethicin recording at +175 mV applied voltage at room temperature (A-C). (D) Histogram of conductance levels corresponding to trace in A. Normalized conductance ratios with respect to the first conductance level are found to be 1:2 (1st to 2nd level), 1:4 (1st to 3rd), 1:5 (1st to 4th) & 1:9 (1st to 5th).

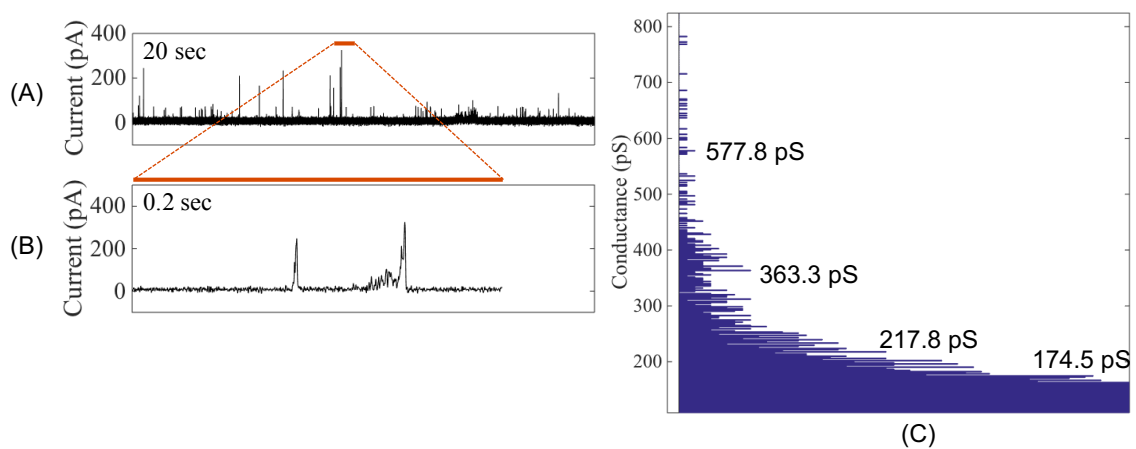


Figure 5.10: Electrical activity of Alamethicin at +175 mV applied voltage at 50°C (A) & (B). (C) The histogram of conductance levels corresponding to the trace shown in (A).

Vibration Experiments to Quantify Durability of DIBs

Two modes of DIB failure are observed during the vibration experiments: droplet separation and droplet coalescence induced by bilayer rupture. In Figure 5.11(a), the data from these experiments are presented in a way that shows, versus frequency, the applied acceleration that induces loss of the bilayer. Note that for liquid-in-liquid DIBs, this value of acceleration does not account for acceleration amplification due to droplet motions relative to the substrate, as described previously.[124] Nonetheless, similar to this prior study, we find that liquid-in-liquid DIBs (o) exhibit droplet separation at a comparable average of 2.1 ± 1.0 g ($n = 14$) across the frequency range from 35 to 60 Hz. In contrast, liquid-in-gel DIBs shaken at maximum achievable accelerations below 50 Hz (due to the power limitation of the shaker) did not separate or rupture (Δ). However, when accelerated at 50 Hz and 60 Hz, liquid-in-gel DIBs (\blacktriangle) ruptured at an average acceleration of 6.0 ± 1.9 g ($n = 9$) (Figure 5.11(b)). An unpaired t-test result of $t(11) = 2.68$, $p = 0.0216$ performed on this subset population (50 & 60 Hz) of bilayer failure accelerations thus confirms that the liquid-in-gel DIBs rupture at a significantly higher applied acceleration. Similar modes of failure were reported for un-encapsulated and PDMS-encapsulated DIBs. Across the frequencies tested herein, SEBS-encapsulated DIBs are found to be comparably durable to PDMS-encapsulated DIBs reported previously by Sarles and Leo.

In addition to the critical accelerations that can be withstood, this experiment again shows that the amount of confinement surrounding the adhesive droplets affects the mode of failure. We observe that droplet pairs placed in liquid hexadecane are not constrained in their relative positions due to the absence of contact to solid supports on all sides, except beneath the droplets. This lack of confinement allows droplets to both deform from their static spherical shapes and move relative to one another, leading to droplet separation, and thus bilayer unzipping, upon vibration. Droplet deformation could also lead to an increase in monolayer tension (due to transient fluctuations in surface area), which may also lead to bilayer unzipping according to

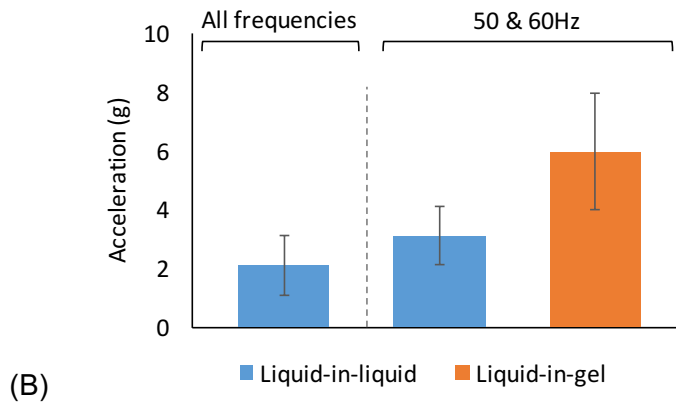
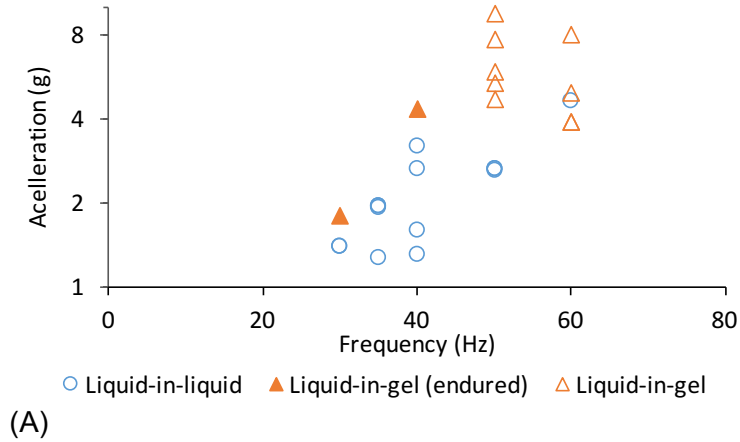


Figure 5.11: Measured values of applied acceleration that triggered bilayer failure for liquid-in-liquid and liquid-in-gel DIBs, plotted with respect to excitation frequency (A). Bar graph comparing the average accelerations at failure across all frequencies ($n = 14$; left), and at 50 & 60 Hz ($n \geq 4$; right) (B). Error bars represent \pm one standard deviation.

the force balance equation described by Young-Dupr e.[92] SEBS-encapsulated droplet pairs, on the other hand, are surrounded by gel (in all directions except for the thin region beneath the droplets) that highly constrains droplet deformation and provides structural support to the droplet pair as a whole. Therefore, when vibrated, due to the minimized droplet deformation and relative motion between the droplets, the droplets do not separate and thus, can withstand higher levels of acceleration because of the additional support when compared to liquid-in-liquid DIBs. However, at high accelerations (>6 g) the bilayer experiences higher magnitude forces and the bilayer

fails, causing the droplets to coalesce. Sarles and Leo reported droplet separation as the mode of failure even for encapsulated DIBs (no electrodes), which is possibly due to the amount of bulk liquid hexadecane that surrounds the aqueous droplets and the extent to which the droplets are still free to move in the compartments.

Nevertheless, with bilayers that can withstand nearly 3X higher applied acceleration, liquid-in-gel DIBs offer a more robust and more portable embodiment than conventional DIBs. Unlike liquid-in-liquid DIB devices, liquid-in-gel DIB devices eliminate spillage of bulk organic phase thus improving handling and portability of the device—a feature desired in many droplet-based applications including DIBs. A liquid-in-gel DIB formed in a PDMS substrate was subjected to a simple drop experiment and is found to withstand a ~ 0.5 -foot drop with an estimated acceleration of $\sim 12g$ felt at impact (see Movie S1 of [193]). In order to demonstrate its improved handling, a liquid-in-gel DIB is formed on a flexible substrate (Dynaflex G6713) as shown in Figure 5.13(a). The rupture of the bilayer is monitored visually by using droplets containing water-soluble food coloring. Once the organogel is cooled to room temperature, the substrate is subjected to simple handling such as moving, lifting, flipping upside down, and bending, and the DIB is found to be preserved. Such manipulations of a substrate containing a liquid DIB would have resulted in DIB failure and droplet and oil spillage.

Developing a portable DIB system that can be used for long-term sensitive measurements must also consider taking preventive measures from possible contaminants such as dust particles and other aqueous droplets. Figure 5.13(b) shows a flexible substrate with a functional DIB being submerged into water, demonstrating the ability of the SEBS-gel to act as a physical barrier to effectively isolate the DIB assembly from the surrounding environment and improving useful longevity (>24 hours) of sensitive experiments in settings outside of laboratories. In addition, because SEBS encapsulation simply replaces the oil phase and does not require a specific substrate, we envision this approach could also help protect large DIB arrays and may even facilitate the fabrication of multilayered droplet assemblies.

Figure 5.13(c) and Movie S2 (see [193]) demonstrates force transmission through the gel by applying force externally to a flexible substrate that contains the DIB. Deformation of droplets and slight increase in bilayer size can be seen when the substrate is subjected to a force from the direction depicted by the arrow mark. Such indirect force transmission capability, in contrast to direct application of force as demonstrated by Najem et al., could be used for activation of mechanosensitive ion channels like MscL by external forces, potentially eliminating the need for a complex droplet-shaking setup and yielding new types of membrane-based materials for cell-inspired transduction.[92]

5.3.5 Wax-encapsulated DIBs

Figure 5.12 shows images of DIBs encapsulated in 40% paraffin/hexadecane mixture. In this experiment, a DIB is formed under 50°paraffin wax as shown in Figure 5.12 (A). As the temperature is reduced to room temperature, the wax solidifies to form an opaque solid. During solidification, the volume of wax reduces and affects the size of the bilayer. Nonetheless, wax-encapsulated DIBs were found to be stable even when held in air as shown in Figure 5.12(C).

5.3.6 Conclusions

Liquid-in-gel DIBs in a polymer-based organogel encapsulation were assembled and found to exhibit improved durability and portability at room temperature when compared to conventional liquid-in-liquid DIBs. SEBS polymer molecules are found to not assemble themselves or interfere with the lipid self-assembly process that forms a monolayer at the oil-water interface. We also found that these polymer molecules are excluded from the bilayer region during the thinning process, yielding a polymer-free lipid bilayer that has statistically similar electrical and structural properties to that of conventional liquid-in-liquid DIBs. The fact that DPhPC bilayers (which do not exhibit a thermotropic transition in the temperature range tested) can withstand

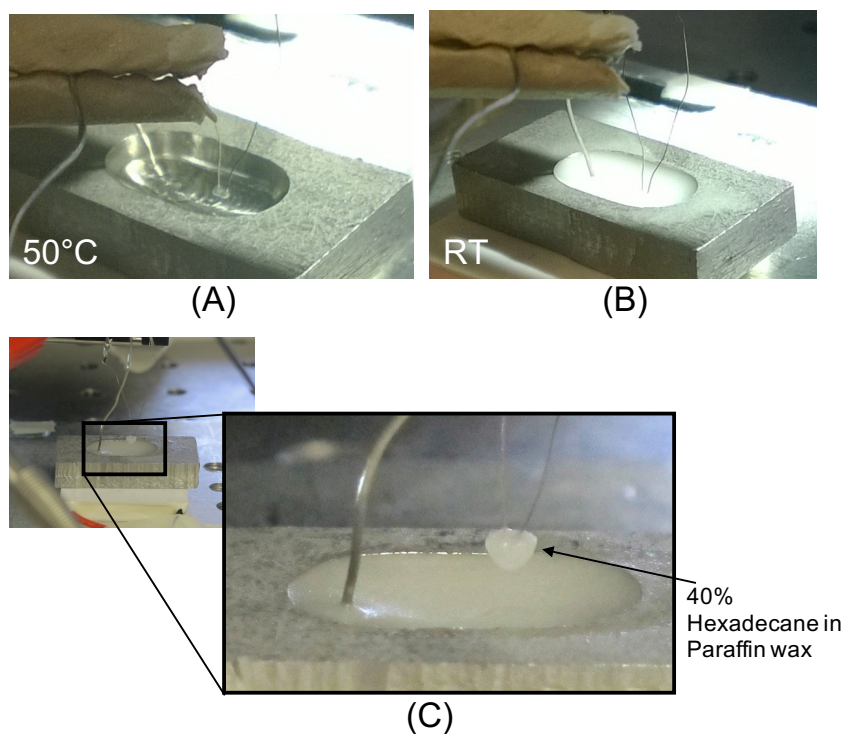


Figure 5.12: DIB formed in 40% hexadecane-paraffin wax at 50°C (A) and cooled to room temperature (B). A wax-encapsulated DIB formed at the tip of two hanging electrodes held in air (C). Shrinkage of paraffin upon solidification causes bilayer size reduction or rupture.

multiple heating (50°C) and cooling (20°C) cycles required to melt and solidify the gel indicates that this approach preserves the ability to add, remove, and rearrange droplets in a DIB network. This temperature range should also be suitable for a wide-variety of phospholipids, surfactants, and other biomolecules that are typically used and studied in model membranes. Unlike a liquid solvent, using a gel-phase material to encapsulate droplet interface bilayers facilitates force transmission to the bilayers through the surrounding medium, enabling membrane-based materials that could be used to sense applied force, stretch, and compression.

Furthermore, we believe that this approach could be integrated with hydrogel-based DIB systems, in which one or both the participating aqueous droplets are replaced with hydrogel (agarose or PEG), [186, 194] to yield gel-in-gel DIB assemblies that could be even more mechanically stable. Our preliminary experiments show that

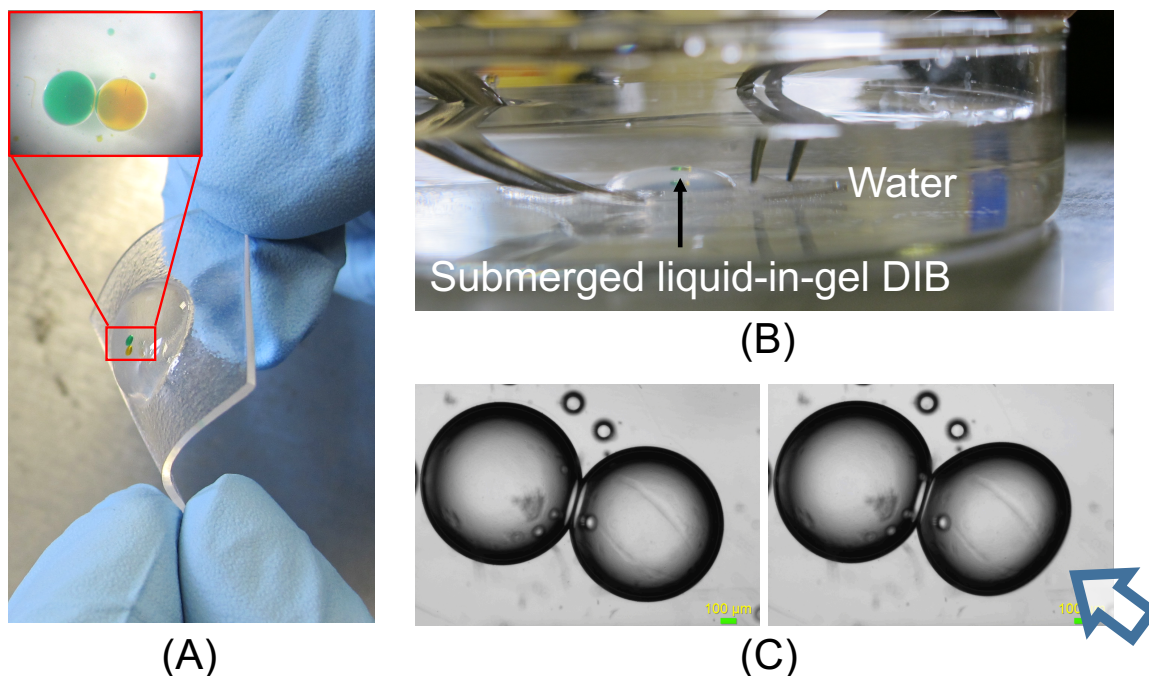


Figure 5.13: Demonstrating the portability and improved handling of SEBS-encapsulated DIBs: A) DIB formed on a flexible, open substrate, and B) DIB submerged under water testifying physical shielding from environment. C) Application of indirect force to perturb the DIB.

SEBS does not affect gel-in-gel bilayer formation. Alternate to a SEBS/hexadecane organogel, SEBS/mineral oil organogel and pure paraffin wax without polymer can also be used to achieve gel- and wax-encapsulated DIBs following the same procedure of DIB formation in the molten organic phase (Figure 5.12). Specific advantages of the organogel material versus paraffin wax include maintaining a transparent encapsulation material upon gelling and a reduced volume shrinkage during the phase transition that helps maintain the bilayer between droplets. Development of such lipid membrane based soft-materials that are more portable and durable enables researchers to design wider range of useful bioinspired membrane-based devices. More broadly, we note that the approach demonstrated here can also be used for solidifying the continuous organic phase in droplet-based emulsions assembled in both closed microfluidic systems[195] and open surface microfluidic systems,[196, 197] where, in

particular, the use of a solidifying external phase can be used to stabilize droplet positions and enhance durability and portability.

Chapter 6

3D-Printed Microscaffolds for Horizontally-oriented Suspended Bilayer Formation

6.1 Introduction

In this chapter, we report results from our attempts to assemble lipid monolayers and bilayers that are positioned within the short working distances of high-resolution microscopy. Usage of Nanoscribe direct laser writing technology to 3D print scaffolds to assemble a non-spherical liposome was recently demonstrated by Inoue et. al.[198] In this work, we explore this technology to print different types of 3D scaffolds that can support horizontally-oriented suspended lipid bilayers that are positioned within the 100-200 μm from microscope objective.

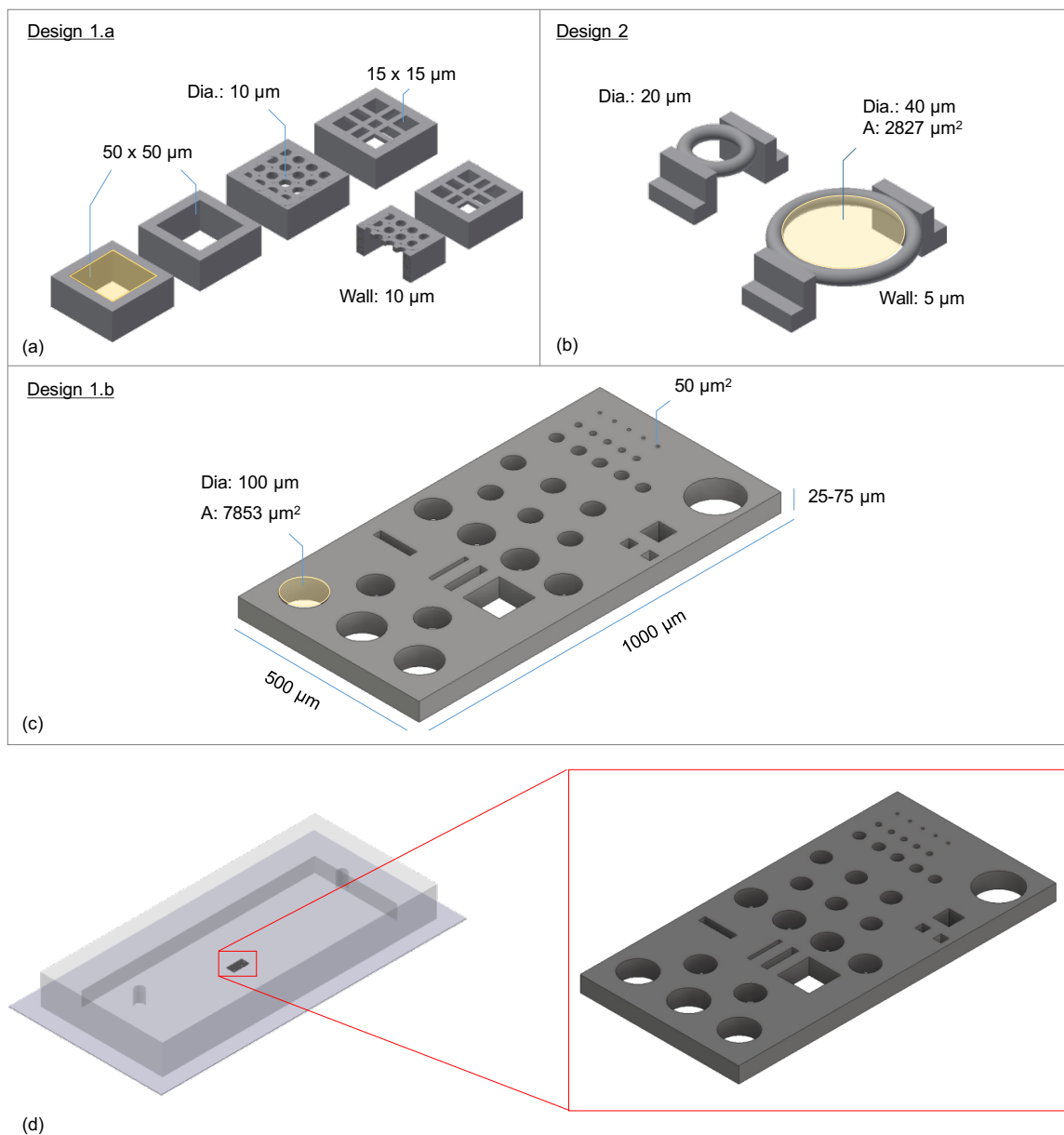


Figure 6.1: 3D models of various designs tested in this Chapter (a-c). (a) and (b) shows the Design style 1 (container-style scaffolds; for bilayer with two different aqueous volumes) while (c) shows the Design type 2 (ring-type; for bilayer surrounded with single aqueous volume). (d) shows a microfluidic chip containing a 3D printed scaffold placed in its liquid chamber.

6.2 Research Objective and Approach

6.2.1 Scaffold Designs

Figure 6.1 shows the two different types of scaffold designs were explored in this work. Design type 1 includes a container-style scaffold which allows for formation of lipid bilayer in between two different aqueous volumes. Under this type, two different scaffold designs were printed and tested. Design 1.a is a cube-shaped micro-container with fully or partially-open top. Partially-open top consists of a mesh-like structure printed at the top of the opening. The thickness of the walls was set between 5 and 10 μm with a height of 10 to 25 μm . Design 1.b is a 25-75 μm tall rectangular slab (1000 x 500 μm) containing micro-wells of various shapes and opening sizes. Slabs containing cylindrical micro-wells with radius ranging from 8 to 120 μm and cuboidal micro-wells with dimensions between 10 and 100 μm were printed. Design type 2 includes an elevated ring-type scaffold that enables the formation of lipid bilayer spanning across the ring. Unlike design type 1, a bilayer formed in this design is surrounded by a single aqueous solution. 20 and 40 μm diameter rings with a wall-thickness of 5 μm were tested in this work. Several different scaffold designs were printed using DiLL method (as discussed in Chapter 2) using IP-S photoresist.

6.3 Method

In order to assemble a lipid bilayer that is spanning across the printed scaffolds, two or three different solutions are needed: 2 different aqueous solutions (1 for Design type 2) and a lipid/organic solvent. Aqueous solutions were made up of buffer containing 100 mM NaCl, 10 mM MOPS, pH 7.0 with different colored solutions (food coloring). 2 mg/ml glyceryl monooleate (GMO)/Hexadecane is used as the lipid/organic solvent solution because of GMO's ability to rapidly self-assemble (within seconds) to form a well-packed monolayer at OW interface. These solutions are sequentially introduced

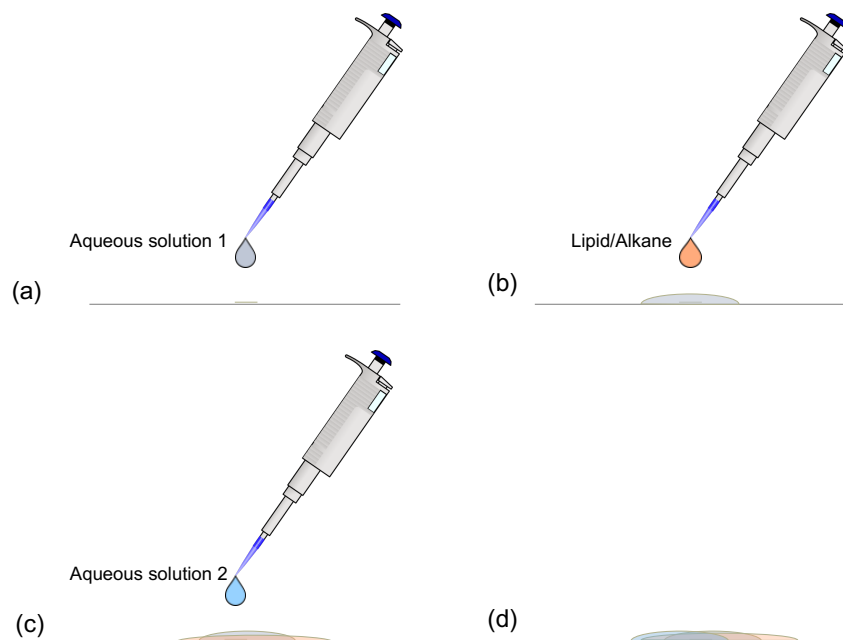


Figure 6.2: Procedure showing sequentially dispensing different solutions using a pipette.

into the system using two different methods: manual pipetting and syringe-pump injection within a microfluidic channel.

Using manual pipetting

First, due to the simplicity of the steps involved, we tested the applicability of sequential dispensing of different solutions using a manual pipette. Figure 6.2 shows the sequence in which different solutions were added onto the printed scaffolds. About 300 to 800 nl of each solution was added in each step.

Using microfluidic chamber

Next, to utilize the controlled flow of liquids offered by microfluidics, we performed another series of experiments using a standard microfluidic setup that consisted of a dual syringe pump (Gemini 88, KD Scientific), syringes, 4-way valve (Cole-Parmer) and a microfluidic chip with printed scaffold is used. Lipid monolayers and bilayers

are assembled on the printed scaffolds by sequential flow of aqueous and lipid-in-oil solutions through the microfluidic chamber. Two slightly different protocols were attempted during the preliminary testing. The first protocol involves flowing aqueous solution 1 (with red food coloring), GMO/Hexadecane and aqueous solution 2 (with yellow food coloring) in the given order (see Figure 6.3). In the second protocol, before passing the aqueous solution 1, the microfluidic chamber is first filled with plain alkane solution in order to achieve different initial wetting conditions. Three different 3 ml syringe (BD Syringe) fitted with blunt needles are filled with liquids and are fitted to the syringe pump. Flow rates between 1 $\mu\text{l}/\text{min}$ to 100 $\mu\text{l}/\text{min}$ were tested. For Design type 2, a single aqueous solution was passed through the chamber before and after passing lipid/alkane solution.

6.4 Results and Discussion

6.4.1 Manual Solution Exchange

Manually pipetting different solutions offers the advantage of quick solution exchange and avoids plasma oxidation (required for bonding PDMS to coverslip). However, with minimal control on flow rate, exchange of solutions is observed to be crude and dependent on coverslip's tendency to preferentially wet different solutions. In addition, removal of solutions had to be performed by using pipettes or cleaning wipes, which often resulted in damaging or dislodging the scaffolds. Results from manual pipetting experiments are not shown here.

6.4.2 Microfluidics for Sequential Solution Exchange

Usage of syringe pump in conjunction with microfluidic chip offers gentle flow of solutions. However, the main drawback of using syringe pump for flowing solutions is the waiting time experienced between different solutions; based on the length of tubing, about 10-20 minute waiting period is noticed between solution exchange inside

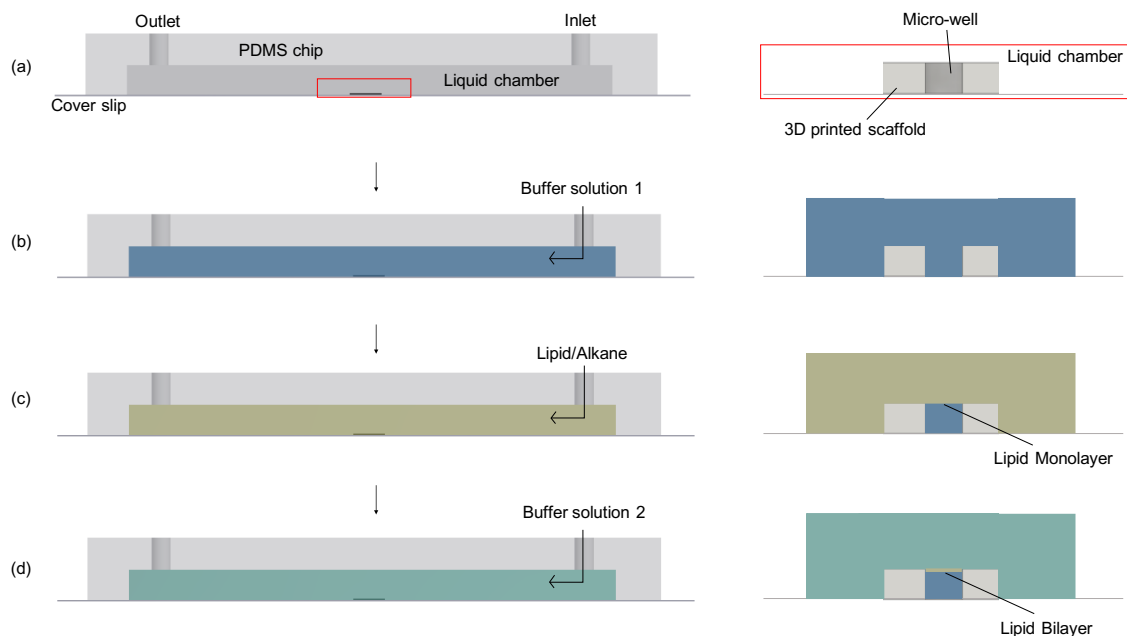


Figure 6.3: (a) Front view of the fully assembled microfluidic chip enclosing the 3D printed scaffold. Red box shows the zoomed-in view of the printed scaffold placed in the liquid chamber. (b-d) show the experimental procedure to assemble a lipid bilayer. First, aqueous solution 1 is filled in the liquid chamber and in the micro-wells of scaffold (b). Following this, lipid/alkane solution is passed through the chamber (c). This displaces the aqueous solution 1 from the chamber leaving behind the volume filled in the micro-well. A lipid monolayer is formed at the water-oil interface on top of the micro-well. Finally, aqueous solution 2 is passed through to replace the lipid/alkane and form a bilayer at the opening of the micro-well (d).

the microfluidic chip. Nonetheless, the results produced with this method are found to be more promising and repeatable. The results discussed in this chapter were performed using microfluidics method.

Figure 6.4(b) shows brightfield micrographs of results obtained using Design 1.a. After the flow of aqueous solution 1, the inside and outside of the cubes were filled both filled with solution 1. Air trapped in these cubes slowly excluded within a minute. After 10-15 minutes, flow of lipid/alkane mixture began to displace the aqueous solution 1 trapped inside the cube. However, after partial exclusion the inside of the cubes were occupied by solution 1 and lipid/alkane mixture. After the flow of aqueous solution 2 through the microfluidic chamber, no change in solution

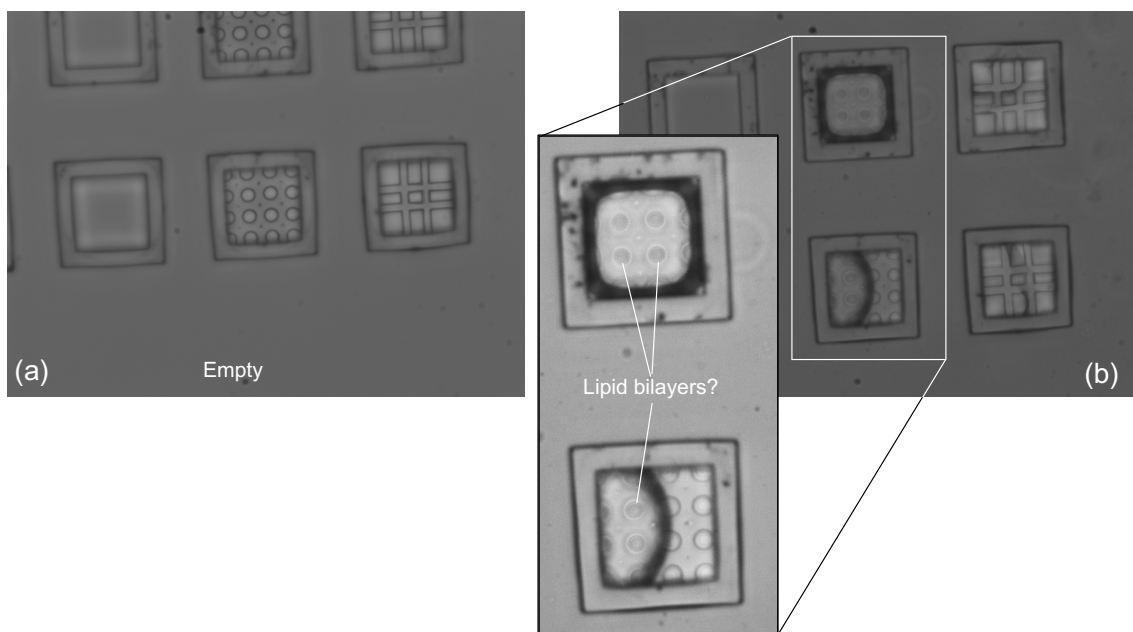


Figure 6.4: Brightfield microscopic images of cube-scaffolds shown in Figure 6.1(a) (Design 1.a). (a) Image of an empty substrate and (b) shows scaffolds partially filled with aq. solution 1 and the chamber filled with aq. solution 2, separated by a layer of lipid/alkane. The dark circles seen on top of the cubes in inset are expected to be lipid bilayers.

1 volume was noticed, confirming the presence of a separation layer between the two aqueous solutions. While the diffraction patterns shown in inset seem to suggest the possibility of lipid bilayers present between the aqueous solutions, this result cannot be used as a confirmation for bilayer formation.

Figure 6.5 shows fluorescence images of results obtained using Design 1.b. The procedure used in this test is same as discussed above. However, aqueous solution 1 in this case contained a 50 mM carboxyfluorescein (CF) dye. This allowed to better assess the presence of different solutions inside and outside the micro-wells. Figure 6.5(a) shows 4 micro-wells filled with CF. After sequential flow of lipid/alkane followed by aqueous solution 2, Figure 6.5(b) shows the presence of CF trapped inside one of the micro-wells. The other 3 micro-wells that previously contained CF coalesced with the aqueous solution 2, thus losing the fluorescent content. After few minutes, the CF trapped inside the cylindrical micro-well too disappeared, possibly due to coalescence

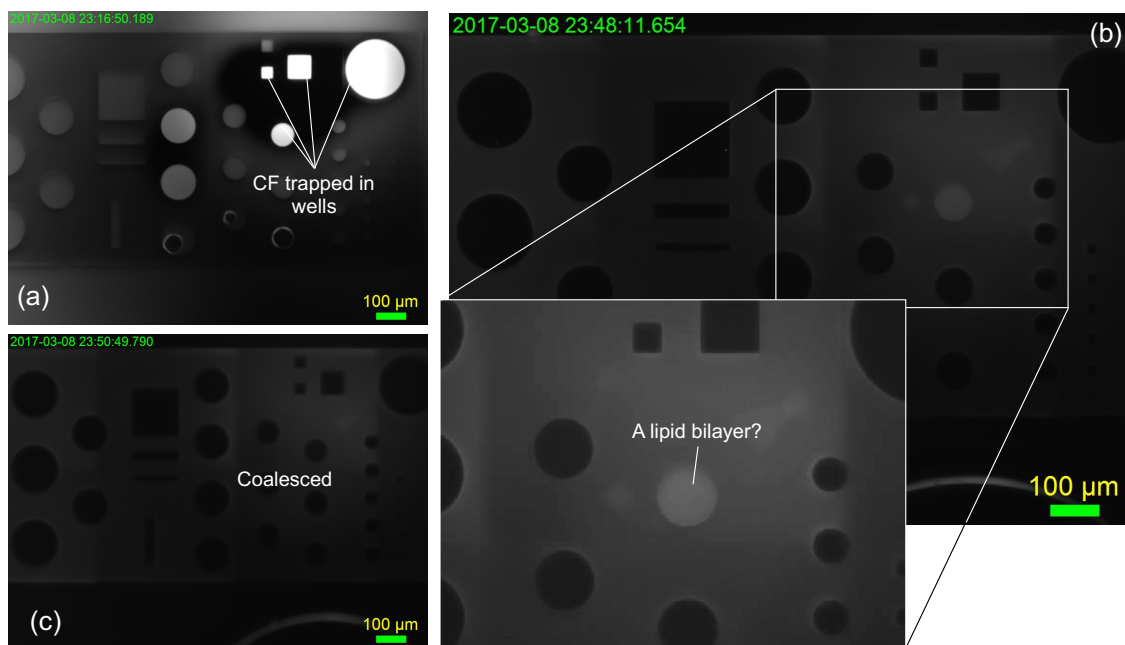


Figure 6.5: Fluorescent images showing CF-filled micro-wells (a), and a possible lipid bilayer assembled on top of a micro-well (b). Inset shows a zoomed-in, contrast-adjusted image of (b). (c) shows the same scaffold without the trapped CF found in (b). 3D view of design 1.b is shown in Figure 6.1(b).

with solution 2. Similar to results discussed in Design 1.a, results observed in this design confirms the entrapment of solution 1 inside and solution 2 outside with a separating lipid/alkane solution but does not confirm the formation of lipid bilayer.

Results obtained from Design 2 are shown in Figure 6.6. First, GMO/hexadecane was passed through the liquid chamber. Flow of aqueous solution 1 through chamber replaced most of the lipid/alkane solution around the scaffold assembly. However, as seen in Figure 6.6(a), some lipid/alkane is found to be trapped within the scaffold structures, which lead to the formation of lipid monolayer. Figure 6.6(b & c) shows the brightfield and phase-contrast images of the scaffolds supporting lipid monolayers, respectively. Successive flow of lipid/alkane replaced the entire aqueous solution, leaving behind a alkane filled scaffold. We conclude that iterating the dimensions, especially the height, of the scaffolds could help replace the lipid/alkane underneath

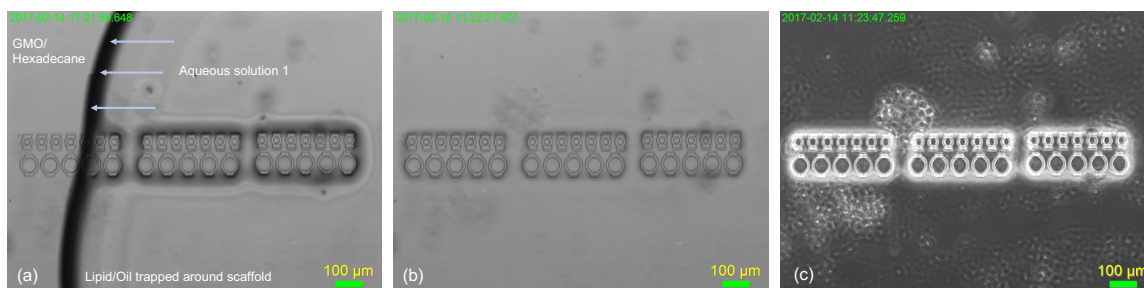


Figure 6.6: Brightfield (a, b) and phase contrast (c) microscopic images showing printed ring-type scaffolds. (Design 2 in Figure 6.1(c))

the rings and lead to the formation of lipid bilayer as opposed to the monolayer formed here.

6.5 Summary and Future Directions

In summary, usage of Nanoscribe direct laser writing to print scaffolds for horizontally-oriented suspended lipid bilayer was explored. Two different types of scaffold designs were tested for monolayer and bilayer formation. First design includes a container-style scaffold which allows for formation of lipid bilayer in between two different aqueous volumes while the second design enables the formation of lipid bilayer spanning a ring-style scaffold surrounded by a single aqueous solution. In general, the wetting properties of printed scaffolds is found to be the leading factor in deciding the ability to assemble lipid bilayers. Therefore, more experiments need to be performed by systematically varying the wetting properties of scaffold. This can either be done by choice of photoresist or by using surface modification methods (such as spatially-controlled silanizing or plasma treating). Another possible design is to print scaffolds with two different photoresists with different wetting conditions: a hydrophilic container to hold water and a hydrophobic layer on top to support oil - mimicking Teflon membrane in BLMs.

While images shown in Figure 6.4 suggest a possibility of lipid bilayer formation spanning the micro-well, we must prove that the interface formed is in fact a lipid

bilayer and not a thick layer of lipid/alkane solution trapped between two monolayers. In order to confirm bilayer formation, an established fluorescent-leakage experiment can be performed. To accomplish this, aqueous solution 1 containing calcein (a fluorescent dye) is filled in the micro-wells. After passing lipid/alkane, aqueous solution 2 containing α -hemolysin (α -HL), a pore-forming transmembrane protein that is known to transport calcein dye across a lipid bilayer, is filled outside the micro-wells. If the interface formed in between is a lipid bilayer, α -HL is expected to insert in the bilayer and transport calcein from inside the micro-well to the aqueous solution 2. This transport of calcein across the bilayer can be quantified by measuring the temporal change in fluorescence intensity inside the micro-wells; over time, the fluorescence intensity is expected to reduce at a rate proportional to the number of α -HL inserted in the bilayer.[199] If the interface formed is not a lipid bilayer, the fluorescence intensity should remain unchanged over time as α -HL is expected to not insert in a thick layer of alkane. This simple fluorescent leakage experiment should help prove the formation of a lipid bilayer. With a proven protocol to assemble lipid bilayers on these printed scaffolds, various scaffold designs can then be explored to create arrays of bilayers suitable for high-resolution microscopy. Addition of thin-film electrodes in each of the micro-wells will enable simultaneous electrical and optical interrogation of lipid bilayers and greatly increase the applicability of these 3D printed scaffolds.

Chapter 7

Summary and Conclusions

7.1 Research Overview

The overarching goal of this work is to further our understanding of lipid self-assembly and its organization at an OW interface to support the development of synthetic lipid bilayer systems that can be used in biologically relevant fields such as membrane biophysics, protein electrophysiology, development of synthetic biomolecules, drugs and nanoparticles for various applications. The primary focus of this work lies on a) improving the success rate and number of lipids that can form DIBs, b) improving the portability and durability of DIB system, and c) development of system to assemble lipid bilayers specifically for high resolution optical techniques. One of the common underlying scientific objective across the above-mentioned goals is to better understand the self-assembly of lipids to form monolayers that are then used to form bilayers. Figure 7.1 lists the scientific gaps identified in Chapter 1 and the contributions from this work.

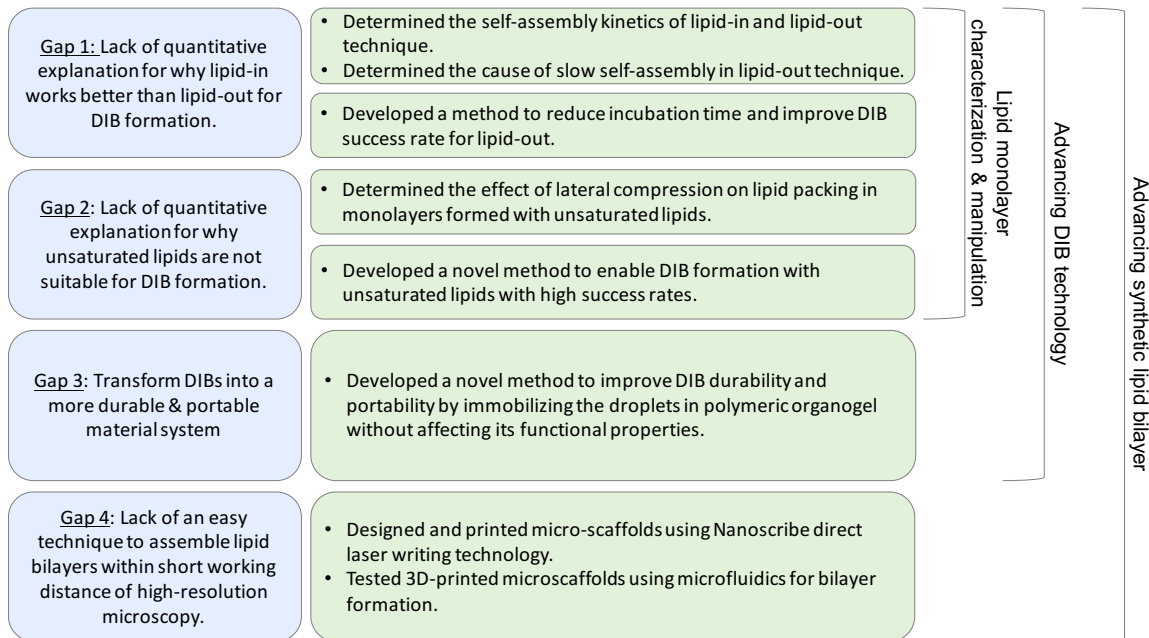


Figure 7.1: Summary of scientific gaps and contributions.

7.1.1 Contributions

Objective 1 (*addressing Gap 1 & 2*). Use dynamic interfacial tension measurements to understand the differences in self-assembly kinetics and organization of phospholipids (DPhPC, DOPC and POPC) at an OW interface when placed in water versus hexadecane. Measuring the interfacial tension will help us answer a) why monolayer formation takes longer for lipid-out method, b) why DIB formation success rate is lower for lipid-out when compared to lipid-in method, and c) why unsaturated lipids have low or zero DIB formation success rates.

- Used pendant drop tensiometer to measure the dynamic change in interfacial tension in order to quantify the differences in self-assembly kinetics of lipids at an OW interface when the lipids are placed in the organic phase versus the aqueous phase. (Chapter 3)
- Utilized mathematical model and supporting molecular dynamic simulations to analyze and explain the reasons for the differences in self-assembly kinetics. We found that the formation of a tightly packed interface was inhibited in lipid-out

method, likely by the formation of inverse micelle aggregates on the oil side of the partially-packed monolayer. This explains the poor DIB formation success rates anecdotally seen when lipid-out method is employed. (Chapter 3)

- Used a stirring mechanism in conjunction with pendant drop tensiometer to study the effect of convective flow in rate of monolayer formation for lipid-out method. (Chapter 3)
- Utilized pendant drop tensiometer and Langmuir-Blodgett trough to understand the compression-induced change in molecular organization of saturated and unsaturated lipids found in the monolayer formed at an OW and OA interface, respectively. We found that, unlike saturated lipids like DPhPC, unsaturated lipids fail to spontaneously assemble to form a monolayer that is in tightest packing state. In addition, we found that laterally compressing the partially-packed monolayers of unsaturated lipids can drive the lipids closer to achieve tighter packing. (Chapter 4)

Objective 2 (*addressing Gap 1 & 2*). Develop methods to reduce incubation time and improve bilayer formation success rate for lipid-out technique. Develop an active-packing technique to achieve monolayers suitable for DIB formation using unsaturated lipids (DOPC and POPC).

- Proved the applicability of convective flow to reduce incubation time and improve monolayer packing to increase DIB formation success rate for lipid-out method. (Chapter 3)
- Developed a simple evaporation-induced monolayer compression technique to condition partially-packed monolayers that are made up of unsaturated lipids (specifically, DOPC and POPC) to reach tightest packing state. This technique was then used to enable formation of stable DIB using unsaturated lipids that

were previously unrealizable. Electrical properties of these DIBs were also characterized. (Chapter 4)

Objective 3 (*addressing Gap 3*). Develop new methods to transform DIB, a lab-based technique, into a more portable and durable material system that is easier to handle without compromising membrane integrity, functionality or losing advantages of a conventional DIB system. This goal will be addressed by examining the usage of a polymer-based organogel to immobilize aqueous droplets in a DIB system in order to achieve the above-mentioned goals.

- Developed novel method to improve the portability and durability of a DIB system by immobilizing the aqueous droplets by replacing the liquid organic phase with a polymer-based organogel that forms a weak-gel at room temperature. (Chapter 5)
- The bilayer formed in this system was then proven to be devoid of polymer molecules by using specific capacitance measurements and voltage-activated peptide activity. (Chapter 5)
- The applicability of this new system was demonstrated by forming DIBs on flexible substrates and submerged under water to showcase the physical stability and shielding offered by the polymer encapsulation. (Chapter 5)

Objective 4 (*addressing Gap 4*). Construct and characterize 3D scaffolds for supporting horizontally-oriented SLBs that are positioned within the short working distance required for high resolution optical techniques. The proposed approach is to use a Nanoscribe direct writing instrument to 3D print micro-scaffolds that can support lipid monolayers and bilayers within 100-200 μ m from the objective for high resolution optical techniques.

- Utilized Nanoscribe direct laser writing technology to print 3D scaffolds that can support horizontally-oriented suspended lipid bilayer positioned within 100-200 μm from the objective. (Chapter 6)
- Explored several 3D scaffold designs that can support lipid monolayers and bilayers. (Chapter 6)
- Tested the applicability of manual pipetting and microfluidics for sequential solution exchange required for bilayer formation and found that usage of microfluidic system offers greater control on flow rate and effective exchange of solutions. (Chapter 6)
- We also found that wetting properties of scaffolds to be the leading factor in deciding the ability to form lipid bilayers.

Bibliography

- [1] Pablo V Escribá, José M González-Ros, Félix M Goñi, Paavo KJ Kinnunen, Lászlo Vigh, Lissete Sánchez-Magraner, Asia M Fernández, Xavier Busquets, Ibolya Horváth, and Gwendolyn Barceló-Coblijn. Membranes: a meeting point for lipids, proteins and therapies. *Journal of cellular and molecular medicine*, 12(3):829–875, 2008.
- [2] Philip L Yeagle. *The membranes of cells*. Academic Press, 2016.
- [3] Jean E Vance and Dennis E Vance. *Biochemistry of lipids, lipoproteins and membranes*. Elsevier, 2008.
- [4] Philipp Bartsch, Claudius Walter, Philipp Selenschik, Alf Honigmann, and Richard Wagner. Horizontal bilayer for electrical and optical recordings. *Materials*, 5(12):2705–2730, 2012.
- [5] Linda C. M. Gross, Andrew J. Heron, Sylvan C. Baca, and Mark I. Wallace. Determining membrane capacitance by dynamic control of droplet interface bilayer area. *Langmuir*, 27(23):14335–14342, 2011. ISSN 0743-7463. doi: 10.1021/la203081v. URL <http://dx.doi.org/10.1021/la203081v>.
- [6] Rob Phillips, Jane Kondev, Julie Theriot, and Hernan Garcia. *Physical biology of the cell*. Garland Science, 2012.
- [7] Thomas Günther Pomorski, Tommy Nylander, and Marité Cárdenas. Model cell membranes: Discerning lipid and protein contributions in shaping the cell. *Advances in colloid and interface science*, 205:207–220, 2014.

- [8] Erik Strandberg, Deniz Tiltak, Sebastian Ehni, Parvesh Wadhvani, and Anne S. Ulrich. Lipid shape is a key factor for membrane interactions of amphipathic helical peptides. *Biochimica et Biophysica Acta (BBA) - Biomembranes*, 1818(7):1764–1776, 2012. ISSN 0005-2736. doi: <http://dx.doi.org/10.1016/j.bbamem.2012.02.027>. URL <http://www.sciencedirect.com/science/article/pii/S0005273612000788>.
- [9] D. Marsh. Intrinsic curvature in normal and inverted lipid structures and in membranes. *Biophysical Journal*, 70(5):2248–2255, 1996. ISSN 0006-3495. doi: [http://dx.doi.org/10.1016/S0006-3495\(96\)79790-4](http://dx.doi.org/10.1016/S0006-3495(96)79790-4). URL <http://www.sciencedirect.com/science/article/pii/S0006349596797904>.
- [10] Markus Antonietti and Stephan Förster. Vesicles and liposomes: a self-assembly principle beyond lipids. *Advanced Materials*, 15(16):1323–1333, 2003.
- [11] Derek Marsh. Thermodynamics of phospholipid self-assembly. *Biophysical Journal*, 102(5):1079–1087, 2012. ISSN 0006-3495. doi: <http://dx.doi.org/10.1016/j.bpj.2012.01.049>. URL <http://www.sciencedirect.com/science/article/pii/S000634951200166X>.
- [12] Dov Lichtenberg, Y Barenholz, and D Glick. Liposomes: preparation, characterization, and preservation. *Methods Biochem. Anal.*, 33:337–462, 1988.
- [13] Peter Walde, Anna Maria Giuliani, C. Andrea Boicelli, and Pier Luigi Luisi. Phospholipid-based reverse micelles. *Chemistry and Physics of Lipids*, 53(4): 265–288, 1990. ISSN 0009-3084. doi: [http://dx.doi.org/10.1016/0009-3084\(90\)90026-N](http://dx.doi.org/10.1016/0009-3084(90)90026-N). URL <http://www.sciencedirect.com/science/article/pii/000930849090026N>.
- [14] S. Morita, H. Narita, T. Matoba, and M. Kito. Synthesis of triacylglycerol by lipase in phosphatidylcholine reverse micellar system. *Journal of the American*

- Oil Chemists Society*, 61(10):1571–1574, 1984. ISSN 0003-021X. doi: 10.1007/BF02541635. URL <http://dx.doi.org/10.1007/BF02541635>.
- [15] Rajan Gupta, H. S. Muralidhara, and H. T. Davis. Structure and phase behavior of phospholipid-based micelles in nonaqueous media. *Langmuir*, 17(17):5176–5183, 2001. ISSN 0743-7463. doi: 10.1021/la0103721. URL <http://dx.doi.org/10.1021/la0103721>.
- [16] Robert A. Walker, John C. Conboy, and Geraldine L. Richmond. Molecular structure and ordering of phospholipids at a liquid–liquid interface. *Langmuir*, 13(12):3070–3073, 1997. ISSN 0743-7463. doi: 10.1021/la961007q. URL <http://dx.doi.org/10.1021/la961007q>.
- [17] Junbai Li, Reinhard Miller, and Helmuth Mühlwald. Characterisation of phospholipid layers at liquid interfaces. 1. dynamics of adsorption of phospholipids at the chloroform/water interface. *Colloids and Surfaces A: Physicochemical and Engineering Aspects*, 114(0):113–121, 1996. ISSN 0927-7757. doi: [http://dx.doi.org/10.1016/0927-7757\(96\)03521-2](http://dx.doi.org/10.1016/0927-7757(96)03521-2). URL <http://www.sciencedirect.com/science/article/pii/0927775796035212>.
- [18] Hãlder A. Santos, Vladimir Garcãa-Morales, and Carlos M. Pereira. Electrochemical properties of phospholipid monolayers at liquid–liquid interfaces. *ChemPhysChem*, 11(1):28–41, 2010. ISSN 1439-7641. doi: 10.1002/cphc.200900609. URL <http://dx.doi.org/10.1002/cphc.200900609>.
- [19] K. M. W. Keough M. W. Hawco, P. J. Davis. Lipid fluidity in lung surfactant: Monolayers of saturated and unsaturated lecithins. *Journal of Applied Physiology*, 51(2), 1981.
- [20] Hilton B. de Aguiar, Alex G. F. de Beer, Matthew L. Strader, and Sylvie Roke. The interfacial tension of nanoscopic oil droplets in water is hardly affected by sds surfactant. *Journal of the American Chemical Society*, 132

- (7):2122–2123, 2010. ISSN 0002-7863. doi: 10.1021/ja9095158. URL <http://dx.doi.org/10.1021/ja9095158>.
- [21] Matthew A. Mitsche, Libo Wang, and Donald M. Small. Adsorption of egg phosphatidylcholine to an air/water and triolein/water bubble interface: Use of the 2-dimensional phase rule to estimate the surface composition of a phospholipid/triolein/water surface as a function of surface pressure. *The Journal of Physical Chemistry B*, 114(9):3276–3284, 2010. ISSN 1520-6106. doi: 10.1021/jp908730t. URL <http://dx.doi.org/10.1021/jp908730t>.
- [22] Benoît Denizot, Pierre Cyril Tchoreloff, Jacques Emile Proust, Francis Puisieux, Albert Lindenbaum, and Michel Dehan. Adsorption of phosphatidylcholine liposomes at the air/water interface. *Journal of Colloid and Interface Science*, 143(1):120–126, 1991. ISSN 0021-9797. doi: [http://dx.doi.org/10.1016/0021-9797\(91\)90444-D](http://dx.doi.org/10.1016/0021-9797(91)90444-D). URL <http://www.sciencedirect.com/science/article/pii/002197979190444D>.
- [23] Guru A. Venkatesan, Joonho Lee, Amir Barati Farimani, Mohammad Heiranian, C. Patrick Collier, Narayana R. Aluru, and Stephen A. Sarles. Adsorption kinetics dictate monolayer self-assembly for both lipid-in and lipid-out approaches to droplet interface bilayer formation. *Langmuir*, 31(47):12883–12893, 2015. ISSN 0743-7463. doi: 10.1021/acs.langmuir.5b02293. URL <http://dx.doi.org/10.1021/acs.langmuir.5b02293>.
- [24] I. Bivas. The dependence of the curvature elasticity moduli of a lipid bilayer on the change of the surface tension at a curving oil-water interface. *Physics Letters A*, 94(2):114–116, 1983. ISSN 0375-9601. doi: [http://dx.doi.org/10.1016/0375-9601\(83\)90222-0](http://dx.doi.org/10.1016/0375-9601(83)90222-0). URL <http://www.sciencedirect.com/science/article/pii/0375960183902220>.

- [25] Robert V. Farese and Tobias C. Walther. Lipid droplets finally get a little r-e-s-p-e-c-t. *Cell*, 139(5):855–860, 2009. ISSN 0092-8674. URL <http://linkinghub.elsevier.com/retrieve/pii/S0092867409014172>.
- [26] Anthony Yasmann and Sergei Sukharev. Properties of diphytanoyl phospholipids at the air–water interface. *Langmuir*, 31(1):350–357, 2015. ISSN 0743-7463. doi: 10.1021/la503800g. URL <http://dx.doi.org/10.1021/la503800g>.
- [27] Svetlana Baoukina, Luca Monticelli, H. Jelger Risselada, Siewert J. Marrink, and D. Peter Tieleman. The molecular mechanism of lipid monolayer collapse. *Proceedings of the National Academy of Sciences*, 105(31):10803–10808, 2008. doi: 10.1073/pnas.0711563105. URL <http://www.pnas.org/content/105/31/10803.abstract>.
- [28] Ethan C Smith, Jonathan M Crane, Ted G Laderas, and Stephen B Hall. Metastability of a supercompressed fluid monolayer. *Biophysical journal*, 85(5):3048–3057, 2003. ISSN 0006-3495.
- [29] Chen Shen. *Molecular Effectors at the Headgroup-Chain Interfaces of Lipids*. Thesis, 2012.
- [30] Aneta D. Petelska and Zbigniew A. Figaszewski. The equilibria of phosphatidylethanolamine-cholesterol and phosphatidylcholine–phosphatidylethanolamine in monolayers at the air/water interface. *Journal of Macromolecular Science, Part A*, 46(6):607–614, 2009. ISSN 1060-1325. doi: 10.1080/10601320902851884. URL <http://dx.doi.org/10.1080/10601320902851884>.
- [31] Izabela Brzozowska and Zbigniew A. Figaszewski. Interfacial tension of phosphatidylcholine–cholesterol system in monolayers at the air/water interface. *Biophysical Chemistry*, 95(2):173–179, 2002. ISSN 0301-4622.

doi: [http://dx.doi.org/10.1016/S0301-4622\(02\)00029-7](http://dx.doi.org/10.1016/S0301-4622(02)00029-7). URL <http://www.sciencedirect.com/science/article/pii/S0301462202000297>.

- [32] Gorgias Garofalakis and Brent S Murray. Surface pressure isotherms, dilatational rheology, and brewster angle microscopy of insoluble monolayers of sugar monoesters. *Langmuir*, 18(12):4765–4774, 2002. ISSN 0743-7463.
- [33] J Miñones, S Pais, O Conde, and P Dynarowicz-Łątka. Interactions between membrane sterols and phospholipids in model mammalian and fungi cellular membranes—A langmuir monolayer study. *Biophysical chemistry*, 140(1):69–77, 2009.
- [34] M Gudmand, Matthias Fidorra, Thomas Björnholm, and T Heimburg. Diffusion and partitioning of fluorescent lipid probes in phospholipid monolayers. *Biophysical journal*, 96(11):4598–4609, 2009. ISSN 0006-3495.
- [35] Grzegorz Chwastek and Petra Schwille. A monolayer assay tailored to investigate lipid–protein systems. *ChemPhysChem*, 14(9):1877–1881, 2013. ISSN 1439-7641.
- [36] Alena Khmelinskaia. *Protein-monolayer interactions investigated by fluorescence microscopy and correlation spectroscopy*. Thesis, 2013.
- [37] Sunghee Lee, Dennis H. Kim, and David Needham. Equilibrium and dynamic interfacial tension measurements at microscopic interfaces using a micropipet technique. 1. a new method for determination of interfacial tension. *Langmuir*, 17(18):5537–5543, 2001. ISSN 0743-7463. doi: 10.1021/la0103259. URL <http://dx.doi.org/10.1021/la0103259>.
- [38] Marja A Oosterlaken-Dijksterhuis, Henk P Haagsman, LM Van Golde, and Rudy A Demel. Characterization of lipid insertion into monomolecular layers mediated by lung surfactant proteins sp-b and sp-c. *Biochemistry*, 30(45):10965–10971, 1991.

- [39] Anke Penno, Gregor Hackenbroich, and Christoph Thiele. Phospholipids and lipid droplets. *Biochimica et Biophysica Acta (BBA) - Molecular and Cell Biology of Lipids*, 1831(3):589–594, 2013. ISSN 1388-1981. doi: <http://dx.doi.org/10.1016/j.bbalip.2012.12.001>. URL <http://www.sciencedirect.com/science/article/pii/S1388198112002557>.
- [40] Joëlle Bigay and Bruno Antony. Curvature, lipid packing, and electrostatics of membrane organelles: defining cellular territories in determining specificity. *Developmental cell*, 23(5):886–895, 2012.
- [41] Raghda Lahdo and Laurence De La FourniÃre-Bessueille. Insertion of the amyloid precursor protein into lipid monolayers: effects of cholesterol and apolipoprotein e. *Biochem. J.*, 382(3):987–994, 2004. doi: 10.1042/bj20040777. URL <http://www.biochemj.org/bj/382/bj3820987.htm>.
- [42] Max C Watson, Evgeni S Penev, Paul M Welch, and Frank LH Brown. Thermal fluctuations in shape, thickness, and molecular orientation in lipid bilayers. *The Journal of chemical physics*, 135(24):244701, 2011. ISSN 0021-9606.
- [43] Abdou Rachid Thiam, Robert V. Farese Jr, and Tobias C. Walther. The biophysics and cell biology of lipid droplets. *Nat Rev Mol Cell Biol*, 14(12):775–786, 2013. ISSN 1471-0072. doi: 10.1038/nrm3699. URL <http://dx.doi.org/10.1038/nrm3699>.
- [44] Johan Marra. Direct measurements of attractive van der waals and adhesion forces between uncharged lipid bilayers in aqueous solutions. *Journal of colloid and interface science*, 109(1):11–20, 1986.
- [45] Gerrit van Meer, Dennis R. Voelker, and Gerald W. Feigenson. Membrane lipids: where they are and how they behave. *Nat Rev Mol Cell Biol*, 9(2):112–124, 2008. ISSN 1471-0072. URL <http://dx.doi.org/10.1038/nrm2330>.

- [46] Michael Edidin. Lipids on the frontier: a century of cell-membrane bilayers. *Nature Reviews Molecular Cell Biology*, 4(5):414–418, 2003.
- [47] R. Fettiplace, D. M. Andrews, and D. A. Haydon. The thickness, composition and structure of some lipid bilayers and natural membranes. *The Journal of Membrane Biology*, 5(3):277–296, 1971. ISSN 0022-2631. doi: 10.1007/BF01870555. URL <http://dx.doi.org/10.1007/BF01870555>.
- [48] Witold K Subczynski and Anna Wisniewska. Physical properties of lipid bilayer membranes: relevance to membrane biological functions. *ACTA BIOCHIMICA POLONICA-ENGLISH EDITION-*, 47(3):613–626, 2000.
- [49] Andreas Blicher, Katarzyna Wodzinska, Matthias Fidorra, Mathias Winterhalter, and Thomas Heimburg. The temperature dependence of lipid membrane permeability, its quantized nature, and the influence of anesthetics. *Biophysical Journal*, 96(11):4581–4591, 2009. ISSN 0006-3495 1542-0086. doi: 10.1016/j.bpj.2009.01.062. URL <http://www.ncbi.nlm.nih.gov/pmc/articles/PMC2711498/>.
- [50] John F Nagle. Theory of the main lipid bilayer phase transition. *Annual Review of Physical Chemistry*, 31(1):157–196, 1980.
- [51] Robert B Gennis. *Biomembranes: molecular structure and function*. Springer Science & Business Media, 2013.
- [52] Shaukat Ali, Sharma Minchey, Andrew Janoff, and Eric Mayhew. A differential scanning calorimetry study of phosphocholines mixed with paclitaxel and its bromoacylated taxanes. *Biophysical journal*, 78(1):246–256, 2000.
- [53] Todd PW McMullen and Ronald N McElhaney. Physical studies of cholesterol-phospholipid interactions. *Current Opinion in Colloid & Interface Science*, 1(1):83–90, 1996.

- [54] Rakesh C YashRoy. Determination of membrane lipid phase transition temperature from ^{13}C -nmr intensities. *Journal of biochemical and biophysical methods*, 20(4):353–356, 1990.
- [55] M Caffrey. The study of lipid phase transition kinetics by time-resolved x-ray diffraction. *Annual review of biophysics and biophysical chemistry*, 18(1):159–186, 1989.
- [56] Nicholas J Brooks and John M Seddon. High pressure x-ray studies of lipid membranes and lipid phase transitions. *Zeitschrift für Physikalische Chemie*, 228(10-12):987–1004, 2014.
- [57] F Jähnig. Structural order of lipids and proteins in membranes: evaluation of fluorescence anisotropy data. *Proceedings of the National Academy of Sciences*, 76(12):6361–6365, 1979.
- [58] SM Campbell, SM Crowe, and J Mak. Lipid rafts and hiv-1: from viral entry to assembly of progeny virions. *Journal of Clinical Virology*, 22(3):217–227, 2001.
- [59] Kai Simons and Robert Ehehalt. Cholesterol, lipid rafts, and disease. *The Journal of clinical investigation*, 110(5):597–603, 2002.
- [60] Sophie Aimon, John Manzi, Daniel Schmidt, Jose Antonio Poveda Larrosa, Patricia Bassereau, and Gilman E. S. Toombes. Functional reconstitution of a voltage-gated potassium channel in giant unilamellar vesicles. *PLoS ONE*, 6(10):e25529, 2011. doi: 10.1371/journal.pone.0025529. URL <http://dx.doi.org/10.1371/journal.pone.0025529>.
- [61] Christa Trandum, Peter Westh, Kent JÄyrgensen, and Ole G Mouritsen. A thermodynamic study of the effects of cholesterol on the interaction between liposomes and ethanol. *Biophysical journal*, 78(5):2486–2492, 2000. ISSN 0006-3495.

- [62] Vladimir Torchilin. Liposomes in drug delivery. In *Fundamentals and Applications of Controlled Release Drug Delivery*, pages 289–328. Springer, 2012.
- [63] S. H. White. Formation of "solvent-free" black lipid bilayer membranes from glyceryl monooleate dispersed in squalene. *Biophysical Journal*, 23(3):337–347, 1978. ISSN 0006-3495. doi: [http://dx.doi.org/10.1016/S0006-3495\(78\)85453-8](http://dx.doi.org/10.1016/S0006-3495(78)85453-8). URL <http://www.sciencedirect.com/science/article/pii/S0006349578854538>.
- [64] Simon D. Ogier, Richard J. Bushby, Yaling Cheng, Stephen D. Evans, Stuart W. Evans, A. Toby A. Jenkins, Peter F. Knowles, and Robert E. Miles. Suspended planar phospholipid bilayers on micromachined supports. *Langmuir*, 16(13):5696–5701, 2000. ISSN 0743-7463. doi: 10.1021/la991367o. URL <http://dx.doi.org/10.1021/la991367o>.
- [65] Paul Mueller, Donald O Rudin, H Ti Tien, and William C Wescott. Reconstitution of cell membrane structure in vitro and its transformation into an excitable system. *Nature*, 194:979–980, 1962.
- [66] M Montal and P Mueller. Formation of bimolecular membranes from lipid monolayers and a study of their electrical properties. *Proceedings of the National Academy of Sciences*, 69(12):3561–3566, 1972.
- [67] H Ti Tien and A Louise Diana. Bimolecular lipid membranes: a review and a summary of some recent studies. *Chemistry and physics of lipids*, 2(1):55–101, 1968.
- [68] Ralf P Richter, Rémi Bérat, and Alain R Brisson. Formation of solid-supported lipid bilayers: an integrated view. *Langmuir*, 22(8):3497–3505, 2006.
- [69] Lukas K Tamm and Harden M McConnell. Supported phospholipid bilayers. *Biophysical journal*, 47(1):105–113, 1985.

- [70] Edward T Castellana and Paul S Cremer. Solid supported lipid bilayers: From biophysical studies to sensor design. *Surface Science Reports*, 61(10):429–444, 2006.
- [71] Kalani J Seu, Anjan P Pandey, Farzin Haque, Elizabeth A Proctor, Alexander E Ribbe, and Jennifer S Hovis. Effect of surface treatment on diffusion and domain formation in supported lipid bilayers. *Biophysical journal*, 92(7):2445–2450, 2007. ISSN 0006-3495.
- [72] Kalani J Seu, Lee R Cambrea, R Michael Everly, and Jennifer S Hovis. Influence of lipid chemistry on membrane fluidity: tail and headgroup interactions. *Biophysical journal*, 91(10):3727–3735, 2006. ISSN 0006-3495.
- [73] HM Seeger, G Marino, A Alessandrini, and P Facci. Effect of physical parameters on the main phase transition of supported lipid bilayers. *Biophysical journal*, 97(4):1067–1076, 2009. ISSN 0006-3495.
- [74] A Sonnleitner, GJ SchÅijtz, and Th Schmidt. Free brownian motion of individual lipid molecules in biomembranes. *Biophysical Journal*, 77(5):2638–2642, 1999. ISSN 0006-3495.
- [75] C Scomparin, S Lecuyer, M Ferreira, T Charitat, and B Tinland. Diffusion in supported lipid bilayers: Influence of substrate and preparation technique on the internal dynamics. *The European Physical Journal E*, 28(2):211–220, 2009.
- [76] A Simon, A Girard-Egrot, F Sauter, C Pudda, N Picollet D’Hahan, L Blum, F Chatelain, and A Fuchs. Formation and stability of a suspended biomimetic lipid bilayer on silicon submicrometer-sized pores. *Journal of colloid and interface science*, 308(2):337–343, 2007. ISSN 0021-9797.
- [77] Suneth P Rajapaksha, Xuefei Wang, and H Peter Lu. Suspended lipid bilayer for optical and electrical measurements of single ion channel proteins. *Analytical chemistry*, 85(19):8951–8955, 2013.

- [78] Michele Zagnoni. Miniaturised technologies for the development of artificial lipid bilayer systems. *Lab on a Chip*, 12(6):1026–1039, 2012.
- [79] Noah Malmstadt, Michael A. Nash, Robert F. Purnell, and Jacob J. Schmidt. Automated formation of lipid-bilayer membranes in a microfluidic device. *Nano Letters*, 6(9):1961–1965, 2006. ISSN 1530-6984. doi: 10.1021/nl0611034. URL <http://dx.doi.org/10.1021/nl0611034>.
- [80] Li-Qun Gu and Ji Wook Shim. Single molecule sensing by nanopores and nanopore devices. *Analyst*, 135(3):441–451, 2010. ISSN 0003-2654. doi: 10.1039/B907735A. URL <http://dx.doi.org/10.1039/B907735A>.
- [81] Kei Funakoshi, Hiroaki Suzuki, and Shoji Takeuchi. Lipid bilayer formation by contacting monolayers in a microfluidic device for membrane protein analysis. *Analytical Chemistry*, 78(24):8169–8174, 2006. ISSN 0003-2700. doi: 10.1021/ac0613479. URL <http://dx.doi.org/10.1021/ac0613479>.
- [82] William L. Hwang, Min Chen, Brid Cronin, Matthew A. Holden, and Hagan Bayley. Asymmetric droplet interface bilayers. *Journal of the American Chemical Society*, 130(18):5878–5879, 2008. ISSN 0002-7863. doi: 10.1021/ja802089s. URL <http://dx.doi.org/10.1021/ja802089s>.
- [83] Ryuji Kawano, Yutaro Tsuji, Koki Kamiya, Taiga Kodama, Toshihisa Osaki, Norihisa Miki, and Shoji Takeuchi. A portable lipid bilayer system for environmental sensing with a transmembrane protein. *PLoS ONE*, 9(7):e102427, 2014. doi: 10.1371/journal.pone.0102427. URL <http://dx.doi.org/10.1371/journal.pone.0102427>.
- [84] Hagan Bayley, Brid Cronin, Andrew Heron, Matthew A. Holden, William L. Hwang, Ruhma Syeda, James Thompson, and Mark Wallace. Droplet interface bilayers. *Molecular BioSystems*, 4(12):1191–1208, 2008. ISSN 1742-206X. doi: 10.1039/B808893D. URL <http://dx.doi.org/10.1039/B808893D>.

- [85] William L. Hwang, Matthew A. Holden, Steven White, and Hagan Bayley. Electrical behavior of droplet interface bilayer networks: experimental analysis and modeling. *Journal of the American Chemical Society*, 129(38):11854–11864, 2007. ISSN 0002-7863. doi: 10.1021/ja074071a. URL <http://dx.doi.org/10.1021/ja074071a>.
- [86] Matthew A. Holden, David Needham, and Hagan Bayley. Functional bionetworks from nanoliter water droplets. *Journal of the American Chemical Society*, 129(27):8650–8655, 2007. ISSN 0002-7863. doi: 10.1021/ja072292a. URL <http://dx.doi.org/10.1021/ja072292a>.
- [87] Gabriel Villar, Alexander D. Graham, and Hagan Bayley. A tissue-like printed material. *Science*, 340(6128):48–52, 2013. doi: 10.1126/science.1229495. URL <http://www.sciencemag.org/content/340/6128/48.abstract>.
- [88] Nima Tamaddoni, Eric C Freeman, and Stephen A Sarles. Sensitivity and directionality of lipid bilayer mechanotransduction studied using a revised, highly durable membrane-based hair cell sensor. *Smart Materials and Structures*, 24(6):065014, 2015. ISSN 0964-1726.
- [89] Peter J. Milianta, Michelle Muzzio, Jacqueline Denver, Geoffrey Cawley, and Sunghee Lee. Water permeability across symmetric and asymmetric droplet interface bilayers: Interaction of cholesterol sulfate with dphpc. *Langmuir*, 31(44):12187–12196, 2015. ISSN 0743-7463. doi: 10.1021/acs.langmuir.5b02748. URL <http://dx.doi.org/10.1021/acs.langmuir.5b02748>.
- [90] Stephen A. Sarles, Pegah Ghanbari Bavarsad, and Donald J. Leo. Incorporation and characterization of biological molecules in droplet-interface bilayer networks for novel active systems. pages 72880H–72880H, 2009. doi: 10.1117/12.815846. URL <http://dx.doi.org/10.1117/12.815846>.

- [91] Srikoundinya Punnamaraju and Andrew J. Steekl. Voltage control of droplet interface bilayer lipid membrane dimensions. *Langmuir*, 27(2):618–626, 2010. ISSN 0743-7463. doi: 10.1021/la1036508. URL <http://dx.doi.org/10.1021/la1036508>.
- [92] Joseph S. Najem, Myles D. Dunlap, Ian D. Rowe, Eric C. Freeman, John W. Grant, Sergei Sukharev, and Donald J. Leo. Activation of bacterial channel mscl in mechanically stimulated droplet interface bilayers. *Scientific Reports*, 5:13726, 2015. doi: 10.1038/srep13726<http://www.nature.com/articles/srep13726#supplementary-information>. URL <http://dx.doi.org/10.1038/srep13726>.
- [93] Hanna MG Barriga, Paula Booth, Stuart Haylock, Richard Bazin, Richard H Templer, and Oscar Ces. Droplet interface bilayer reconstitution and activity measurement of the mechanosensitive channel of large conductance from escherichia coli. *Journal of The Royal Society Interface*, 11(98):20140404, 2014. ISSN 1742-5689.
- [94] Graham J. Taylor and Stephen A. Sarles. Heating-enabled formation of droplet interface bilayers using escherichia coli total lipid extract. *Langmuir*, 31(1): 325–337, 2015. ISSN 0743-7463. doi: 10.1021/la503471m. URL <http://dx.doi.org/10.1021/la503471m>.
- [95] Tobias Wauer, Holger Gerlach, Shiksha Mantri, Jamie Hill, Hagan Bayley, and K. Tanuj Sapra. Construction and manipulation of functional three-dimensional droplet networks. *ACS Nano*, 8(1):771–779, 2013. ISSN 1936-0851. doi: 10.1021/nm405433y. URL <http://dx.doi.org/10.1021/nm405433y>.
- [96] Prachya Mruetusatorn, Jonathan B. Boreyko, Guru A. Venkatesan, Stephen A. Sarles, Douglas G. Hayes, and C. Patrick Collier. Dynamic morphologies of microscale droplet interface bilayers. *Soft Matter*, 10(15):2530–2538, 2014. ISSN

1744-683X. doi: 10.1039/C3SM53032A. URL <http://dx.doi.org/10.1039/C3SM53032A>.

- [97] Takasi Nisisako, Shiva A Portonovo, and Jacob J Schmidt. Microfluidic passive permeability assay using nanoliter droplet interface lipid bilayers. *Analyst*, 138(22):6793–6800, 2013.
- [98] Mary-Anne Nguyen, Bernadeta Srijanto, C Patrick Collier, Scott T Retterer, and Stephen A Sarles. Hydrodynamic trapping for rapid assembly and in situ electrical characterization of droplet interface bilayer arrays. *Lab on a Chip*, 16(18):3576–3588, 2016.
- [99] CI Xavier et al. Microfluidic generation of encapsulated droplet interface bilayer networks (multisomes) and their use as cell-like reactors. *Chemical Communications*, 52(35):5961–5964, 2016.
- [100] Edmond Walsh, Alexander Feuerborn, and Peter R Cook. Formation of droplet interface bilayers in a teflon tube. *Scientific Reports*, 6, 2016.
- [101] M. Ferrari, L. Liggieri, F. Ravera, C. Amodio, and R. Miller. Adsorption kinetics of alkylphosphine oxides at water/hexane interface: 1. pendant drop experiments. *Journal of Colloid and Interface Science*, 186(1):40–45, 1997. ISSN 0021-9797. doi: <http://dx.doi.org/10.1006/jcis.1996.4579>. URL <http://www.sciencedirect.com/science/article/pii/S0021979796945798>.
- [102] Qiang He, Yi Zhang, Gang Lu, Reinhard Miller, Helmuth MÃuhwald, and Junbai Li. Dynamic adsorption and characterization of phospholipid and mixed phospholipid/protein layers at liquid/liquid interfaces. *Advances in Colloid and Interface Science*, 140(2):67–76, 2008. ISSN 0001-8686. doi: <http://dx.doi.org/10.1016/j.cis.2007.12.004>. URL <http://www.sciencedirect.com/science/article/pii/S000186860700187X>.

- [103] Sebastian Leptihn, Oliver K. Castell, Brid Cronin, En-Hsin Lee, Linda C. M. Gross, David P. Marshall, James R. Thompson, Matthew Holden, and Mark I. Wallace. Constructing droplet interface bilayers from the contact of aqueous droplets in oil. *Nat. Protocols*, 8(6):1048–1057, 2013. ISSN 1754-2189. doi: 10.1038/nprot.2013.061. URL <http://dx.doi.org/10.1038/nprot.2013.061>.
- [104] Srihoundinya Punnamaraju. *Voltage and Photo Induced Effects in Droplet-Interface-Bilayer Lipid Membranes*. PhD thesis, University of Cincinnati, 2011.
- [105] Jean-Christophe Baret, Felix Kleinschmidt, Abdeslam El Harrak, and Andrew D. Griffiths. Kinetic aspects of emulsion stabilization by surfactants: A microfluidic analysis. *Langmuir*, 25(11):6088–6093, 2009. ISSN 0743-7463. doi: 10.1021/la9000472. URL <http://dx.doi.org/10.1021/la9000472>.
- [106] F. Zhang and A. Proctor. Rheology and stability of phospholipid-stabilized emulsions. *Journal of the American Oil Chemists' Society*, 74(7):869–874, 1997. ISSN 0003-021X. doi: 10.1007/s11746-997-0230-x. URL <http://dx.doi.org/10.1007/s11746-997-0230-x>.
- [107] K. Ogino and M. Onishi. Interfacial action of natural surfactants in oil/water systems. *Journal of Colloid and Interface Science*, 83(1):18–25, 1981. ISSN 0021-9797. doi: [http://dx.doi.org/10.1016/0021-9797\(81\)90004-7](http://dx.doi.org/10.1016/0021-9797(81)90004-7). URL <http://www.sciencedirect.com/science/article/pii/0021979781900047>.
- [108] M. C. R. Johnson and L. Saunders. Time dependent interfacial tensions of a series of phospholipids. *Chemistry and Physics of Lipids*, 10(4):318–327, 1973. ISSN 0009-3084. doi: [http://dx.doi.org/10.1016/0009-3084\(73\)90057-1](http://dx.doi.org/10.1016/0009-3084(73)90057-1). URL <http://www.sciencedirect.com/science/article/pii/0009308473900571>.
- [109] Tz Ivanova, V. Raneva, I. Panaiotov, and R. Verger. Kinetics of spreading of dopc liposomes at the air-water interface subjected to phospholipase

- a2 hydrolysis. *Colloid and Polymer Science*, 271(3):290–297, 1993. ISSN 0303-402X. doi: 10.1007/BF00652369. URL <http://dx.doi.org/10.1007/BF00652369>.
- [110] V. Raneva, Tz Ivanova, G. Lazarova, J. Proust, and I. Panaiotov. Kinetics of spreading of photodamaged dopc liposomes at the air-water interface. *Colloid and Polymer Science*, 273(2):150–155, 1995. ISSN 0303-402X. doi: 10.1007/BF00654012. URL <http://dx.doi.org/10.1007/BF00654012>.
- [111] I. Panaiotov, Tz Ivanova, K. Balashev, and J. Proust. Spreading kinetics of dimyristoylphosphatidylcholine liposomes at the air/water interface below and above the main phase-transition temperature. *Colloids and Surfaces A: Physicochemical and Engineering Aspects*, 102(0):159–165, 1995. ISSN 0927-7757. doi: [http://dx.doi.org/10.1016/0927-7757\(95\)03253-A](http://dx.doi.org/10.1016/0927-7757(95)03253-A). URL <http://www.sciencedirect.com/science/article/pii/092777579503253A>.
- [112] M. A. Launois-Surpas, Tz Ivanova, I. Panaiotov, J. E. Proust, F. Puisieux, and G. Georgiev. Behavior of pure and mixed dppc liposomes spread or adsorbed at the air-water interface. *Colloid and Polymer Science*, 270(9):901–911, 1992. ISSN 0303-402X. doi: 10.1007/BF00657735. URL <http://dx.doi.org/10.1007/BF00657735>.
- [113] M Thoma and H Möhwald. Phospholipid monolayers at hydrocarbon/water interfaces. *Journal of colloid and interface science*, 162(2):340–349, 1994.
- [114] A Lucero, MR Rodriguez Nino, AP Gunning, VJ Morris, PJ Wilde, and JM Rodriguez Patino. Effect of hydrocarbon chain and ph on structural and topographical characteristics of phospholipid monolayers. *The Journal of Physical Chemistry B*, 112(25):7651–7661, 2008.
- [115] VB Fainerman, EV Aksenenko, and Reinhard Miller. Influence of alkane and perfluorocarbon vapors on adsorbed surface layers and spread insoluble

monolayers of surfactants, proteins and lipids. *Advances in colloid and interface science*, 2015.

- [116] Shashi Thutupalli, Jean-Baptiste Fleury, Audrey Steinberger, Stephan Herminghaus, and Ralf Seemann. Why can artificial membranes be fabricated so rapidly in microfluidics? *Chemical Communications*, 49(14):1443–1445, 2013. ISSN 1359-7345. doi: 10.1039/C2CC38867G. URL <http://dx.doi.org/10.1039/C2CC38867G>.
- [117] Haden L Scott, Vanessa P Nguyen, Daiane S Alves, Forrest L Davis, Kristen R Booth, Jordan Bryner, and Francisco N Barrera. The negative charge of the membrane has opposite effects on the membrane entry and exit of ph-low insertion peptide. *Biochemistry*, 54(9):1709–1712, 2015.
- [118] Sara Aghdaei, Mairi E Sandison, Michele Zagnoni, Nicolas G Green, and Hywel Morgan. Formation of artificial lipid bilayers using droplet dielectrophoresis. *Lab on a Chip*, 8(10):1617–1620, 2008.
- [119] Shiv A Acharya, Alexander Portman, Carl S Salazar, and Jacob J Schmidt. Hydrogel-stabilized droplet bilayers for high speed solution exchange. *Scientific reports*, 3:3139, 2013.
- [120] Dae-Woong Jeong, Hyunwoo Jang, Siyoung Q Choi, and Myung Chul Choi. Enhanced stability of freestanding lipid bilayer and its stability criteria. *Scientific Reports*, 6, 2016.
- [121] Satoshi Nakata, Ayano Deguchi, Yota Seki, Koichi Fukuhara, Makiko Goto, and Mitsuhiro Denda. Ability of sodium dodecyl sulfate to transiently stabilize a phospholipid molecular layer. *Thin Solid Films*, 615:215–220, 2016.
- [122] Sung-Ho Jung, Sangbaek Choi, Young-Rok Kim, and Tae-Joon Jeon. Storable droplet interface lipid bilayers for cell-free ion channel studies. *Bioprocess and biosystems engineering*, 35(1-2):241–246, 2012. ISSN 1615-7591.

- [123] Tae-Joon Jeon, Jason L. Poulos, and Jacob J. Schmidt. Long-term storable and shippable lipid bilayer membrane platform. *Lab on a Chip*, 8(10):1742–1744, 2008. ISSN 1473-0197. doi: 10.1039/B807932C. URL <http://dx.doi.org/10.1039/B807932C>.
- [124] Stephen A. Sarles, L. Justin Stiltner, Christopher B. Williams, and Donald J. Leo. Bilayer formation between lipid-encased hydrogels contained in solid substrates. *ACS Applied Materials Interfaces*, 2(12):3654–3663, 2010. ISSN 1944-8244. doi: 10.1021/am100826s. URL <http://dx.doi.org/10.1021/am100826s>.
- [125] Xiao-feng Kang, Stephen Cheley, Allison C Rice-Ficht, and Hagan Bayley. A storable encapsulated bilayer chip containing a single protein nanopore. *Journal of the American Chemical Society*, 129(15):4701–4705, 2007. ISSN 0002-7863.
- [126] S. Ladha, A. R. Mackie, L. J. Harvey, D. C. Clark, E. J. Lea, M. Brullemans, and H. Duclohier. Lateral diffusion in planar lipid bilayers: a fluorescence recovery after photobleaching investigation of its modulation by lipid composition, cholesterol, or alamethicin content and divalent cations. *Biophysical Journal*, 71(3):1364–1373, 1996. ISSN 0006-3495. doi: [http://dx.doi.org/10.1016/S0006-3495\(96\)79339-6](http://dx.doi.org/10.1016/S0006-3495(96)79339-6). URL <http://www.sciencedirect.com/science/article/pii/S0006349596793396>.
- [127] Jonas Korlach, Petra Schwille, Watt W Webb, and Gerald W Feigenson. Characterization of lipid bilayer phases by confocal microscopy and fluorescence correlation spectroscopy. *Proceedings of the National Academy of Sciences*, 96(15):8461–8466, 1999. ISSN 0027-8424.
- [128] Ewa Banachowicz, Adam Patkowski, Gerd Meier, Kamila Klamecka, and Jacek GapinÅski. Successful fcs experiment in nonstandard conditions. *Langmuir*, 30(29):8945–8955, 2014. ISSN 0743-7463.

- [129] Michael L Wagner and Lukas K Tamm. Tethered polymer-supported planar lipid bilayers for reconstitution of integral membrane proteins: silane-polyethyleneglycol-lipid as a cushion and covalent linker. *Biophysical Journal*, 79(3):1400–1414, 2000.
- [130] James R. Thompson, Andrew J. Heron, Yusdi Santoso, and Mark I. Wallace. Enhanced stability and fluidity in droplet on hydrogel bilayers for measuring membrane protein diffusion. *Nano Letters*, 7(12):3875–3878, 2007. ISSN 1530-6984. doi: 10.1021/nl071943y. URL <http://dx.doi.org/10.1021/nl071943y>.
- [131] Linda C. M. Gross, Oliver K. Castell, and Mark I. Wallace. Dynamic and reversible control of 2d membrane protein concentration in a droplet interface bilayer. *Nano Letters*, 11(8):3324–3328, 2011. ISSN 1530-6984. doi: 10.1021/nl201689v. URL <http://dx.doi.org/10.1021/nl201689v>.
- [132] Andrew J. Heron, James R. Thompson, BrÃ¡nd Cronin, Hagan Bayley, and Mark I. Wallace. Simultaneous measurement of ionic current and fluorescence from single protein pores. *Journal of the American Chemical Society*, 131(5):1652–1653, 2009. ISSN 0002-7863. doi: 10.1021/ja808128s. URL <http://dx.doi.org/10.1021/ja808128s>.
- [133] Bruno Le Pioufle, Hiroaki Suzuki, Kazuhito V. Tabata, Hiroyuki Noji, and Shoji Takeuchi. Lipid bilayer microarray for parallel recording of transmembrane ion currents. *Analytical Chemistry*, 80(1):328–332, 2007. ISSN 0003-2700. doi: 10.1021/ac7016635. URL <http://dx.doi.org/10.1021/ac7016635>.
- [134] Victor Marin, Roland Kieffer, Raymond Padmos, and Marie-Eve Aubin-Tam. Stable free-standing lipid bilayer membranes in norland optical adhesive 81 microchannels. *Analytical Chemistry*, 88(15):7466–7470, 2016.
- [135] Janine Drexler and Claudia Steinem. Pore-suspending lipid bilayers on porous alumina investigated by electrical impedance spectroscopy. *The Journal of*

- Physical Chemistry B*, 107(40):11245–11254, 2003. ISSN 1520-6106. doi: 10.1021/jp030762r. URL <http://dx.doi.org/10.1021/jp030762r>.
- [136] Toru Ide, Yuko Takeuchi, and Toshio Yanagida. Development of an experimental apparatus for simultaneous observation of optical and electrical signals from single ion channels. *Single Molecules*, 3(1):33–42, 2002. ISSN 1438-5171. doi: 10.1002/1438-5171(200204)3:1<33::AID-SIMO33>3.0.CO;2-U. URL [http://dx.doi.org/10.1002/1438-5171\(200204\)3:1<33::AID-SIMO33>3.0.CO;2-U](http://dx.doi.org/10.1002/1438-5171(200204)3:1<33::AID-SIMO33>3.0.CO;2-U).
- [137] Prasad V. Ganesan and Steven G. Boxer. A membrane interferometer. *Proceedings of the National Academy of Sciences*, 2009. doi: 10.1073/pnas.0901770106. URL <http://www.pnas.org/content/early/2009/03/20/0901770106.abstract>.
- [138] Peter J Beltramo, Rob Van Hooghten, and Jan Vermant. Millimeter-area, free standing, phospholipid bilayers. *Soft matter*, 12(19):4324–4331, 2016.
- [139] Sumit Kalsi, Andrew M Powl, Bonnie A Wallace, Hywel Morgan, and Maurits RR de Planque. Shaped apertures in photoresist films enhance the lifetime and mechanical stability of suspended lipid bilayers. *Biophysical journal*, 106(8):1650–1659, 2014.
- [140] Xiaojun Han, André Studer, Harald Sehr, Isabelle Geissbühler, Marco Di Berardino, Fritz K Winkler, and Louis X Tiefenauer. Nanopore arrays for stable and functional free-standing lipid bilayers. *Advanced Materials*, 19(24):4466–4470, 2007.
- [141] Christian Hennessal and Claudia Steinem. Pore-spanning lipid bilayers visualized by scanning force microscopy. *Journal of the American Chemical Society*, 122(33):8085–8086, 2000.

- [142] V. Borisenko, T. Loughheed, J. Hesse, E. FÄijreder-KitzmÄijller, N. Fertig, J. C. Behrends, G. A. Woolley, and G. J. SchÄijtz. Simultaneous optical and electrical recording of single gramicidin channels. *Biophysical Journal*, 84(1):612–622, 2003. ISSN 0006-3495. doi: [http://dx.doi.org/10.1016/S0006-3495\(03\)74881-4](http://dx.doi.org/10.1016/S0006-3495(03)74881-4). URL <http://www.sciencedirect.com/science/article/pii/S0006349503748814>.
- [143] Michele Zagnoni. Miniaturised technologies for the development of artificial lipid bilayer systems. *Lab on a Chip*, 12(6):1026–1039, 2012.
- [144] Sanhita S. Dixit, Alexandra Pincus, Bin Guo, and Gregory W. Faris. Droplet shape analysis and permeability studies in droplet lipid bilayers. *Langmuir*, 28(19):7442–7451, 2012. ISSN 0743-7463. doi: 10.1021/la3005739. URL <http://dx.doi.org/10.1021/la3005739>.
- [145] Miho Yanagisawa, Taka-aki Yoshida, Miyuki Furuta, Satoshi Nakata, and Masayuki Tokita. Adhesive force between paired microdroplets coated with lipid monolayers. *Soft Matter*, 9(25):5891–5897, 2013. ISSN 1744-683X. doi: 10.1039/C3SM50938A. URL <http://dx.doi.org/10.1039/C3SM50938A>.
- [146] Stephen Andrew Sarles. *Physical encapsulation of interface bilayers*. PhD thesis, Virginia Tech, 2010.
- [147] Graham J. Taylor, Guru A. Venkatesan, C. Patrick Collier, and Stephen A. Sarles. Direct in situ measurement of specific capacitance, monolayer tension, and bilayer tension in a droplet interface bilayer. *Soft Matter*, 11(38):7592–7605, 2015. ISSN 1744-683X. doi: 10.1039/C5SM01005E. URL <http://dx.doi.org/10.1039/C5SM01005E>.
- [148] Maurits R. R. de Planque, Sara Aghdaei, Tiina Roose, and Hywel Morgan. Electrophysiological characterization of membrane disruption by nanoparticles.

- ACS Nano*, 5(5):3599–3606, 2011. ISSN 1936-0851. doi: 10.1021/nm103320j. URL <http://dx.doi.org/10.1021/nm103320j>.
- [149] Roman Pichot, Richard Watson, and Ian Norton. Phospholipids at the interface: Current trends and challenges. *International Journal of Molecular Sciences*, 14(6):11767–11794, 2013. ISSN 1422-0067. URL <http://www.mdpi.com/1422-0067/14/6/11767>.
- [150] Michinao Hashimoto, Piotr Garstecki, Howard A. Stone, and George M. Whitesides. Interfacial instabilities in a microfluidic hele-shaw cell. *Soft Matter*, 4(7):1403–1413, 2008. ISSN 1744-683X. doi: 10.1039/B715867J. URL <http://dx.doi.org/10.1039/B715867J>.
- [151] Yurii A. Shchipunov and Alexander F. Kolpakov. Phospholipids at the oil/water interface: adsorption and interfacial phenomena in an electric field. *Advances in Colloid and Interface Science*, 35(0):31–138, 1991. ISSN 0001-8686. doi: [http://dx.doi.org/10.1016/0001-8686\(91\)80020-K](http://dx.doi.org/10.1016/0001-8686(91)80020-K). URL <http://www.sciencedirect.com/science/article/pii/000186869180020K>.
- [152] Anda Vintiloiu and Jean-Christophe Leroux. Organogels and their use in drug delivery – a review. *Journal of Controlled Release*, 125(3):179–192, 2008. ISSN 0168-3659. doi: <http://dx.doi.org/10.1016/j.jconrel.2007.09.014>. URL <http://www.sciencedirect.com/science/article/pii/S0168365907005391>.
- [153] C. Jarzynski. Nonequilibrium equality for free energy differences. *Physical Review Letters*, 78(14):2690–2693, 1997. URL <http://link.aps.org/doi/10.1103/PhysRevLett.78.2690>.
- [154] Qing Song, Alexander Couzis, Ponisseril Somasundaran, and Charles Maldarelli. A transport model for the adsorption of surfactant from micelle solutions onto a clean air/water interface in the limit of rapid aggregate

- disassembly relative to diffusion and supporting dynamic tension experiments. *Colloids and Surfaces A: Physicochemical and Engineering Aspects*, 282(0):162–182, 2006. ISSN 0927-7757. doi: <http://dx.doi.org/10.1016/j.colsurfa.2006.03.006>. URL <http://www.sciencedirect.com/science/article/pii/S0927775706002123>.
- [155] Milton J. Rosen and Xi Yuan Hua. Dynamic surface tension of aqueous surfactant solutions: 2. parameters at 1 s and at mesoequilibrium. *Journal of Colloid and Interface Science*, 139(2):397–407, 1990. ISSN 0021-9797. doi: [http://dx.doi.org/10.1016/0021-9797\(90\)90114-4](http://dx.doi.org/10.1016/0021-9797(90)90114-4). URL <http://www.sciencedirect.com/science/article/pii/0021979790901144>.
- [156] Srinivas Nageswaran Moorkanikkara and Daniel Blankschtein. New methodology to determine equilibrium surfactant adsorption properties from experimental dynamic surface tension data. *Langmuir*, 25(11):6191–6202, 2009. ISSN 0743-7463. doi: 10.1021/la804324e. URL <http://dx.doi.org/10.1021/la804324e>.
- [157] D. J. Mitev, Tz Ivanova, and C. S. Vassilieff. Kinetics of lipid layer formation at interfaces. *Colloids and Surfaces B: Biointerfaces*, 24(3):185–192, 2002. ISSN 0927-7765. doi: [http://dx.doi.org/10.1016/S0927-7765\(01\)00245-4](http://dx.doi.org/10.1016/S0927-7765(01)00245-4). URL <http://www.sciencedirect.com/science/article/pii/S0927776501002454>.
- [158] J. Eastoe and J. S. Dalton. Dynamic surface tension and adsorption mechanisms of surfactants at the air/water interface. *Advances in Colloid and Interface Science*, 85(2):103–144, 2000. ISSN 0001-8686. doi: [http://dx.doi.org/10.1016/S0001-8686\(99\)00017-2](http://dx.doi.org/10.1016/S0001-8686(99)00017-2). URL <http://www.sciencedirect.com/science/article/pii/S0001868699000172>.
- [159] G. Bleys and P. Joos. Adsorption kinetics of bolaform surfactants at the air/water interface. *The Journal of Physical Chemistry*, 89(6):1027–1032, 1985.

ISSN 0022-3654. doi: 10.1021/j100252a028. URL <http://dx.doi.org/10.1021/j100252a028>.

- [160] Oualid Hamdaoui and Emmanuel Naffrechoux. Modeling of adsorption isotherms of phenol and chlorophenols onto granular activated carbon: Part i. two-parameter models and equations allowing determination of thermodynamic parameters. *Journal of Hazardous Materials*, 147(1&A2):381–394, 2007. ISSN 0304-3894. doi: <http://dx.doi.org/10.1016/j.jhazmat.2007.01.021>. URL <http://www.sciencedirect.com/science/article/pii/S0304389407000568>.
- [161] Florly S. Ariola, Zaiguo Li, Christine Cornejo, Robert Bittman, and Ahmed A. Heikal. Membrane fluidity and lipid order in ternary giant unilamellar vesicles using a new bodipy-cholesterol derivative. *Biophysical Journal*, 96(7):2696–2708, 2009. ISSN 0006-3495. doi: <http://dx.doi.org/10.1016/j.bpj.2008.12.3922>. URL <http://www.sciencedirect.com/science/article/pii/S0006349509003907>.
- [162] H Lindsey, NO Petersen, and Sunney I Chan. Physicochemical characterization of 1, 2-diphytanoyl-sn-glycero-3-phosphocholine in model membrane systems. *Biochimica et Biophysica Acta (BBA)-Biomembranes*, 555(1):147–167, 1979. ISSN 0005-2736.
- [163] Emanuel Schneck, Felix Sedlmeier, and Roland R. Netz. Hydration repulsion between biomembranes results from an interplay of dehydration and depolarization. *Proceedings of the National Academy of Sciences*, 109(36):14405–14409, 2012. doi: 10.1073/pnas.1205811109. URL <http://www.pnas.org/content/109/36/14405.abstract>.
- [164] B. V. Zhmud, F. Tiberg, and J. Kizling. Dynamic surface tension in concentrated solutions of cnem surfactants: a comparison between the theory and experiment. *Langmuir*, 16(6):2557–2565, 2000. ISSN 0743-7463. doi: 10.1021/la991144y. URL <http://dx.doi.org/10.1021/la991144y>.

- [165] Sophie Pautot, Barbara J. Frisken, Ji-Xin Cheng, X. Sunney Xie, and D. A. Weitz. Spontaneous formation of lipid structures at oil/water/lipid interfaces. *Langmuir*, 19(24):10281–10287, 2003. ISSN 0743-7463. doi: 10.1021/la034532f. URL <http://dx.doi.org/10.1021/la034532f>.
- [166] Hansgeorg Schindler. Exchange and interactions between lipid layers at the surface of a liposome solution. *Biochimica et Biophysica Acta (BBA) - Biomembranes*, 555(2):316–336, 1979. ISSN 0005-2736. doi: [http://dx.doi.org/10.1016/0005-2736\(79\)90171-8](http://dx.doi.org/10.1016/0005-2736(79)90171-8). URL <http://www.sciencedirect.com/science/article/pii/0005273679901718>.
- [167] D. Needham and D. A. Haydon. Tensions and free energies of formation of "solventless" lipid bilayers. measurement of high contact angles. *Biophysical Journal*, 41(3):251–257, 1983. ISSN 0006-3495. doi: [http://dx.doi.org/10.1016/S0006-3495\(83\)84435-X](http://dx.doi.org/10.1016/S0006-3495(83)84435-X). URL <http://www.sciencedirect.com/science/article/pii/S000634958384435X>.
- [168] Sean F Gilmore, Andrew I Yao, Zipora Tietel, Tobias Kind, Marc T Facciotti, and Atul N Parikh. Role of squalene in the organization of monolayers derived from lipid extracts of halobacterium salinarum. *Langmuir*, 29(25):7922–7930, 2013.
- [169] Asya Tsanova, A Jordanova, and Z Lalchev. Effects of leucin-enkephalins on surface characteristics and morphology of model membranes composed of raft-forming lipids. *The Journal of membrane biology*, 249(3):229–238, 2016.
- [170] Linas Mazutis and Andrew D Griffiths. Selective droplet coalescence using microfluidic systems. *Lab on a Chip*, 12(10):1800–1806, 2012.
- [171] Małgorzata Jurak. Thermodynamic aspects of cholesterol effect on properties of phospholipid monolayers: Langmuir and langmuir–blodgett monolayer study. *The Journal of Physical Chemistry B*, 117(13):3496–3502, 2013.

- [172] Thomas Husslein, Dennis M Newns, Pratap C Pattnaik, Qingfeng Zhong, Preston B Moore, and Michael L Klein. Constant pressure and temperature molecular-dynamics simulation of the hydrated diphytanolphosphatidylcholine lipid bilayer. *The Journal of chemical physics*, 109(7):2826–2832, 1998.
- [173] Stefano Vanni, Hisaaki Hirose, H el ene Barelli, Bruno Antony, and Romain Gautier. A sub-nanometre view of how membrane curvature and composition modulate lipid packing and protein recruitment. *Nature communications*, 5, 2014.
- [174] Matthias Garten, Coline Pr evost, Clotilde Cadart, Romain Gautier, Luc Bousset, Ronald Melki, Patricia Bassereau, and Stefano Vanni. Methyl-branched lipids promote the membrane adsorption of α -synuclein by enhancing shallow lipid-packing defects. *Physical Chemistry Chemical Physics*, 17(24):15589–15597, 2015.
- [175] Sarah L Keller. Miscibility transitions and lateral compressibility in liquid phases of lipid monolayers. *Langmuir*, 19(5):1451–1456, 2003.
- [176] Friederike Giebel, Michael Paulus, Julia Nase, Irena Kiesel, Steffen Bieder, and Metin Tolan. The interaction between stearic acid monolayers and butane under elevated pressures. *Colloids and Surfaces A: Physicochemical and Engineering Aspects*, 504:126–130, 2016.
- [177] Qunfang Lei and Colin D. Bain. Surfactant-induced surface freezing at the alkane-water interface. *Physical Review Letters*, 92(17):176103, 2004. URL <http://link.aps.org/doi/10.1103/PhysRevLett.92.176103>.
- [178] Shai Yefet, Eli Sloutskin, Lilach Tamam, Zvi Sapir, Moshe Deutsch, and Benjamin M Ocko. Surfactant-induced phases in water-supported alkane monolayers: Ii. structure. *Langmuir*, 30(27):8010–8019, 2014.

- [179] JA Marqusee and Ken A Dill. Solute partitioning into chain molecule interphases: monolayers, bilayer membranes, and micelles. *The Journal of chemical physics*, 85(1):434–444, 1986.
- [180] Petra B Welzel, Ingrid Weis, and Gerhard Schwarz. Sources of error in langmuir trough measurements: Wilhelmy plate effects and surface curvature. *Colloids and Surfaces A: Physicochemical and Engineering Aspects*, 144(1):229–234, 1998.
- [181] T. DÄijrrschmidt and H. Hoffmann. Organogels from aba triblock copolymers. *Colloid and Polymer Science*, 279(10):1005–1012, 2001. ISSN 0303-402X. doi: 10.1007/s003960100532. URL <http://dx.doi.org/10.1007/s003960100532>.
- [182] Masataka Sugimoto, Keisuke Sakai, Yuji Aoki, Takashi Taniguchi, Kiyohito Koyama, and Toshihiro Ueda. Rheology and morphology change with temperature of sebs/hydrocarbon oil blends. *Journal of Polymer Science Part B: Polymer Physics*, 47(10):955–965, 2009. ISSN 1099-0488.
- [183] N Mischenko, K Reynders, Kell Mortensen, R Scherrenberg, F Fontaine, R Graulus, and Harry Reynaers. Structural studies of thermoplastic triblock copolymer gels. *Macromolecules*, 27(8):2345–2347, 1994. ISSN 0024-9297.
- [184] G Andrew Woolley and BA Wallace. Temperature dependence of the interaction of alamethicin helices in membranes. *Biochemistry*, 32(37):9819–9825, 1993. ISSN 0006-2960.
- [185] J MÄijller, C MÄijnster, and T Salditt. Thermal denaturing of bacteriorhodopsin by x-ray scattering from oriented purple membranes. *Biophysical journal*, 78(6):3208–3217, 2000. ISSN 0006-3495.
- [186] Yunpeng Bai, Ximin He, Dingsheng Liu, Santoshkumar N. Patil, Dan Bratton, Ansgar Huebner, Florian Hollfelder, Chris Abell, and Wilhelm T. S. Huck.

- A double droplet trap system for studying mass transport across a droplet-droplet interface. *Lab on a Chip*, 10(10):1281–1285, 2010. ISSN 1473-0197. doi: 10.1039/B925133B. URL <http://dx.doi.org/10.1039/B925133B>.
- [187] Jiang-Jen Lin, I-Jein Cheng, Chou-Nan Chen, and Chang-Chin Kwan. Synthesis, characterization, and interfacial behaviors of poly (oxyethylene)-grafted sebs copolymers. *Industrial engineering chemistry research*, 39(1): 65–71, 2000. ISSN 0888-5885.
- [188] Thomas J. McIntosh, Alan D. Magid, and Sidney A. Simon. Range of the solvation pressure between lipid membranes: dependence on the packing density of solvent molecules. *Biochemistry*, 28(19):7904–7912, 1989. ISSN 0006-2960. doi: 10.1021/bi00445a053. URL <http://dx.doi.org/10.1021/bi00445a053>.
- [189] P. Poulin and J. Bibette. Adhesion of water droplets in organic solvent. *Langmuir*, 14(22):6341–6343, 1998. ISSN 0743-7463. doi: 10.1021/la9801413. URL <http://dx.doi.org/10.1021/la9801413>.
- [190] Tanya L. Chantawansri, Andrew J. Duncan, Jan Ilavsky, Kristoffer K. Stokes, Michael C. Berg, Randy A. Mrozek, Joseph L. Lenhart, Frederick L. Beyer, and Jan W. Andzelm. Phase behavior of sebs triblock copolymer gels. *Journal of Polymer Science Part B: Polymer Physics*, 49(20):1479–1491, 2011. ISSN 1099-0488. doi: 10.1002/polb.22335. URL <http://dx.doi.org/10.1002/polb.22335>.
- [191] Stephen A. Sarles, John D. W. Madden, and Donald J. Leo. Hair cell inspired mechanotransduction with a gel-supported, artificial lipid membrane. *Soft Matter*, 7(10):4644–4653, 2011. ISSN 1744-683X. doi: 10.1039/C1SM05120B. URL <http://dx.doi.org/10.1039/C1SM05120B>.

- [192] Mois̃s Eisenberg, James E Hall, and CA Mead. The nature of the voltage-dependent conductance induced by alamethicin in black lipid membranes. *The Journal of membrane biology*, 14(1):143–176, 1973. ISSN 0022-2631.
- [193] Guru A Venkatesan and Stephen A Sarles. Droplet immobilization within a polymeric organogel improves lipid bilayer durability and portability. *Lab on a Chip*, 16(11):2116–2125, 2016.
- [194] C. H. Hsieh, S. C. Sue, P. C. Lyu, and W. G. Wu. Membrane packing geometry of diphytanoylphosphatidylcholine is highly sensitive to hydration: phospholipid polymorphism induced by molecular rearrangement in the headgroup region. *Biophys J*, 73(2):870–7, 1997. ISSN 0006-3495 (Print) 1542-0086 (Electronic).
- [195] Richard B Fair. Digital microfluidics: is a true lab-on-a-chip possible? *Microfluidics and Nanofluidics*, 3(3):245–281, 2007. ISSN 1613-4982.
- [196] Andrew J. Heron, James R. Thompson, Amy E. Mason, and Mark I. Wallace. Direct detection of membrane channels from gels using water-in-oil droplet bilayers. *Journal of the American Chemical Society*, 129(51):16042–16047, 2007. ISSN 0002-7863. doi: 10.1021/ja075715h. URL <http://dx.doi.org/10.1021/ja075715h>.
- [197] Jonathan B. Boreyko, Georgios Polizos, Panos G. Datskos, Stephen A. Sarles, and C. Patrick Collier. Air-stable droplet interface bilayers on oil-infused surfaces. *Proceedings of the National Academy of Sciences of the United States of America*, 111(21):7588–7593, 2014. ISSN 0027-8424 1091-6490. doi: 10.1073/pnas.1400381111. URL <http://www.ncbi.nlm.nih.gov/pmc/articles/PMC4040577/>.
- [198] K Inoue, K Kamiya, T Osaki, N Miki, and S Takeuchi. Non-spherical liposome formation using 3d-laser-printed micro-cube structures. In *2016 IEEE 29th*

International Conference on Micro Electro Mechanical Systems (MEMS), pages 197–199. IEEE.

- [199] R Watanabe, N Soga, M Hara, and H Noji. Arrayed water-in-oil droplet bilayers for membrane transport analysis. *Lab on a Chip*, 2016.

Appendices

Appendix A

Lipid Composition of Biological Membranes

Membrane lipid composition data plotted in Figure 1.6 and 1.7 are taken from the Tables given below.

Table A.1: Lipid composition of biological membranes

Source	Cholesterol	PC	SPM	PE	PI	PS	PG	Other
E Coli	0	-	0	80	0	0	15	5
Sindbis virus	0	26	18	35	0	20	0	0
Rat Liver ER smooth	10	55	12	21	6.7	0	0	1.9
Rat Liver Mitochondria (inner)	3	45	2.5	25	6	1	2	18.7
Rat Liver Mitochondria (outer)	5	50	5	23	13	2	2.5	4.8

Data reproduced from [2]

Table A.2: Phospholipid fatty acid chain composition in human red blood cell

Chain length and unsaturation	Total Phospholipid	SPM	PC	PE	PS
16:0	20.1	23.6	31.2	12.9	2.7
18:0	17	5.7	11.8	11.5	37.5
18:1	13.3	1	18.9	18.1	8.1
18:2	8.6	1	22.8	7.1	3.1
20:0	1	1.9	1	1	1
20:3	1.3	0	1.9	1.5	2.6
22:0	1.9	9.5	1.9	1.5	2.6
20:4	12.6	1.4	6.7	23.7	24.2
23:0	1	2	1	1	1
24:0	4.7	22.8	1	1	1
22:4	3.1	0	1	7.5	4
24:1	4.8	24	1	1	1
22:5	2	0	1	4.3	3.4
23:0	4.2	0	2.1	8.2	10.1

Data reproduced from [3]

Appendix B

Exponential Model for Lipid Self-assembly

Here, we consider a time-variable adsorption rate constant, and thus the surface pressure, as given by

$$k_a(t) = k_a(\Gamma_\infty - \Gamma(t)) \quad (\text{B.1})$$

In this form, the adsorption rate constant k_a is proportional to the difference in surface pressure from its final value. Substituting 1 into Equation 2 in Chapter 3 yields an exponential, converging relationship for surface density versus time:

$$\Gamma(t) = \Gamma_\infty(1 - e^{-k_a C_0 t}) \quad (\text{B.2})$$

Taking the logarithm of both sides and rearranging yields the following linear equation in time that can be used to test the appropriateness of Equation 1:

$$\ln(\Gamma_\infty - \Gamma(t)/\Gamma_\infty) = -k_a C_0 t \quad (\text{B.3})$$

The figure below shows values of surface pressure measured for DPhPC-in and DOPC-in (2 mg/ml) plotted versus time as given in Equation 3. The fact that the

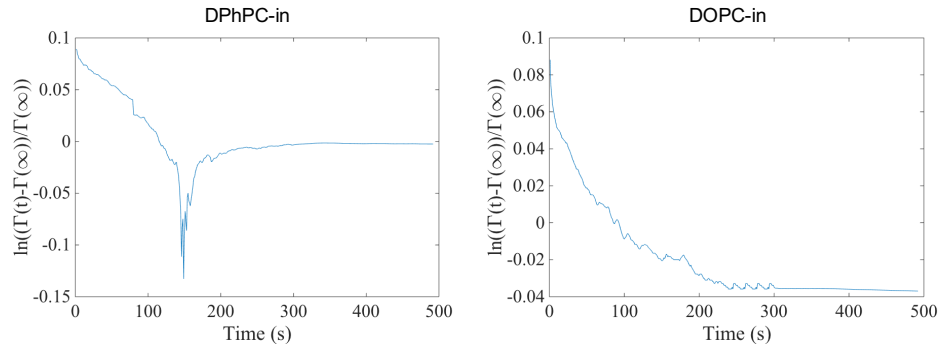


Figure B.1: Values of left hand side of Equation 3 plotted versus time for DPhPC-in and DOPC-in.

data do not adhere to a single linear relationship across the time required to reach equilibrium indicate that a single exponent, exponential model fails to capture the evolution in surface pressure. A similarly poor fit is found for other cases (DPhPC-out and DOPC-out) as well (not shown).

Appendix C

DI Water Evaporation Rate at Oil-Air Interface

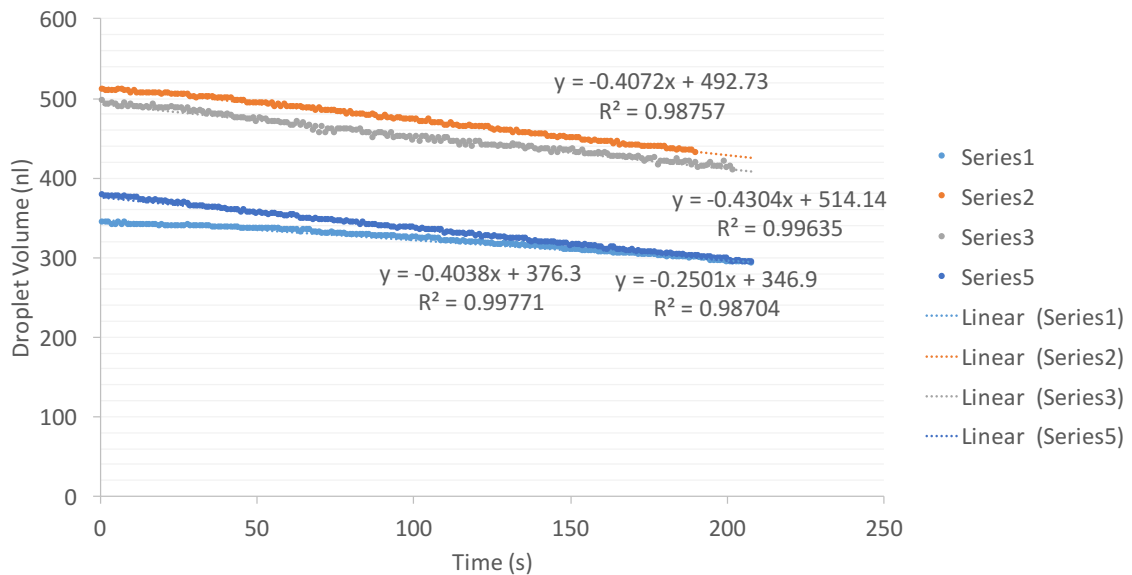


Figure C.1: Rate of evaporation of DI water droplet held close to Hexadecane-Air interface. Volumes are estimated from droplet diameter by assuming a spherical droplet. Droplet diameter is measured using MATLAB image processing.

Vita

Guru A. Venkatesan was born in Neyveli, a small town in southern part of India, on July 22, 1990. After finishing his high-school in 2007 at Jawahar Senior Secondary School, he received a B.Tech. in Biomedical Engineering at the Sathyabama University, Chennai, India in May 2011. During his undergraduate studies, he collaborated with Sri Ramachandra Medical College and Research Institute to develop an image processing algorithm to analyze biopsy samples to grade prostate cancers.

Guru began his graduate studies under Dr. Andy Sarles in August 2011 and is currently set to graduate in spring 2017 with a Ph.D. in Biomedical Engineering from the University of Tennessee, Knoxville. As a graduate student, his work has been in understanding how biomolecules behave at liquid interfaces to advance the droplet interface bilayer technology that is used to create model cell membranes. His research work has resulted in two published first-author papers, with one more in preparation. He has also contributed to three other journal papers as a co-author.

Outside of the lab, Guru founded a student organization called Tech Carnival to host annual science and engineering festival for students of all levels. This organization has hosted two annual festivals so far and has directly impacted over 500 high school and college level students. Prior to this, he also served as the president of Manthan - Indian student association at UT. During his spare time, Guru enjoys and ponders about music, philosophy and art. He has co-composed original artworks with his friend Jordan Kear and showcased them at local galleries in Knoxville.